

**DEVELOPMENT OF NOVEL MODELS AND CRISPR-BASED GENE EDITING
THERAPEUTICS FOR RETINAL DEGENERATION IN *XENOPUS LAEVIS***

by

Amirfarhad Ghaseminejad Tafres

B.Sc. (Hons), The University of British Columbia, 2018

A THESIS SUBMITTED IN PARTIAL FULFILLMENT OF

THE REQUIREMENTS FOR THE DEGREE OF

MASTER OF SCIENCE

in

The Faculty of Graduate and Postdoctoral studies

(Experimental Medicine)

THE UNIVERSITY OF BRITISH COLUMBIA

(Vancouver)

June 2021

© Amirfarhad Ghaseminejad Tafres, 2021

The following individuals certify that they have read, and recommend to the Faculty of Graduate and Postdoctoral Studies for acceptance, the thesis entitled:

Development of novel models and Crispr-based gene editing therapeutics for retinal degeneration in *Xenopus laevis*

submitted by Amirfarhad Ghaseminejad Tafres in partial fulfilment of the requirements for

the degree of Master of Science

in Experimental Medicine

Examining Committee:

Orson Moritz, Experimental Medicine, UBC

Supervisor

Cheryl Gregory-Evans, Experimental Medicine, UBC

Supervisory Committee Member

Robert Molday, Biochemistry and Molecular Biology, UBC

Additional Examiner

ABSTRACT

Mutations in the rhodopsin gene (*RHO*) are the most common cause of autosomal dominant retinitis pigmentosa (adRP). Previously, our research group has identified two distinct mechanisms of light-exacerbated retinal degeneration (RD) associated with P23H and T4K *RHO* mutations. Here, we developed a transgenic *X. laevis* carrying human/mouse hybrid T4K *RHO* and compared the light-exacerbated RD phenotype to human/mouse wildtype, human-T4K and mouse-T4K *RHO* transgenic *X. laevis* models. For animals reared in cyclic light, expression of T4K rhodopsin in rods caused significant RD regardless of whether the transgene was human, mouse, or a human/mouse hybrid *RHO*. When raised in the dark, no significant RD was detected in animals expressing T4K *RHO*. Therefore, the light-exacerbated RD phenotype associated with the *RHO* T4K mutation is relatively independent of the underlying *RHO* cDNA. This hybrid animal model allows us to explore treatment strategies directly on the human gene, streamlining the transfer of therapeutics from lab benches into clinical trials.

To date, RP remains an incurable disease. Utilizing a previously developed *X. laevis* model for adRP, we tested multiple CRISPR/Cas9-based gene-editing strategies to prevent RD in our adRP model. We designed highly specific guide RNAs to 1. Edit the mutant allele and allow for the error-prone non-homologous end joining (NHEJ) repair mechanism to result in a premature stop codon, nullifying the mutant allele 2. Induce simultaneous double-strand breaks on both sides of the start codon, generating large inactivating deletions and 3. Edit the mutant allele and utilize the homology-directed recombination repair mechanism to restore the mutant allele to wildtype. Remarkably, the CRISPR-induced NHEJ repair mechanism appeared to be the most efficient treatment in preventing RD. We postulate that in developing gene editing therapeutics for human RP, similar results are likely to occur, suggesting that the simplest approach may be the most

effective. Moreover, our *X. laevis* models can be used to characterize and understand the pathomechanism of human RP mutations, as well as to develop novel gene-editing treatment strategies. Lastly, our findings demonstrate that CRISPR/Cas9 technology is an effective therapeutic tool for adRP with potential clinical implications for other dominant diseases of the human retina.

LAY SUMMARY

Retinitis Pigmentosa (RP) is a vision-threatening disorder that is characterized by progressive blindness due to retinal degeneration. There are currently no treatments available for this disease, mainly due to the diversity of its underlying genetic mutations. A large portion of these mutations affect the gene encoding rhodopsin, a key protein in visual function. Here, we have developed a novel *Xenopus laevis* model that carries a human/mouse hybrid rhodopsin gene. This model allows us to better understand the mechanisms underlying RP as well as to develop treatments specific to the human gene. We also tested multiple therapeutic approaches in our autosomal dominant RP model, using the cutting-edge CRISPR/Cas9 gene editing tool. Remarkably, we were able to prevent retinal degeneration by specifically eliminating the mutant allele. Given the rapid technological advancements in delivering human gene-therapeutics, we believe our findings highlight the most efficient treatment approach once translation into human patients becomes feasible.

PREFACE

All data collection and analysis presented in this dissertation were conducted by myself. Research goals were designed in collaboration with my supervisor, Dr. Orson Moritz. A subset of injection experiments was carried out with the assistance of Beatrice Tam, Aaron Loewen and Ross Scharbach. Aaron Loewen was responsible for conducting the dot blot assay and taking the confocal images presented in Figure 2-1.

At the time of submission, no publications have arisen from work presented in this dissertation.

All procedures involving animals were approved by the UBC animal care committee under certificates A18-0257 Analysis of mechanisms underlying retinal degeneration 2018, and A18-0259 In vivo analysis of mechanisms underlying retinal degeneration and photoreceptor structure 2018 issued to Orson L. Moritz.

TABLE OF CONTENTS

ABSTRACT.....	iii
LAY SUMMARY.....	v
PREFACE.....	vi
TABLE OF CONTENTS.....	vii
LIST OF FIGURES	x
LIST OF ABBREVIATIONS.....	xii
ACKNOWLEDGMENTS	xiv
1. INTRODUCTION.....	1
1.1 The eye.....	1
1.1.1 The retina.....	1
1.1.2 Rod and cone photoreceptors	1
1.1.3 Phototransduction and rhodopsin.....	2
1.1.4 Genetic diseases of the retina.....	4
1.2 Retinitis Pigmentosa.....	7
1.2.1 <i>Xenopus laevis</i> as a genetic model for RP	8
1.3 Gene editing	10
1.3.1 Gene therapy	10
1.3.1 CRISPR/Cas9	13
1.4 Electrophysiology, Fundus Imaging and Optical Coherence Tomography	18
2. MODELING A HYBRID HUMAN/MOUSE RHODOPSIN TRANSGENE IN <i>XENOPUS LAEVIS</i>	20
2.1 Introduction	20
2.1.1 Objectives and hypothesis	21
2.2 Methods.....	22
2.2.1 Construct design.....	22
2.2.2 Gibson assembly, transformation and miniprep	23
2.2.3 Transgenesis and animal rearing	24
2.2.4 Dot blot assay.....	24
2.2.5 Immunohistochemical labeling and confocal microscopy.....	25
2.2.6 Statistical analyses	26
2.3 Results	26

2.3.1	Human/mouse hybrid T4K rhodopsin – dark-reared vs. cyclic light	26
2.3.2	ChiWT, ChiT4K and hT4K – dark-reared	28
2.3.3	Mouse T4K rhodopsin – dark-reared vs. cyclic light	30
3.	CRISPR-BASED TREATMENT STRATEGIES FOR SELECTIVE EDITING OF MUTANT RHODOPSIN.....	32
3.1	Introduction	32
3.1.1	Genetically modified model for adRP (12bp deletion)	33
3.1.2	Objectives and hypotheses	34
3.2	Methods.....	37
3.2.1	Characterization of the 12bp-deletion animals	37
3.2.2	Designing single-guide RNA oligonucleotides	37
3.2.3	Oligonucleotide ligation into the pDR274 and transformation	39
3.2.4	Diagnostics to ensure proper insertion of the oligonucleotides	41
3.2.5	PCR Primers.....	41
3.2.6	<i>In-vitro</i> transcription of sgRNA.....	42
3.2.7	CRISPR <i>in-vitro</i> digestion assay	43
3.2.8	Designing a single-stranded oligonucleotide as an HDR template sequence... ..	43
3.2.9	RNA microinjection	44
3.2.10	Genomic DNA extraction, fragment analysis and Sanger sequencing	45
3.2.11	Dot blot assay, immunohistochemical labeling and confocal microscopy	45
3.2.12	Western Blotting	46
3.2.13	ERG recordings.....	46
3.2.14	OCT and fundus photography.....	47
3.2.15	Statistical analyses	47
3.3	Results	48
3.3.1	Characterizing the animals with the 12bp deletion mutation.....	48
3.3.2	<i>In-vitro</i> and <i>in-vivo</i> testing of the designed guides	50
3.3.3	Comparing the single-guide and double-guide CRISPR-based treatment approaches.....	52
3.3.4	Significantly higher rod opsin levels in the treated groups compared to untreated ones	52
3.3.5	Retinal degeneration was prevented in 12bp-deletion animals treated with a single-guide edit in exon 1	53

3.3.6	Simultaneous treatment with two guides also prevented RD	54
3.3.7	Simultaneous treatment with Sg2 and Sg5 resulted in large inactivating deletions in 7 out of 11 cases	55
3.3.8	The single guide (Sg2) editing the promoter regulatory region upstream from the start codon does not cause retinal degeneration	57
3.3.9	Distinguishing the mutant rhodopsin from WT endogenous rhodopsin protein via immunolabeling and western blotting	59
3.3.10	ERG recordings from 9-months old animals	61
3.3.11	OCT and fundus photography in 9-months old animals	63
3.3.12	Histology sections from 9-months old animals	66
3.3.13	CRISPR-mediated HDR as a treatment approach for adRP	66
3.3.14	Toxicity test to optimize the amount of single-stranded oligonucleotide injected into each embryo	67
3.3.15	Significant improvement in phenotype was observed in treated groups	69
3.3.16	The HDR repair pathway was inefficient for the recombination of the designed ssDNA template into the mutant rhodopsin gene	70
4.	CONCLUSION	73
	BIBLIOGRAPHY	80
	APPENDICES	91
	Appendix A. Rhodopsin promoter sequence	91
	Appendix B. HDR template design	92

LIST OF FIGURES

Figure 1-1. The phototransduction pathway in photoreceptors.	3
Figure 1-2. Rod-cone dystrophy and the progressive pattern of disease.	5
Figure 1-3. Flow chart summarizing dominant mutation types and corresponding therapeutic approaches.....	13
Figure 1-4. Different gene editing strategies using CRISPR/Cas9.....	15
Figure 1-5. CRISPR-Cas9 and sgRNA genome editing strategy and the following repair mechanisms of NHEJ and HDR.	17
Figure 2-1. ChiT4K transgenic animals raised in the dark compared to cyclic light.	27
Figure 2-2. ChiT4K, ChiWT and hT4K transgenic animals raised in the dark.	29
Figure 2-3. MT4K transgenic animals raised in the dark compared to cyclic light.....	31
Figure 3-1. Allele-specific gene therapeutic strategy for autosomal dominant diseases.	33
Figure 3-2. sgRNA designed to target the mutant allele, leaving the WT allele unaffected due to a single base discrepancy.....	35
Figure 3-3. <i>X. laevis Rho.L</i> gene carrying the 12bp deletion at the start of exon 1.....	39
Figure 3-4. Retinal histology and rhodopsin levels in 12bp deletion animals compared to WT..	49
Figure 3-5. CRISPR <i>in-vitro</i> digestion assay.....	50
Figure 3-6. CRISPR <i>in-vivo</i> testing assay.....	51
Figure 3-7. Total rod opsin levels assayed by dot blotting and rhodopsin labeling with B630N antibody.....	53
Figure 3-8. Significant RD observed in 12bp deletion animals was prevented in treated groups with a single guide.	54

Figure 3-9. Significant RD observed in 12b deletion animals was prevented in treated groups with two guides.	55
Figure 3-10. Removal of the start codon induced by large deletions in the 12bp-deletion animals prevented retinal degeneration in animals treated with simultaneous treatment of Sg2 and Sg5.	57
Figure 3-11. Comparing the Sg2-treated WT animals to untreated WT animals.	58
Figure 3-12. Rhodopsin localization in WT and 12bp deletion animals labelled by 11D5 antibody.....	60
Figure 3-13. Western blotting to compare 11D5 and B630N rhodopsin labeling in three WT solubilized eyes and three 12bp deletion eyes.	61
Figure 3-14. Scotopic ERG assay in 12bp deletion and WT animals.....	62
Figure 3-15. Scotopic ERG assay in treated and untreated animals.	63
Figure 3-16. OCT comparing WT and 12bp deletion 9 months old <i>X. laevis</i>	65
Figure 3-17. Histology sections from 9-months old animals.....	66
Figure 3-18. The effect of the concentration of ssDNA injected on the survival of <i>X. laevis</i> embryos.....	68
Figure 3-19. Comparing phenotypes between untreated, Sg5-treated and Sg5+ssDNA treated animals.	70
Figure 3-20. Dot blot assay comparing the 514-18 to B630N antibody labeling ratios between experimental and control groups.....	71
Figure 3-21. Histological evidence for a 2B2-positive cell, indicating the recombination of the designed template via HDR.	72

LIST OF ABBREVIATIONS

AAV	Adeno-associated virus
bp	Base pair
BRB	Blood-retinal-barrier
Cas	CRISPR-associated
CNS	Central nervous system
CRISPR	Clustered regularly interspaced short palindromic repeats
DNA	Deoxyribonucleic acid
dpf	Days-post-fertilization
DSB	Double-stranded DNA break
eGFP	Enhanced green fluorescent protein
ER	Endoplasmic reticulum
ERG	Electroretinogram
GCL	Ganglion cell layer
GDP	Guanosine 3'-diphosphate
GPCR	G protein coupled receptor
GTP	Guanosine 3'-triphosphate
HCG	Human chorionic gonadotropin
HDR	Homology directed repair
Indel	insertion or deletion
INL	Inner nuclear layer
IRD	Inherited retinal dystrophies
IS	Inner segment

IVF	In vitro fertilization
KO	Knock-out
NHEJ	Non-homologous end joining
NMD	Nonsense-mediated decay
OCT	Optical coherence tomography
ONL	Outer nuclear layer
OS	Outer segment
PAM	Promoter-adjacent motif
PCR	Polymerase chain reaction
PDE	Phosphodiesterase
RD	Retinal degeneration
RdCVF	Rod-derived cone viability factor
RNA	Ribonucleic acid
RNP	Ribonucleoprotein
ROS	Reactive oxygen species
RP	Retinitis pigmentosa
<i>S. pyogenes</i>	<i>Streptococcus pyogenes</i>
sgRNA	single-guide RNA
ssDNA	Single-stranded DNA
WGA	Wheat germ agglutinin
WT	Wildtype
<i>X. laevis</i>	<i>Xenopus laevis</i>

ACKNOWLEDGMENTS

I would like to sincerely thank my research supervisor, Dr. Orson Moritz, for his valuable guidance throughout my thesis project. I am truly grateful for his continuous support despite the challenges of the global pandemic and for accommodating uncertainties with patience, knowledge and understanding. His genuine scientific curiosity and genius has certainly been a source of motivation and inspiration for me throughout my project as well as my personal life. I truly could not have asked for a better supervisor.

I would also like to express my gratitude to my committee member, Dr. Cheryl Gregory-Evans, for her insightful suggestions and guidance. I have admired her scientific work since before I started my graduate studies, and it was a pleasure for me to have her on my committee.

I would like to thank my amazing lab members, without whom this thesis project would not have been possible. I learned several laboratory techniques from Beatrice Tam, and I am very appreciative of her thorough and knowledgeable guidance throughout my project. Her detail-oriented and hard work is an inspiration, and any student would be lucky to have her as a teacher. I thank Aaron Loewen for his help since the first day I joined the lab and for sharing his knowledge in the most effective way. I thank Dr. Brittany Carr for her valuable advice, training me in conducting ERG recordings, teaching me to communicate scientific data more effectively and passing on her knowledge and experience. I thank Ross Scharbach for his valuable assistance in experiment set ups, teaching me his skills and for being a great colleague to work with in every way. I thank Colette Chiu for training me in different laboratory techniques and sharing her extensive knowledge and experience. It has been a great pleasure to work with each and every one of them and I feel grateful to have been a part of the frog squad.

Lastly, special thanks to my parents and my sister for always being there for me and supporting me in every possible way, regardless of the adventure I embark on. I am forever grateful to them.

1. INTRODUCTION

1.1 The eye

1.1.1 The retina

The retina is a central nervous tissue lining the inner back of the eye comprised of five main classes of neurons including photoreceptors, bipolar cells, amacrine cells, horizontal cells and ganglion cells¹. In vertebrate retinas, the cell bodies from these neurons are found the inner nuclear layer (INL), outer nuclear layer (ONL) and ganglion cell layers (GCL), while the synapses are located in the inner plexiform and outer plexiform layers². More specifically, photoreceptor cell bodies are in the ONL; bipolar, horizontal and amacrine cell bodies are in the INL and ganglion cell bodies are in the GCL³. The multilayered neuroretina detects the incoming light signal and relays the signal to the brain via electrical signals for image interpretation⁴. Photoreceptors are the class of cells responsible for detecting incoming light. Horizontal and amacrine cells are interneurons that regulate and integrate the signals from multiple photoreceptors and are responsible for lateral interactions within the retina before transmitting signals to the ganglion cells¹. The signal is then relayed to the lateral geniculate nucleus of the thalamus via a bundle of ganglion cell axons, called the optic nerve, before ultimately reaching the visual cortex of the brain for visual perception processing⁵.

1.1.2 Rod and cone photoreceptors

Photoreceptors are mainly involved in absorbing light photons and converting them into electrical signals in a process referred to as phototransduction⁶. Photoreceptors are classified into two broad groups of rods and cones based on their structural and functional differences. The rod-shaped

photoreceptors of the retina are highly light-sensitive at a level that they can detect single photons of light with a peak absorption of ~500nm. Cones are much less sensitive and rather respond to visible light from ~350 to 560nm⁷. Generally, dim-light and peripheral vision are mostly dependent on rods while cones are responsible for bright-light and high acuity color vision⁸.

Structurally, photoreceptors cells consist of an outer segment (OS), a connecting cilium, an inner segment (IS), cell body and a synaptic terminal⁹. The OS is the main distinguishing feature between the structure of cone and rod photoreceptors. Rod OS are elongated with densely packed discs of rhodopsin photopigment that are individually enclosed by a separate membrane. In contrast, cones tend to have shorter OS with a series of open discs that are not separately enclosed and are continuously connected to the cilium¹⁰. The connecting cilium links the OS to the IS where cell organelles including the nucleus, mitochondria, endoplasmic reticulum (ER) and the Golgi complex are contained¹¹.

1.1.3 Phototransduction and rhodopsin

Rhodopsin is a 7-transmembrane G-protein-coupled receptor (GPCR) and is known to function as a light sensor in rod photoreceptors. Rhodopsin is comprised of the rod opsin protein and the 11-*cis*-retinal chromophore ligand¹². The key involvement of rhodopsin in the phototransduction process begins with light-induced isomerization of its 11-*cis*-retinal chromophore into all-*trans* retinal (Figure 1-1). The change in conformation of the opsin protein subsequently activates the transducin G-protein, leading to the dissociation of its alpha subunit from the beta and gamma subunits. The alpha subunit bound to GTP further stimulates the activity of phosphodiesterase (PDE), which in turn hydrolyzes the conversion of cGMP into GMP. The cGMP bound to Na⁺ channels maintains their opening and the inflow of Na⁺ ions to depolarize the photoreceptors.

When the concentration of cGMP is lowered due to its conversion to GMP, Na⁺ ion channels begin to close which leads to hyperpolarization of photoreceptors. The resulting hyperpolarization then causes voltage-gated calcium channels to close, lowering Ca⁺ ion levels which causes a decrease in glutamate neurotransmitter release¹³.

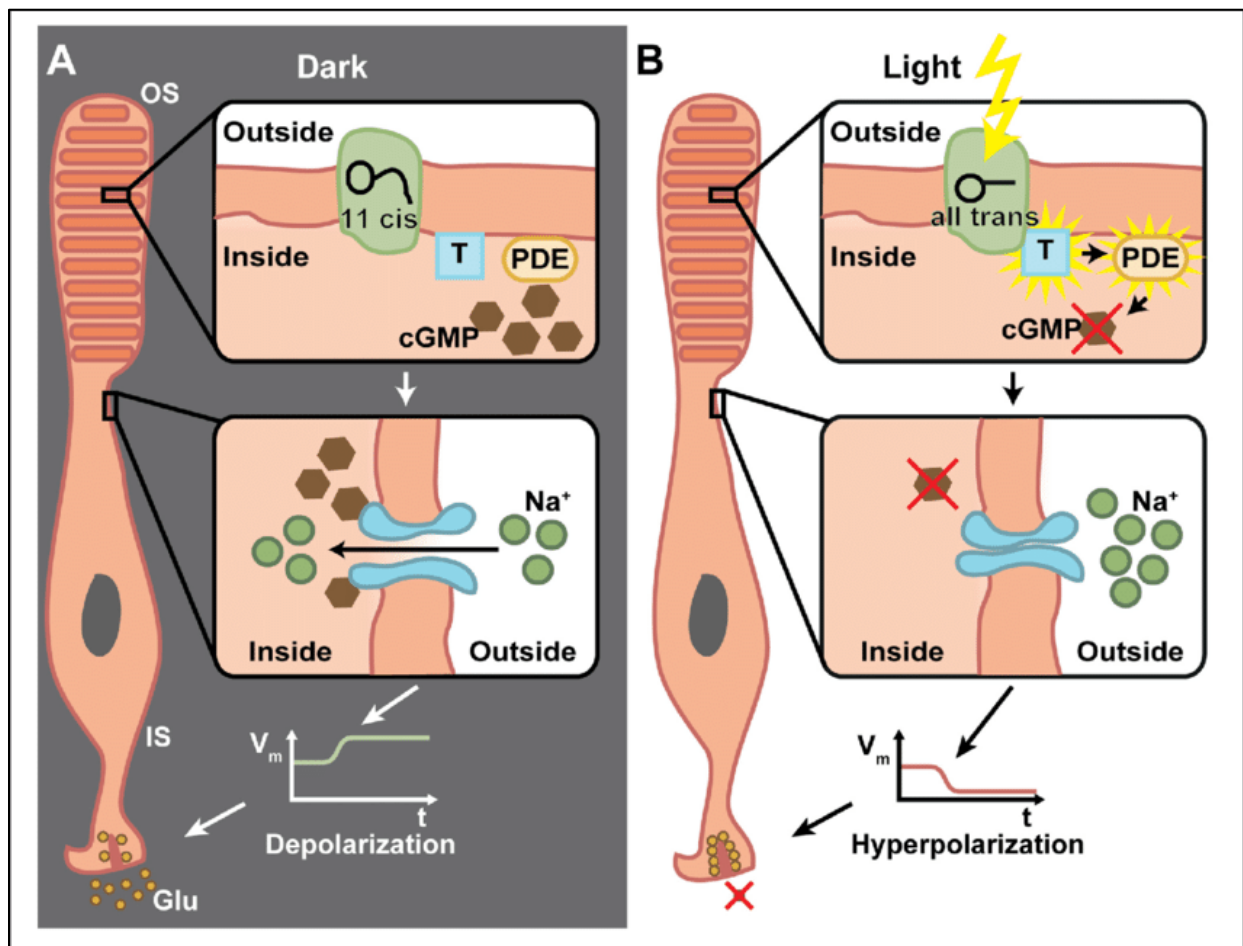


Figure 1-1. The phototransduction pathway in photoreceptors. (A) In the absence of light, the 11-*cis* retinal chromophore remains bound to rhodopsin while the transducin G-protein (T) and PDE are inactive. This allows cGMP to maintain Na⁺ channels open in the IS of photoreceptors. The inflow of Na⁺ ions depolarize the membrane potential and induce glutamate neurotransmitter release. (B) In the presence of light, rhodopsin's 11-*cis* retinal chromophore converts to all-*trans* retinal, which in turn activates the transducin. Transducin subsequently activates PDE, an enzyme that degrades cGMP and converts it to GMP. The resulting decline in cGMP concentration leads to the closure of Na⁺ channels and hyperpolarization of the membrane potential. Ultimately, glutamate neurotransmitter release comes to a halt (Figure acquired from Klapper et al. 2016¹⁴).

Rhodopsin is synthesized and folded in the ER of rod cell IS, traverses the Golgi apparatus, and is transported to rod OS via the connecting cilium. It is then stored in densely packed stacks of membranous disks in the OS⁷. More than 85% of the OS protein content is comprised of rhodopsin in a highly concentrated manner¹⁵. Following its synthesis in the IS, the N-terminus of rhodopsin is glycosylated at two asparagine residues (N2 and N15) and trafficked to the OS. Previous research has illustrated that mutations that prevent glycosylation at these residues cause light-dependent retinal degeneration¹⁶. In other words, photoactivation of non-glycosylated rhodopsin exacerbates retinal degeneration.

1.1.4 Genetic diseases of the retina

Inherited retinal dystrophies (IRDs) are a heterogeneous group of conditions caused by genetic mutations that result in vision loss. The majority of IRDs are progressive conditions that worsen over time and often lead to complete blindness. IRDs are further categorized into syndromic and non-syndromic diseases⁴. Syndromic IRDs are less prevalent and are associated with extra-ocular phenotypes. Yet, more than 80 different forms of syndromic IRDs have been described¹⁷. Alternatively, non-syndromic IRDs are isolated to the retina and are classified according to the cell types and specific regions that they affect. Conditions that uniquely affect the macula are referred to as macular dystrophies¹⁸. In contrast, diseases that affect the entire retina are categorized based on the order that photoreceptors begin to degenerate. Rod-cone dystrophies refer to conditions in which rods start to degenerate first and the loss of rods progressively results in the loss of cones (Figure 1-2). Cone-rod dystrophies on the other hand affect only cones, or both rods

and cones simultaneously¹⁹. Retinitis pigmentosa (RP) is the most prevalent type of IRD and is categorized as a non-syndromic, progressive rod-cone dystrophy⁴.

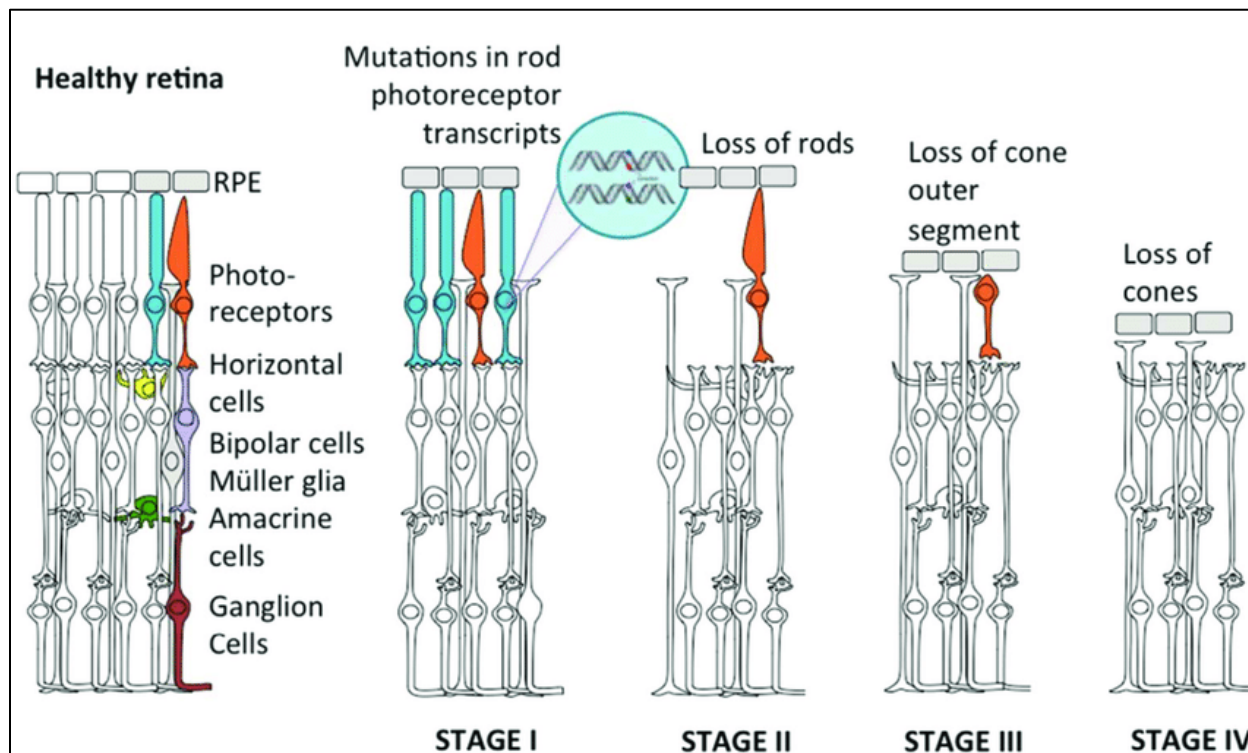


Figure 1-2. Rod-cone dystrophy and the progressive pattern of disease. The five main classes of retinal cells are illustrated in a healthy retina. Progression of disease is shown starting with mutations in rod photoreceptors which lead to the loss of rods in the outer segment, ultimately resulting in the loss of cones. Rods are shown in blue and cone are shown in red (Figure acquired from Dalkara et al. 2016¹³⁸).

The mechanism through which the loss of rods leads to the loss of cones is not yet fully understood. However, there are several theories that attempt to explain the secondary loss of cones in rod-cone dystrophies such as RP. A review by Narayan *et al.* described five prevailing theories²⁰. One theory is that the trophic factors that are produced by rods are required for the growth of developing cones. Hence, loss of rods and their inability to provide the necessary trophic factors impede the maturation of cones. The importance of such trophic factors has further been elucidated in models

where supplementing trophic factors delayed or prevented cone death²¹. Rod-derived cone viability factor (RdCVF) is a trophic factor produced by rods that is found to be involved in cone photoreceptor's cellular metabolism. Therefore, another theory suggests that secondary death of cones occurs due to nutrient deficiency following the loss of RdCVF through disruption of the insulin/mTOR pathway that leads to the activation of autophagy²². Oxidative stress as a result of imbalance in reactive oxygen species (ROS) has also been suggested as a potential cause of cell death. With the primary loss of rods, the amount of oxygen consumption in the outer retina begins to decrease while the supply of oxygen by the choroidal vessels remains unchanged²³. Subsequently, increased ROS levels overwhelms the antioxidant defense system of cones which leads to cell damage. Another theory involves microglial activation in response to the death of rods that can lead to neuro-destructive effects, similar to many neurodegenerative diseases in the CNS²⁴. Activated microglia release various pro-inflammatory cytokines such as tumor necrosis factor-alpha (TNF- α) and nitric oxide synthase-2 (NOS-2) at the site of disease²⁵. TNF- α can further induce apoptotic pathways²⁶ and NOS-2 results in oxidative stress and caspase activation²⁷, both leading to cell death. Some have also suggested that dying rods release toxic substances into the extracellular space between photoreceptors that lead to cone death²⁸. Viringipurampeer *et al.* have identified one of these substances to be adenosine triphosphate (ATP), an increase in extracellular concentration of which triggers the activation of inflammasomes and cell death²⁹. More recently, a sixth theory has been introduced by Samardzija *et al.*, highlighting the role of epigenetics in the secondary loss of cones³⁰. They have shown that excessive histone deacetylase (HDAC) activity is associated with the loss of cones, and that pharmacological inhibition of HDAC was highly effective in prolonging cone degeneration in mouse models³¹. Although a single overarching explanation has not yet been proposed to describe the underlying mechanism for rod-cone

dystrophies, a combination of the events described above appear to be key contributing factors in the process.

1.2 Retinitis Pigmentosa

Retinitis pigmentosa (RP) is a vision-threatening disorder that is characterized by loss of functional and viable photoreceptors as well as retinal degeneration (RD)³². According to Fighting Blindness Canada, 1 in 3500-4500 Canadians are affected by RP, making it one of the most common inherited diseases of the retina³³. RP is a rod-cone dystrophy, in which initial symptoms of night-blindness associated with the rods progress into secondary cone death, resulting in the loss of day-light peripheral vision, and may ultimately lead to complete blindness³⁴.

RP symptoms typically begin to develop in childhood and are detected when children struggle to get around in the dark or their visual field becomes restricted, a phenomenon referred to as tunnel vision³⁴. However, given the heterogeneity in the underlying mutations and the diversity in pathomechanisms, disease progression is highly variable and in some cases RP patients retain their vision until later in adulthood. That being said, the vast majority of cases ultimately lead to significant loss of sight.

There are several ways for an ophthalmologist to diagnose a patient with RP. Primarily, viewing the patients' retina using an ophthalmoscope may allow for the detection of potential dark pigment deposits. Visual field testing is also another tool to assess the extent of potential peripheral vision loss. Additionally, an electroretinogram (ERG) can be used to measure the electrical activity of photoreceptor cells. In RP patients, the signal from rod photoreceptors is primarily diminished due to the loss of rods³². Lastly, genetic testing can be elucidating in the expected progression of a patient's particular genetic mutation as well as the mode of inheritance to their offspring. Different

subtypes of RP can be inherited through autosomal recessive, autosomal dominant as well as X-linked inheritance, depending on the underlying mutation³⁵.

Although most cases of RP are monogenic, thousands of different mutations have been identified that underlie this blinding disease. The genetic heterogeneity of RP has made treatment development quite complex, leaving it untreatable for more than a million affected individuals worldwide³⁶. In 30-40% of cases, RP is inherited as an autosomal-dominant trait, labeled as autosomal dominant RP (adRP)³⁶. Notably, 25% of adRP cases stem from mutations in the rhodopsin gene (*RHO*), making *RHO* mutations the most common cause of adRP. To date, more than 150 distinct missense/nonsense *RHO* mutations have been identified to be associated with adRP⁷.

1.2.1 *Xenopus laevis* as a genetic model for RP

Historically, *Xenopus laevis* (*X. laevis*), has commonly been used as a model organism in developmental biology. This vertebrate model, also known as the African clawed frog, has also been utilized to model human genetic diseases including the diseases of the retina. There are unique features associated with *X. laevis* that make this animal a valuable and practical model to better understand and develop treatments for human conditions. Primarily, whole genome sequencing of *X. laevis* has uncovered extensive similarity to the human genome with at least 1700 orthologs of human disease genes³⁷. Secondly, the retina of *X. laevis* has the same layered structure and cell types as the human retina. Thirdly, relatively larger oocytes and fertilized *X. laevis* embryos are able to tolerate extensive manipulation and injection of nucleic acids and proteins, allowing for relatively easy genetic manipulation, and the development of highly specific models and treatment approaches³⁸. Additionally, significantly shorter experimental timeframes can be expected as the

F0 animals can be studied as opposed to F1 offspring³⁹. In the case of F1 animals, the large numbers of offspring allow experiments with high “n” values⁴⁰.

RP has been modeled in a number of different animals. The similarities in disease progression and resulting phenotypes compared to humans have allowed for a better understanding of this blinding disease. RP animal models can be categorized into two broad groups: 1. Animals with naturally occurring mutations and 2. Transgenic animals with foreign genes or mutations inserted into their genome⁴¹. Natural mutations detected in canines, cats, and chickens have made these animals valuable models to represent the real disease. Studying specific mutations that mimic the process in RP, however, has been made possible with the generation of transgenic animals. The available transgenic models for RP include but are not limited to mice, rats, frogs, zebrafish and pigs⁴².

In studying the retina specifically, one unique advantage of *X. laevis* is the relatively large size of rods, which allows for better resolution under light or confocal microscopy, electrophysiological recordings and detecting histology-related phenotypes. In addition, *X. laevis* retina contains both rod and cone photoreceptors, with rods comprising 53% of all photoreceptors⁴³. Similar to humans, photoreceptors synapse with horizontal and bipolar cells to transmit signals within the retina⁴⁴.

One challenge associated with the use of *X. laevis* as a genetic model for human disease is the fact that they are allotetraploids, as opposed to diploid humans. *X. laevis*, with a chromosome number $2n=36$, consists of two sub-genomes labelled as L (long chromosomes) and S (short chromosomes)⁴⁵. The genome duplication is believed to have resulted from an interspecific hybridization of diploid progenitors $2n=18$ ⁴⁶. In case of rhodopsin, there are three distinct genes identified to encode rhodopsin on *X. laevis*'s chromosome-4 labelled as *Rho.L*, *Rho.S* and *Rho.2.L*⁴⁷.

1.3 Gene editing

1.3.1 Gene therapy

There are currently no known cures for adRP. Additionally, developing treatment for this blinding disease is highly challenging as the underlying mutation, age of onset, disease progression and type of cellular dysfunction are vastly heterogenous across diagnosed patients⁴. Therefore, a single treatment will not be applicable to all adRP patients. However, considering the advancements in our ability to identify specific underlying mutations in the patient population and the monogenic root of disease in many instances, gene-based therapies appear to be the main candidates for treatment development.

The unique characteristics of the retina have made this tissue an ideal environment to develop gene-based therapies⁴⁸. These features include the following: 1) the retina is a highly accessible tissue for surgical procedures as well as imaging, 2) small amounts of therapeutic products can be administered in a localized fashion to the subretinal area without affecting the surrounding tissues and 3) the retina is immune-privileged due to the presence of the blood-retinal-barrier (BRB) and its isolation from systemic blood circulation⁴⁹. Given the concerns surrounding the use of adeno-associated viral (AAVs) vectors as means to administer gene-editing drugs, the isolation of the retina from the systemic circulation has instigated a lot of interest for the use of AAV-driven gene-editing therapies³⁶.

Within the identified dominant mutations in RP, there are three main disease-causing mechanisms that each require a specific therapeutic approach accordingly: 1. Loss-of-function mutations 2. Dominant-negative mutations 3. Gain-of-function mutations⁵⁰ (Figure 1-3).

Loss-of-function mutations result in a non-functional gene and only cause disease if the other copy of the gene is not sufficient to assure WT phenotype (i.e. haploinsufficiency). This type of mutation is less prevalent amongst adRP mutations and are more commonly present in autosomal recessive forms of IRDs. The *PRPF31* gene is one example of a haploinsufficient gene encoding pre-mRNA splicing factor that if mutated, can lead to adRP⁵¹. In such cases where higher levels of protein are required, gene supplementation through AAV vectors allows for the adequate restoration of phenotype⁵².

Dominant-negative mutations result in mutant proteins that disrupt the activity of the WT protein. This type of mutation has been characterized to eliminate one or more functions of the rhodopsin protein, resulting in dominant RP⁵³. For instance, if the mutant form of rhodopsin GPCR maintains its ability to dimerize with the WT during the phototransduction process in the rod OS, the mutant may interfere with the function of the WT protein⁵⁴. In diseases caused by dominant-negative mutations, addition of the WT form can outcompete the mutant and diminish its effects. Hence, the resulting RD will be less severe as the ratio of the mutant to WT becomes smaller⁵⁰.

Gain-of-function refers to mutations that alter protein function and can lead to novel activity toxic to the cell. This type of mutation is the most common in the *RHO* gene⁵⁵. Considering the high levels of rhodopsin expression in photoreceptors, the mutant forms may lead to detrimental effects including toxic aggregation, dysregulated activation, structural instability and disrupted trafficking⁵⁶. In gain-of-function mutations, unlike dominant-negative mutations, changing the concentration of the WT protein does not affect the severity of RD. This is mainly because the mutant is often performing a new toxic function regardless of the concentration of the WT protein. Various treatment strategies are currently being explored for gain-of-function mutations in adRP.

Cideciyan *et al.* have identified a short hairpin RNA (shRNA) that effectively targets human *RHO*, silencing gene expression through RNA interference (RNAi)⁵⁷. By supplying the resistant form of the human *RHO* simultaneously, they were able to prevent RD progression in a canine model for *RHO*-adRP⁵⁷. Other therapeutic approaches have been proposed to utilize CRISPR/Cas9 gene editing for the ablation or correction of the mutated allele at the DNA level. Diakatou *et al.* have used CRISPR-induced non-homologous end-joining (NHEJ) to specifically knockout mutant alleles in induced pluripotent stem cells (iPSCs) from an adRP patient⁵⁸. Alternatively, both mutated and WT alleles can be targeted and inactivated using CRISPR/Cas9, if supplying an exogenous gene copy is possible⁵⁹. Lastly, correction of the mutant allele utilizing CRISPR/Cas9 followed by the homology-directed recombination (HDR) repair mechanism has also been proposed as a way to correct mutations at a DNA level^{4,60}.

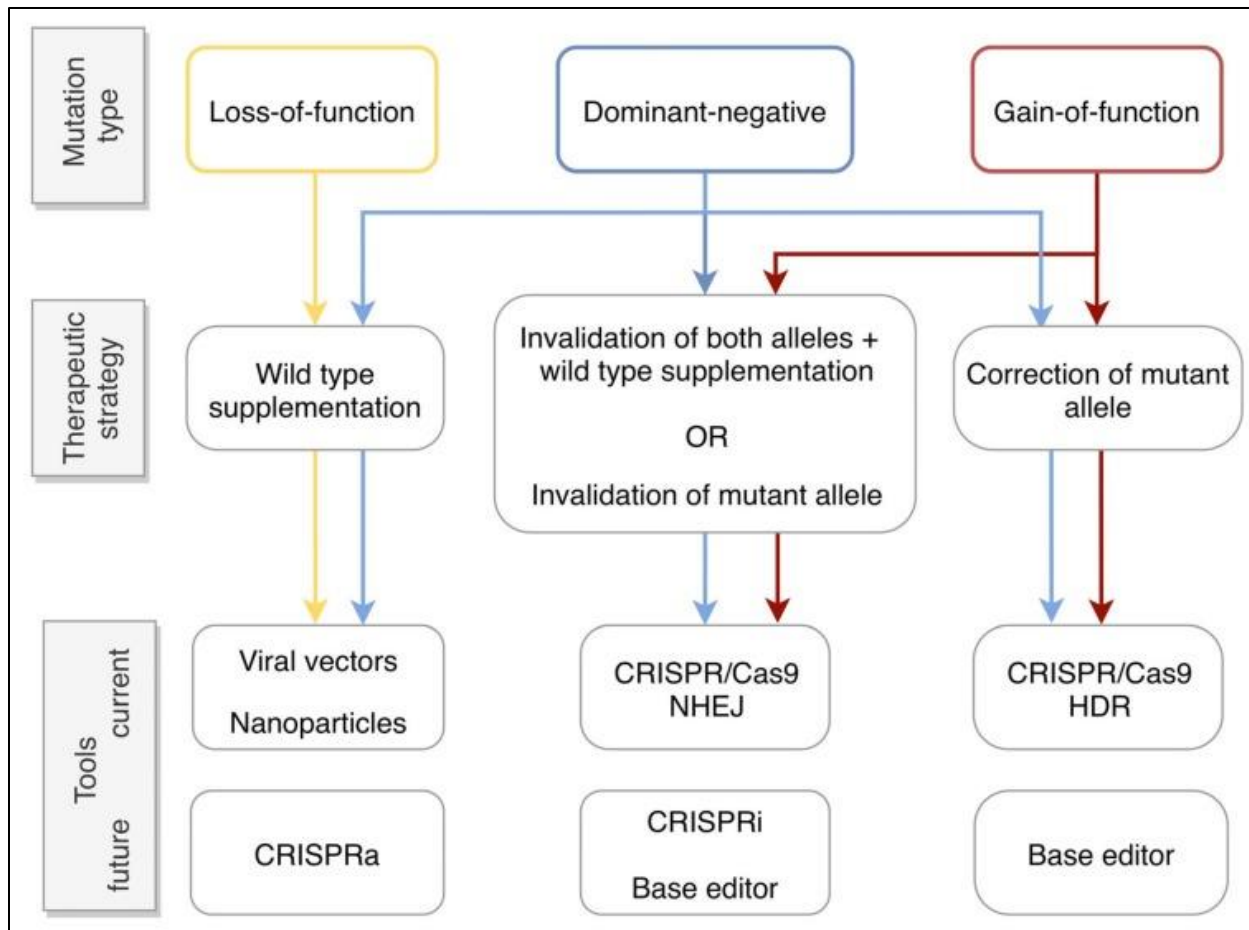


Figure 1-3. Flow chart summarizing dominant mutation types and corresponding therapeutic approaches. (Figure adapted from Diakatou *et al.*, 2019⁴).

1.3.1 CRISPR/Cas9

CRISPR/Cas9 is a two-component gene editing system that allows for a diverse range of genetic modifications⁶¹. CRISPR (Clustered Regularly Interspaced Short Palindromic Repeat) is an RNA-mediated protective mechanism against invading nucleic acids found in bacteria⁶². The naturally occurring CRISPR system in bacteria is a form of adaptive immune system functioning as a genomic memory for invading pathogens⁶³. Using this highly specific system, bacteria are able to scan invading DNA sequences and introduce destructive double strand DNA breaks through

guided endonucleases⁶³. Various types and classes of CRISPR with differing components have been identified so far, from which the Type II CRISPR/Cas9 system has been most commonly used and optimized in experimental settings⁶⁴. This is mainly because the type II CRISPR system is able to bind and edit target DNAs, requiring only one protein. Relying on the simplicity of the Type II CRISPR/Cas9 and utilizing the Cas9 (Crispr-associated protein 9) system derived from *Streptococcus pyogenes*, CRISPR/Cas9 was first used by Jinek *et al.* in 2012 to introduce double strand breaks (DSBs) in targeted DNA sequences⁶². The CRISPR/Cas9 complex is made up of a DNA-cleaving enzyme called Cas9 and an RNA molecule that is used as a guide for Cas9 to a specific target site in the genome, referred to as single guide RNA (sgRNA)⁶². An sgRNA recognizes a unique ~20 nucleotides target sequence on the foreign DNA⁶⁵. Guided to the location of interest by an sgRNA, Cas9 introduces DSBs 3bp upstream from the PAM site (promoter-adjacent motif site: e.g. NGG from *S. pyogenes*). In terms of its delivery, different approaches have been taken to inject the CRISPR/Cas9 components into individual cells including: 1. Plasmid encoding the Cas9 protein and the sgRNA in the same vector, 2. mRNA encoding Cas9 with sgRNA and 3. Cas9 protein with sgRNA (Figure 1-4)⁶⁶. The plasmid-based delivery is the simplest strategy where a single component is being introduced to the cell and it is more stable than combining Cas9 mRNA with sgRNA⁶⁷. However, plasmid-based CRISPR has been found to lead to more off-target effects⁶⁸. Additionally, more time is required for efficient editing with this strategy, because the plasmid needs to be translated into Cas9 protein after the injection⁶⁶. Delivering Cas9-encoding mRNA with the sgRNA allows for faster editing, following the formation of the Cas9/sgRNA complex inside the cell, and has been reported to result in fewer off-target effects⁶⁹. However, mRNA instability is a key limiting factor in this type of delivery⁷⁰. Lastly, in the strategy with Cas9 protein and sgRNAs, purified positively charged Cas9 protein is

combined with the sgRNA prior to delivery. The resulting complex is referred to as a ribonucleoprotein (RNP)⁶⁴. Direct delivery of RNPs provides high editing efficiency, reduced off-target effects and lower toxicity and immune responses⁷¹.

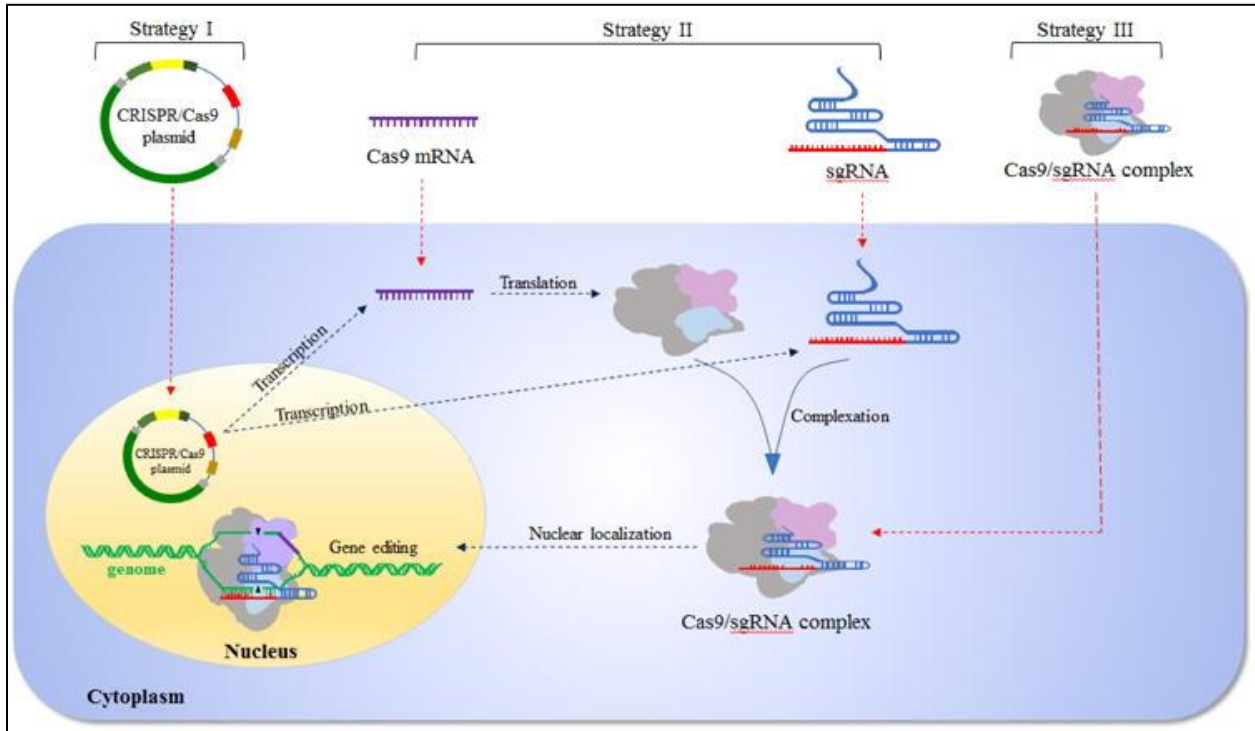


Figure 1-4. Different gene editing strategies using CRISPR/Cas9. Strategy (I) uses a plasmid DNA encoding the Cas9 protein and sgRNA. Strategy (II) uses Cas9 mRNA in combination with the sgRNA. Strategy (III) utilizes a Cas9 protein in a complex with sgRNA (Figure adapted from Liu *et al.*⁶⁶).

When the CRISPR/Cas9 system is employed in vertebrate cells, the introduced cleavage in the DNA sequence most prominently leads to the initiation of either NHEJ or HDR repair pathways⁷² (Figure 1-5). These crucial repair mechanisms have evolved to preserve genomic integrity following DNA damage. NHEJ is an error-prone response that promotes direct ligation of DNA sequences at the DSB site⁷³. In doing so, insertions and deletions (indels) of short DNA sequences are likely to occur. Indels that result in frameshift mutations instigate nonsense-mediated decay

(NMD), a surveillance pathway present in all eukaryotic cells that reduces error in gene expression by omitting mRNA transcripts with premature stop codons⁷⁴. Hence, in case of a frameshift mutation, NMD may lead to a loss-of-function mutation and generate knockout (KO) phenotype. Alternatively, indels can create in-frame mutations that cause gain-of-function phenotypes or protein instability and loss of function. Although NHEJ is thought to be favoured in the G1 stage of the cell cycle, it appears to be active throughout the entire cell cycle⁷³.

Alternatively, the HDR pathway utilizes a homologous DNA sequence as a template for repairing the broken ends at the DSB site⁷⁵. Therefore, HDR appears to be more prevalent following DNA replication in S and G2 phases of the cell cycle where it is able to use the intact sister chromatid as a homologous template sequence⁷⁶. For this reason, HDR is believed to be a high-fidelity mechanism compared to the NHEJ but with a much lower incidence rate. Combining the HDR repair mechanism with the CRISPR/Cas9 system has been shown to be a valuable genome editing tool⁷⁷. In experimental settings, the homologous template sequence can be artificially provided through specifically designed donor sequences of interest. Hence, accurate gene knock-ins, gene replacement, point mutations and conditional gene knockout gene editing strategies can be carried out utilizing the HDR pathway⁷⁸.

The designed exogenous HDR repair templates typically consist of an insert designed to be recombined at the Cas9 cleavage site, with homology arm lengths of varying sizes extending from both ends. Several studies have been conducted to improve the incidence of the HDR repair mechanism and to exploit its remarkable ability in genome editing by optimizing the HDR template. Circular and linear double-stranded DNA molecules as well as single-stranded oligonucleotides of different lengths have been used as repair templates⁷⁹. Single-stranded

oligonucleotides have been found to be more efficient in activating the HDR mechanism, while causing the lowest levels of toxicity^{80,81}. Additionally, the length of the homology arms has been explored as another potential contributing factor. HDR efficiency has been shown to increase significantly with increasing lengths of the homology arms, although longer oligonucleotides appeared to cause toxicity and reduced efficiency⁸². Therefore, homology arm lengths need to be optimized for maximal efficiency. Generally, 30-80 nucleotides long homology arms have been found to be optimal in different experimental models with varying sizes of inserts⁸³⁻⁸⁵.

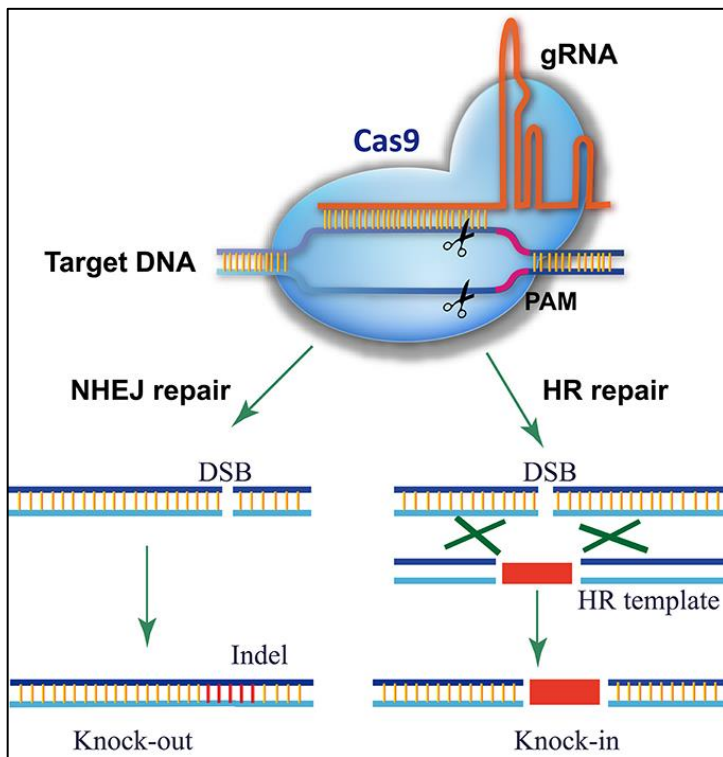


Figure 1-5. CRISPR-Cas9 and sgRNA genome editing strategy and the following repair mechanisms of NHEJ and HDR. Uniquely designed guide RNA (gRNA) directs the Cas9 cleaving enzyme to a specific target site, where it introduces DSBs 3 bases upstream from the PAM sequence. The introduced DSB on the target DNA then activates the NHEJ (non-homologous end joining) or the HR (homologous recombination) repair mechanisms. The error prone NHEJ pathway results in the introduction of insertions and deletions (indels) at the cleavage site, potentially leading to a knockout due to a premature stop codon. The HR pathway requires a template (HR template) with homology arms that allow for an insert (shown in red) knock-in at the DSB site (Figure adapted from Ding *et al.* 2016⁸⁶).

1.4 Electrophysiology, Fundus Imaging and Optical Coherence Tomography

There are several robust tools available to ophthalmologists and research scientists to assess the functional and structural state of the retina. These tools not only allow for clinicians to diagnose and monitor disease progression but are also reliable measures for changes in visual function and structural health of retinal tissue in animal models. For the purposes of this dissertation, I will briefly introduce three of the commonly used tools that were also used in my experiments.

The electroretinogram (ERG) is a non-invasive tool that measures the electrical activity of various cells within the retina in response to light signals⁸⁷. A typical ERG response consists of negatively deflected a-wave which corresponds to photoreceptor response, followed by a positively deflected b-wave that is believed to be associated with the inner retinal cells⁸⁸. Since the 1940s, ERGs have been used in the clinics to diagnose diverse retinal disease including RP⁸⁹. Given that RP is known to directly affect photoreceptor function, almost all symptomatic RP patients have significant measurable changes in their ERG recordings. Additionally, the function of cones and rods can be distinguished by light adaptation and dark adaptation of subjects, respectively. Photopic ERG refers to the measurement of cone-mediated retinal signal in response to bright flashes of light following light adaptation⁹⁰. Conversely, scotopic ERG is a method through which the unique signals of rods in response to low levels of white or blue light is measured in dark-adapted subjects⁹¹. In RP patients where rods begin to degenerate first, rod photoreceptor signals noticeably reduce in young adulthood. As the disease progresses however, decreased levels of signal from both rods and cones become detectable in ERG measurements.

Fundus photography is another widely used imaging technique that allows for a two-dimensional demonstration of the retinal tissue⁹². Appearance of pigment deposits, attenuation of the blood

vessels and a waxy optic disk pallor are some of the key features of progressed disease in fundus images from RP patients⁹³.

Lastly, optical coherence tomography (OCT) is an imaging technique that takes cross-section pictures of the retina⁹⁴. OCT allows us to distinguish the layers of the retina and measure their thickness, a non-invasive and informative approach that is widely used in the clinical setting. Previous studies have illustrated differences in thickness measurements and retinal nerve fiber layer atrophies detected by OCT in RP patients⁹⁵.

2. MODELING A HYBRID HUMAN/MOUSE RHODOPSIN TRANSGENE IN *XENOPUS LAEVIS*

2.1 Introduction

Although more than 100 different mutations in the *RHO* gene have been identified to underly adRP, the pathways that lead to retinal degeneration remain largely unknown. A major obstacle in understanding the underlying pathways stems from the heterogeneity of RP pathomechanisms and the lack of mutation-specific models that can be easily manipulated. Transgenic *X. laevis* has shown to be an effective model system for RP where large numbers of offspring can be generated, and disease symptoms and phenotypes can be distinguished in short time frames⁹⁶.

Many RP-inducing rhodopsin mutations are located in *RHO*'s N-terminus and disrupt proper glycosylation of this protein. T4K, T17M and P23H are prominent instances of such mutations that are known to cause sector RP, a condition in which retinal degeneration is disproportionately higher in inferior retina^{16,39}. One explanation for asymmetric RD in human patients with sector RP is the greater light exposure of inferior retina, especially in N15S, T17M and T4K mutations⁹⁷. Previous research has explored this possibility and illustrated that these mutations cause light-exacerbated RD in transgenic animals. They demonstrated that inactive glycosylation-deficient rhodopsin alone does not induce significant RD; rather the detrimental effects are aggravated by photoactivation⁹⁸. Tam *et al.* illustrated that elimination of chromophore-binding site or chromophore precursor vitamin A through dietary deprivation reduced the toxic effects of T4K and T17M mutations⁹⁸. Hence, light activation is necessary for cell death in these mutants. Similar outcomes have also been previously observed in mice with T17M mutation⁹⁹ and dogs with T4R mutation¹⁰⁰.

In contrast, P23H rhodopsin is associated with a different cell death mechanism distinct from that of T4K and T17M. Reported as the most prevalent mutation underlying adRP in North America, P23H rhodopsin is one of the most studied RP mutations¹⁰¹. Tam *et al.* demonstrated that preventing chromophore binding and dietary deprivation of vitamin A in transgenic animals carrying P23H rhodopsin mutation further exacerbates RD, even in the absence of light¹⁰². They suggest that chromophore acts as a “pharmacological chaperone” for P23H rhodopsin by illustrating that in its absence, mutant rhodopsin begins to accumulate in the ER. Similarly, when exposed to light, 11-*cis* retinal is depleted as a result of photoisomerization, leading to ER stress and subsequent cell death¹⁰².

2.1.1 Objectives and hypothesis

Unlike other studied mutations, T4K-induced RD has been found to be particularly associated with photoactivation of mutant rhodopsin, making it an important pathomechanism to explore. Our long-term goal is to generate humanized knock-in mice, carrying a human/mouse hybrid T4K mutated *RHO* gene, as a model of RP for the purpose of developing translational gene-editing therapeutics and investigating the underlying mechanisms of cell death. In these Crispr-Humanized Minimally Mouse Models (CHuMMMs; term coined by Dr. Elizabeth Simpson), the first exon of the mouse rhodopsin gene and its immediate surrounding sequence will be substituted by the equivalent human gene, containing the T4K adRP-causing mutation (methods described by Miura *et al.*¹⁰³).

To ensure that the hybrid gene design does not alter the mechanism of RD, we aimed to generate transgenic *X. laevis* carrying human/mouse hybrid T4K *RHO* and to characterize the light-exacerbated RD phenotype in comparison to human/mouse hybrid WT (ChiWT), human T4K and

mouse T4K *RHO* models in transgenic *X. laevis*. The human/mouse hybrid T4K *RHO X. laevis* (ChiT4K) is identical to the proposed CHuMMMS mouse model as it expresses the mouse gene for rhodopsin, with its first exon replaced by the T4K mutated human exon 1 *RHO*. The human T4K (hT4K) and mouse T4K *RHO* (MT4K) models carry the human and mouse T4K mutated *RHO* exon 1, respectively. We hypothesized that the ChiT4K transgenic model will express the light-exacerbated RD phenotype indistinguishable from human T4K rhodopsin, making it a robust model for understanding the underlying mechanism of this unique phenotype using mammalian transgenes. Additionally, if generated successfully, this hybrid model can further elucidate the viability of our proposed humanized knock-in mouse as a novel mammalian model for T4K mutation-induced light-exacerbated RD.

2.2 Methods

Transgenes were designed wherein expression of the human/mouse hybrid T4K, human/mouse hybrid WT, and mouse T4K *RHO* cDNAs were driven by 0.8 Kb of the *X. laevis* opsin promoter. The human T4K (hT4K) animals used were generated from mating adult animals with the hT4K transgene that were already available in our laboratory.

2.2.1 Construct design

Oligonucleotide-directed mutagenesis was utilized to introduce the T4K mutation of interest in our construct design. Oligonucleotide sequences were selected in a region starting 19-20 bp upstream from the mutation site in the 5' direction and continuing for 25-29 bp in the 3' direction downstream from the mutation site (starting and ending on G/C). The T_M was kept within a range

of 3°C for both strands while keeping the length of the oligonucleotides at or below 50 bp. The designed forward and reverse oligonucleotides were then purchased from Integrated DNA Technologies (IDT) to be generated.

2.2.2 Gibson assembly, transformation and miniprep

The XOP0.8-eGFP-N1 plasmid was used as a vector for each insert of interest to generate the *X. laevis RHO* transgene construct. eGFP was excised out from the plasmid using restriction digests at the *EcoRI* and *NotI* sites and the linearized DNA was treated with Calf Intestinal Phosphatase (CIP) to catalyze the dephosphorylation of 5' and 3' ends. The restriction digest products were then run on a 1% agarose gel and gel-purified to generate the vector backbone. Gibson Assembly¹⁰⁴ was then performed to replace the eGFP cDNA sequence of the vector with the 1. Mouse *RHO* exon 1 carrying the T4K mutation (MT4K), 2. Human-mouse *RHO* sequence combining human *RHO* exon 1 with mouse *RHO* exons 2-5 (ChiWT) or 3. Human-mouse *RHO* carrying the T4K mutation (ChiT4K). Both human and mouse T4K *RHO* constructs were created via a PCR mutagenesis protocol, previously described by Tam and Moritz¹⁶.

The products were then transformed into competent *E. coli* cells on LB agar plates with Kanamycin. Two to three colonies were selected and grown in liquid culture. Following the overnight liquid culture, miniprep protocol was carried out followed by nanodrop measurement to quantify the final DNA concentration. The products were then verified via Sanger sequencing to confirm the insertion of the mutation of interest without introduction of other undesired changes. Prior to injection of embryos, the plasmids were linearized with *FseI* (New England Biolabs - NEB) digest and then purified utilizing the QIAquick Gel Extraction Kit (Qiagen) for integration into sperm nuclei.

2.2.3 Transgenesis and animal rearing

Primary transgenic *X. laevis* were generated and reared based on methods described by Tam *et al.*¹⁰⁵. For each experiment, the designed linearized plasmids were incubated with permeabilized sperm preparation. Treated with *X. laevis* egg extract and restriction enzyme, the mixture was injected into unfertilized eggs from three different adult female frogs. Female frogs were previously primed with human chorionic gonadotropin (HCG) subcutaneous injections 48 hours and 9 hours prior to microinjections. Normally fertilized and developed embryos were then selected and housed in 4 L tanks in 18°C incubator. The dark-reared groups were placed in complete darkness and the light-reared groups were exposed to a 12 h light cycle with an average light intensity of 1700 lux. During the initial 4-5 days post-fertilization (dpf), embryos were exposed to 20 µg/ml G418 in order to eliminate non-transgenic tadpoles. Once the transgenic tadpoles began to swim, they were fed ground frog brittle (Nasco). At 14dpf, normally developed tadpoles at developmental stage 48 were sacrificed by pithing. The left eye was dissected and solubilized in 100 µl of a 1:1 mixture of PBS and SDS-PAGE loading buffer containing 1mM EDTA and 100 µg/ml PMSF, while the contralateral eye was fixed in 4% paraformaldehyde buffered with 0.1 M sodium phosphate pH 7.4.

2.2.4 Dot blot assay

Dot blot assay was performed in accordance to the methods described by Tam *et al.*¹⁰⁵. The solubilized eye from each tadpole was diluted 1:300 in 20 mM NaPO₄ buffer pH 7.4 and drawn by suction through Immobilon P membrane. As controls, each dot blot also contained 100% *X. laevis* rhodopsin extracted from WT tadpole retinas as well as 100% human WT rhodopsin from transfected cultured cells. Primary antibodies mAb B630N¹⁰⁶ (at 1:10 dilution of tissue culture

supernatant) and mAb 1D4¹⁰⁷ (at 1:750 dilution of 1 mg/ml solution) were used to probe the duplicate dot blots on separate membranes. The mAb B630N antibody binds to both endogenous *X. laevis* and human rhodopsin while mAb 1D4 only recognizes human rhodopsin and not *X. laevis* rhodopsin. IR-dye800-conjugated goat anti-mouse was then used as secondary antibody at 1:10000 of 1 mg/ml solution (LI-COR Biosciences). Following antibody probing, LI-COR Odyssey imaging system was utilized to image and quantify rhodopsin levels on each blot. In order to determine the relative levels of total and transgenic rhodopsin, antibody affinity was compared between test and control samples.

2.2.5 Immunohistochemical labeling and confocal microscopy

The right eye from each tadpole, which was placed in fixative after being sacrificed at 14dpf, was then sucrose infiltrated in a 20% sucrose solution within 48 hours. Sucrose infiltrated eyes were embedded in OCT (Sakura Finetek) and stored at -80°C. Embedded eyes were sectioned in 12µm slices and labelled overnight with mAb 2B2¹⁰⁷ (at 1:10 cell culture supernatant), a primary antibody which specifically recognizes the N-terminus mammalian rhodopsin. Secondary antibody labelling was done with Cy3-conjugated anti-mouse antibody (1:750 dilution, Jackson Immunoresearch), AlexaFluor 488-conjugated wheat germ agglutinin (WGA; Life Technologies) and Hoechst 33342 (Sigma-Aldrich). MOWIOL 4-88 reagent (EMD Millipore) was used to mount the labelled sections prior to imaging. The Zeiss (Oberkochen, Germany) 510 laser scanning confocal microscope was used for imaging with 10X and 40X objectives and the Zen software. Adobe Photoshop (Adobe Systems, San Jose, Ca) was used for post-imaging processing. To improve image detail, non-linear adjustments were performed in Hoechst 33342 and WGA

labeling channels. Rhodopsin antibody labeling was only linearly adjusted where necessary for better visualization.

2.2.6 Statistical analyses

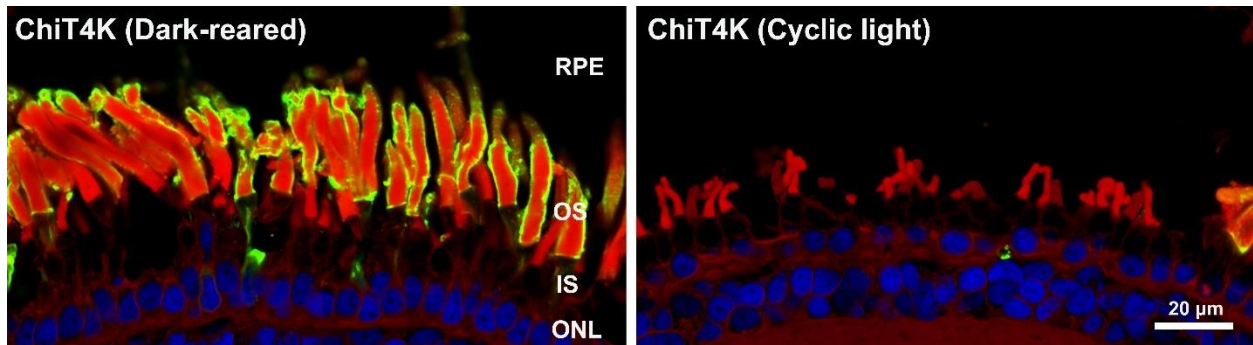
GraphPad Prism software (version 9.0.0, San Diego, California, USA) was used to perform statistical analyses and to generate figures. The Mann-Whitney U test was used to compare levels of rhodopsin quantified from dot blot assays. This non-parametric test allows us to assess the likelihood of two samples being derived from the same or differing populations¹⁰⁸. When comparing more than two groups, the Kruskal-Wallis one-way analysis of variance was used instead¹⁰⁹. P-values smaller than 0.05 were deemed statistically significant.

2.3 Results

2.3.1 Human/mouse hybrid T4K rhodopsin – dark-reared vs. cyclic light

ChiT4k refers to transgenic tadpoles expressing mouse *RHO* with sequence derived from its first exon replaced with sequence derived from human exon 1 carrying the T4K mutation. G418-selected transgenic animals were raised to 14 days in dark-reared (n=44) and cyclic light conditions (n=35). Total amount of rod opsin protein expressed, determined by the dot blot assay, was significantly lower in the cyclic light group (Figure 2-1, B; dark-reared (n=44), cyclic light (n=35); p=0.0003 by Mann-Whitney U test). Additionally, immunolabelled sections demonstrated severe light-exacerbated RD in cyclic light, while dark-rearing prevented T4K mutation-induced RD (Figure 2-1, A). Hence, ChiT4K transgenic animals displayed a light-exacerbated RD phenotype similar to that obtained with human T4K rhodopsin transgene.

A.



B.

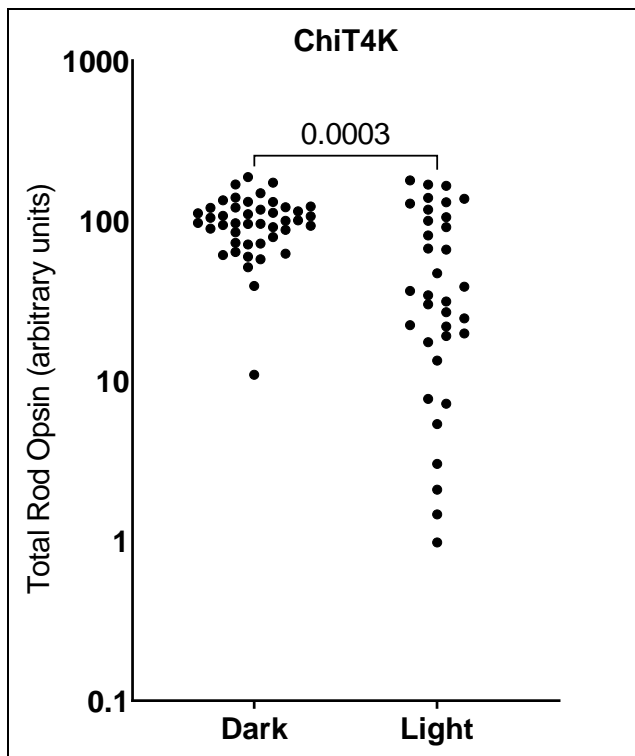
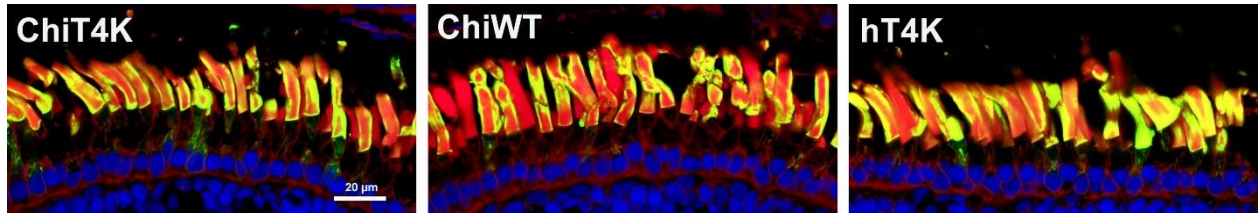


Figure 2-1. ChiT4K transgenic animals raised in the dark compared to cyclic light. (A) Significant RD was observed in animals raised in cyclic light. Photoreceptors were protected in animals raised in complete darkness. Green=2b2 (mammalian rod opsin); red=WGA; blue=Hoechst dye. **(B)** Transgenic rod opsin levels assayed by dot blotting and probing with 1D4 antibody. Rhodopsin levels are compared between the two groups on a log-scale (dark-reared (n=44), cyclic light (n=35); p=0.0003 by Mann-Whitney U test).

2.3.2 ChiWT, ChiT4K and hT4K – dark-reared

In order to verify whether the human/mouse hybrid construct alone can introduce any detrimental effects, a follow-up experiment was designed to compare the phenotypes of transgenic ChiWT (WT human/mouse hybrid rhodopsin; n=19), transgenic ChiT4k (T4K human/mouse hybrid rhodopsin; n=20) and hT4K (human T4K rhodopsin from mating; n=22). All three groups were raised for 14 days in the dark. As expected, dark rearing demonstrated protective effects against RD and similar phenotypes were observed in all three groups. No significant difference in rhodopsin levels were observed between dark-reared ChiT4K, ChiWT and hT4K animals (Figure 2-2, B; ChiT4K (n=20), ChiWT (n=19), hT4K (n=22); Kruskal-Wallis test) and RD was prevented in all groups (Figure 2-2, A). Next to the evidence gathered from the initial experiment, these results suggest that the ChiT4K construct can be a reliable model for T4K-induced light-exacerbated RD.

A.



B.

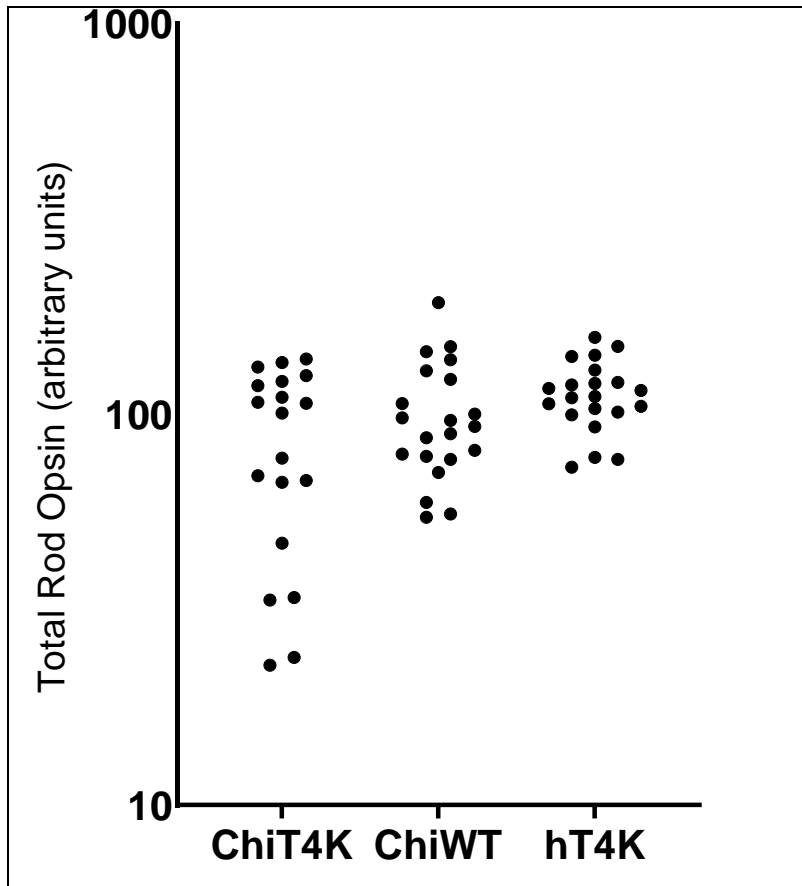
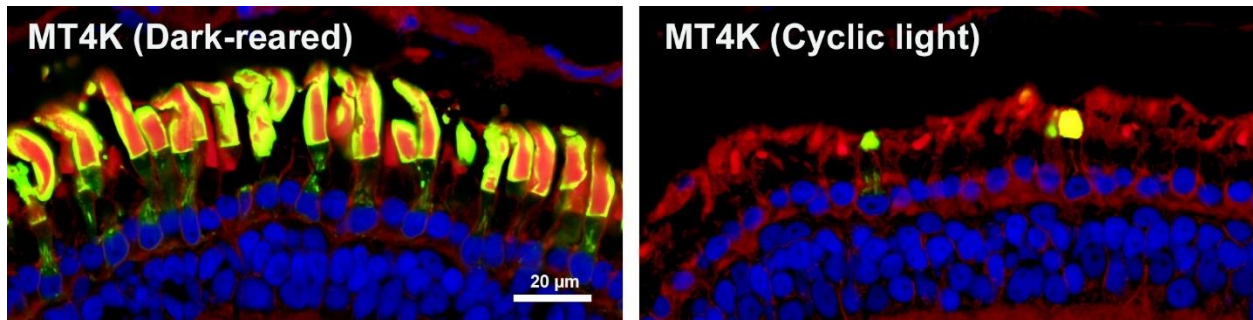


Figure 2-2. ChiT4K, ChiWT and hT4K transgenic animals raised in the dark. (A) RD was prevented in all animals protected from light, regardless of their transgene. Green=2b2 (mammalian rod opsin); red=WGA; blue=Hoechst dye. (B) Transgenic rod opsin levels assayed by dot blotting and probing with 1D4 antibody. Rhodopsin levels are compared between groups on a log-scale (ChiT4K (n=20), ChiWT (n=19), hT4K (n=22); no statistical difference was detected between groups with Kruskal-Wallis test).

2.3.3 Mouse T4K rhodopsin – dark-reared vs. cyclic light

Lastly, the light-exacerbated RD phenotype was tested in *X. laevis* tadpoles expressing the mouse T4K rhodopsin (MT4K) transgene. Transgenic MT4K rhodopsin animals were raised for 14 days, half of them under the cyclic light condition and the other half in complete darkness. The light-exacerbated RD phenotype observed in hT4K and ChiT4k animals was similarly detected in the MT4K rhodopsin animals. As illustrated by the dot blot assay, animals raised in cyclic light had significantly lower levels of rod opsin compared to dark-reared tadpoles (Figure 2-3, B; dark-reared (n=14), cyclic light (n=18); $p=0.0223$ by Mann-Whitney U test). Severe RD was observed in transgenic MT4K rhodopsin tadpoles raised in cyclic light, while RD was prevented in dark-reared animals (Figure 2-3, A).

A.



B.

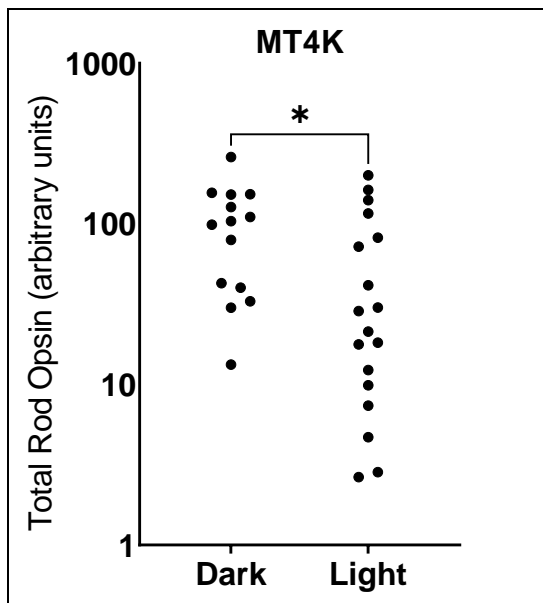


Figure 2-3. MT4K transgenic animals raised in the dark compared to cyclic light. (A) Significant RD was observed in animals raised in cyclic light. Photoreceptors were protected in animals raised in complete darkness. Green=2b2 (mammalian rod opsin); red=WGA; blue=Hoechst dye. (B) Transgenic rod opsin levels assayed by dot blotting and probing with 1D4 antibody. Rhodopsin levels are compared between the two groups on a log-scale (dark-reared (n=14), cyclic light (n=18); p=0.0223 by Mann-Whitney U test).

3. CRISPR-BASED TREATMENT STRATEGIES FOR SELECTIVE EDITING OF MUTANT RHODOPSIN

3.1 Introduction

In autosomal dominant diseases, the mutant allele either acquires a new toxic function (gain of function mechanism) or disrupts the functioning of the remaining endogenous WT allele (dominant negative mechanism). One treatment strategy for autosomal dominant diseases is to develop allele-specific therapeutics that knockout the mutant allele, leaving the endogenous WT allele unaffected (as shown in Figure 3-1)¹¹⁰. A previous study in rhodopsin knockout mice has shown that mice with a single copy of the rhodopsin gene do not develop retinal degeneration¹¹¹. Although these heterozygous knockout mice had half the normal complement of rhodopsin and their photoreceptor OS were shorter compared to WT controls, a single copy of the gene appeared to be haplo-sufficient¹¹¹. Furthermore, previous studies have explored the haplo-sufficiency of the rhodopsin gene by investigating families of patients with null rhodopsin mutations with autosomal recessive RP. These studies have reported that heterozygous carrier parents of individuals with autosomal recessive RP do not develop retinal degeneration and appear to have WT phenotype with slightly reduced rod sensitivity^{112,113}. Therefore, phenotypes associated with single null alleles are significantly milder than the phenotypes associated with dominant RP alleles, making the allele-specific therapeutics that knockout the mutant allele viable treatment options for adRP. Other potential solutions are to restore the mutant allele into WT or replace the mutant with an exogenous copy. In this chapter, I will introduce and characterize a previously developed adRP *X. laevis* model from our research group. I will then explore three different CRISPR-based gene-editing strategies to prevent RD in our adRP model. We hope that the comparison in precision and

efficiency of these therapeutic approaches can be informative for developing similar treatments in human patients suffering from adRP.

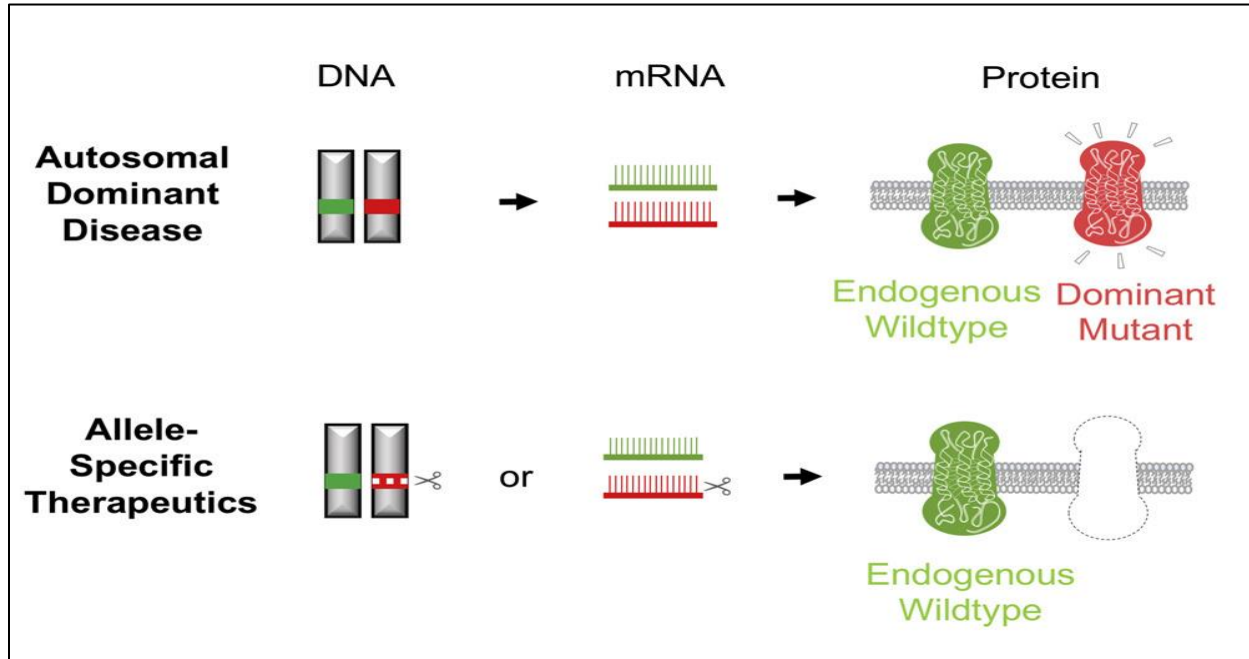


Figure 3-1. Allele-specific gene therapeutic strategy for autosomal dominant diseases. In autosomal dominant diseases where the dominant mutant allele disrupts the function of the endogenous wildtype allele, allele-specific therapeutics can be designed to knockout the mutant allele without affecting the wildtype. Therefore, allowing the endogenous wildtype allele to lead to wildtype phenotype (Modified from Meng *et al.*, 2020)¹¹⁰.

3.1.1 Genetically modified model for adRP (12bp deletion)

The Moritz lab has previously generated multiple functional KO in the F0 generation of various genes critical to photoreceptor function, utilizing CRISPR/Cas9-mediated editing strategies in *X. laevis*¹¹⁴. Feehan *et al.* designed an sgRNA (labelled as Rhosg3) that in combination with the Cas9 protein selectively edits the *X. laevis Rho.L* gene, immediately downstream from the start codon⁴⁹. Indels induced by the NHEJ repair mechanism following the Rhosg3 edit led to a desirable model with a 12bp deletion in the first exon of the *Rho.L* gene. The resulting animals (referred to as

‘12bp-deletion’) appear to be a useful model for adRP, as extensive RD is observed in heterozygous animals with this mutation.

3.1.2 Objectives and hypotheses

Utilizing the previously developed 12bp-deletion *X. laevis* model for adRP, we aimed to develop and compare CRISPR-based gene-therapeutic approaches to prevent the detrimental effects of this mutation by inactivating the malfunctioning gene. This model can be considered analogous to a hypothetical adRP patient with a mutation in the first exon of *RHO* undergoing gene editing therapy under idealized circumstances. Three different gene therapeutic approaches were explored in this dissertation:

1. The first approach was to design a highly specific sgRNA that is able to introduce DSBs immediately downstream from the start codon of the *Rho.L* gene’s exon 1, where the 12bp deletion occurs (Figure 3-2). By designing a guide that only edits the sequence with the 12bp deletion, the WT allele in heterozygous animals as well as the other rhodopsin genes of the *X. laevis* (*Rho.S* and *Rho.2.L*) remain unaffected. Furthermore, introducing a DSB at the beginning of the first exon will activate the error prone NHEJ repair mechanism that will subsequently lead to indels within the coding sequence. The introduced indels are likely to cause an out-of-frame mutation in 2/3 of cases where the edit has occurred, while in 1/3 of cases an in-frame mutation is expected. Given that the following several start codons are out-of-frame, we expect the out-of-frame mutations in 2/3 of the cases to knockout the mutated allele. Considering that heterozygous loss of function alleles in rhodopsin have no RD phenotype in humans¹¹² or *X. laevis*¹¹⁵, knocking out the mutated allele should be curative in 2/3 of the photoreceptors. However, in 1/3 cases the in-frame

indels should result in neutral or aggravating phenotypes that can be problematic for an ideal treatment strategy. Therefore, we hypothesized that the sgRNA treatment of the 12bp deletion sequence will significantly reduce RD, though the treatment will only improve phenotypes in 2/3 of the photoreceptors on average, and treated animals will remain phenotypically inferior to WT.

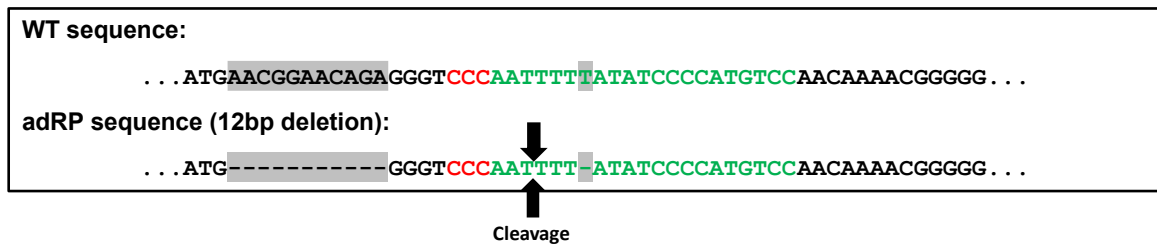


Figure 3-2. sgRNA designed to target the mutant allele, leaving the WT allele unaffected due to a single base discrepancy. The top sequence illustrates the first bases of exon-I of the WT *Rho.L X. laevis* gene. The bottom sequence demonstrates the 12 (11+1) bases deleted in our adRP model immediately downstream from the start codon (highlighted in grey). The 20 bases-long sgRNA target sequence unique to the mutant is shown in green, with only a single base difference compared to the WT sequence. The PAM sequence is shown in green with the cleavage site indicated 3 bases upstream from the PAM site.

2. To tackle the challenge described in the first objective above, a novel second approach was designed. This approach involved generation of two simultaneous DSBs on both sides of the first exon's start codon, one in the non-conserved upstream promoter regulatory region and the other within the first exon. By introducing simultaneous edits upstream and downstream from the start codon, we aimed to remove a piece of DNA containing the *Rho.L* start codon. Given that the following several start codons are out-of-frame, assuming 100% editing, eliminating the first start codon will lead to a loss-of-function allele and

removal of the misfolded protein. In order to examine the efficacy of this therapeutic approach, highly specific sgRNAs were designed to target only the defective *Rho.L* gene, similar to the first objective. Additionally, a second unique target site was identified in the upstream promoter regulatory region of the *Rho.L* gene. Despite the fact that the sgRNA editing the promoter region would introduce DSBs in both the WT and mutated alleles of the *Rho.L* gene, we expected the edit in the non-conserved promoter regulatory region of the WT allele to be innocuous in the majority of cases. Assuming efficient simultaneous editing, we hypothesized that removing the start codon of the mutated allele will lead to the desirable KO and prevents RD in 12bp deletion animals, with a potentially superior efficacy to approach 1 above.

3. The third proposed treatment approach aimed to utilize the HDR repair mechanism as opposed to the NHEJ. As explained previously (section 1.3.1), the HDR pathway requires a homologous template sequence for repairing the broken ends at the DSB site allowing error-free repair, or the introduction of specific sequences⁷⁵. By designing a single-stranded DNA (ssDNA) identical to the WT sequence and combining it with the previously described sgRNA that targets the mutated sequence, we aimed to correct the 12bp deletion using HDR. Depending on the efficiency of the HDR mechanism in our experimental settings, we hypothesized that this treatment could completely prevent RD, comparable to WT animals.

3.2 Methods

3.2.1 Characterization of the 12bp-deletion animals

Primarily, the animals were genotypically and phenotypically characterized. This was done by performing blood draws from mature animals previously edited and by sequencing the blood genomic preparation samples to identify the animals expressing the 12bp deletion in the first exon of the *Rho.L* gene. Secondly, a mature identified 12bp deletion animal was mated with a WT and 100 fertilized embryos were raised to 14-days-old tadpoles. At 14dpf, 40 tadpoles were sacrificed, and the remaining tadpoles were raised to maturity. For each sacrificed tadpole, the left eye was solubilized to be used for dot blot analysis while the contralateral eye was fixed, cryo-sectioned, labelled and imaged by confocal microscopy.

3.2.2 Designing single-guide RNA oligonucleotides

In order to target highly specific regions within the *Rho.L* gene, sgRNAs were designed and generated as previously described by Feehan *et al.*¹¹⁵. The ZiFit online tool was utilized to identify 20bp-long sequences of oligonucleotides containing PAM sites appropriate for CRISPR experiments. A total of six candidates were found in the *Rho.L* gene, that were absent in the *Rho.2.L* and *Rho.S* rhodopsin encoding genes (highlighted in blue in Figure 3-3). Two of these target sites were selected in exon-1 of the 12bp-deletion mutated version of the *Rho.L* gene (Sg5 and Sg6), one site was found in the 5'UTR (Sg4) and 3 other unique sites were found in the upstream promoter region (Sg1, Sg2 and Sg3). The closest target site in the promoter regulatory region was at least 1200 bases upstream of the start codon due to the highly conserved regulatory region immediately preceding the start codon, as no unique target sites could be found in that

region (Appendix A). Additionally, editing the conserved promoter regulatory region seemed more likely to induce unwanted detrimental effects in gene expression.

In order to prevent off-target effects, the uniqueness of the identified target sites was verified using the Xenbase blast database search software to ensure that no other identical sites were present in the entire genome. The designed phosphorylated oligos and primers were synthesized (IDT), and ligated into linearized pDR274 (gift of Keith Joung) to generate constructs for in-vitro transcription.

TGTGGGACTTTTGAAGTGTTCAGGGAGGGGGGCGAGACAGAAGTGAACAAAAACCTCCAAAA
AACAAAGAACTACAAAAAATAAACTAAAAAACTAAAATTATTTGGGGGCAAAGTAAATTT
G**FAAAGGGTCTCTGGGAGTGG**GACTGTGACTGGCTTGTGAGGGGAGGAGGGCCAGGCTGGCAG
GTTGTGCTGTAGCCATTTGAAAGTGATCTGGGGGTAGGCTTGCACCTTTCTGGAAAAAATA
CCGGCTTTCCT**CTATTCTTGACATTTTTTCC**TATTAATAACATTGGCATCAAGCATAATTTTTA
CCGGCCA**GGCCGAACATGGTAATTAGG**GGTGTGGCCACAAAACAGGTGTGGTCAATTTTTTTT
TGCTGTGCTTTCACGCTGCAACTTTTTTATACTCTTTCTATTTCCAAAATGTTGGGAGGTATGC
GCTAGCATAGCAGTGCCTTTTTTACAACCTGTAACCTT**GGAGGTTCAAGGTGGTGGGG**GGGGGG
CAGAAGCACTACCTTCATGCTAATACTAGAAGCATTGATCTTGGGGCCTGACTGCACTGTGGG
GTTGTAGAAGGTTGTACATGCTTCCCCTCATGAATATATGGCTGTTGAATACAGGAATGAT
GTATTCCGGTCTCTCCCTATTTTTGAGTGAAGGCAGGGCACAAAATGCAAAAACAAGGTG
GATTGCACCAGTTTTTTGTACTTAAAGGGATTCATTCTGTGATGATTATGGTTGATTTTTATT
TGTAATTTACTGTTTACACTACAATATAAAATCTCATTCTGAAACGGACAAGTGTATCTTTT
TTAGTTGTAATATTGGTGTGTAGGCACCATCTCAGGTCATTTGACTGGTCATCTTCCTCAGA
AAGAGCTATTGTTCTCCTACTAAAATGTA**CTGATGTGTTGCAATGGGAC**CTGGATTTTACCAT
TGAGTGTGTTCTTAGACCTACCAGGCAGCTGTTATCTTGTGTTAGGGAGCTGTTATCTGGTTA
CCTTCCCATTGGCATGTGGTTAGGCTGCTGGGGGGGAGAGGTTATATCACTCCAACCTGCAGT
AAAGCAGTAAAGAGCAAGTACATGACTGGGGCAGCTGGGAACTGACAACATGTCTAGCCCCA
TGTCAGATTTCAAATTTAAATATAAAAAATCTGTGTCTTTTTGAAAGAGCCCTTATTTAC
CCCTGGTCCATGCCGGTGTCTCAGTTAAAAATCCACATAATTTGTGAAGTTCTAATTTAACA
CACTAAATGGTAACGAAGGGGAGAGGGAACAGAGCAAAACCCAAAAATGGCTGTCTTTGCTCC
TACAATATGGAATTATCCCTTGTAGGTCAGACCTGGATTTCTTCCGTCACTTTTAAATACACT
TTCTTCTGTGTGTTTAAACAGAGAGAGAGAGAGAGAGATTGACAGGTGTAGACTTAAATACGT
TTATGGGAAGCAATTAACACTTTGCAACCTTAGCTTGCATTACAGTGATTAATAGTGGCCTAA
ATCCTTTGTGTGCTGACGCTGGGGGTTGCAAGCTTACTCCAGGTGAGACTTTAAAAGGACCAGGG
GACAGTGGGTCACTACTGTAGAACAGCT**AGTTGGGATCAAGGCTTC**TAAGGATCCTTTGGGC
AAAAAGAAACAGAGAAGGCATTTCTTCTATCAAGAAAGGACTTGATAGAGCTGCTACCA**ATGG**
GGTCCC**AAATTTAAAT****CCCCATGTCC****AACAAAACGGGGTGGTACGAAGCCATTTCGATTACCC**
TCAGTATTACTTAGCAGAGCCATGGCAATATTTCAGCACTGGCTGCTTACATGTTCTCTGCTCATC
CTGCTGGGTTACCAATCAACTTCATGACCTTGTGTTTACCATCCAGCACAGAAGAACTCAGAA
CACCCCTAAACTACATCTCTGCTGAACCTGGTATTTGCCAATCACTTCATGGTCTGTGGGTT
CACGGTGACAATGTACACCTCAATGCACGGCTACTTCATCTTTGGCCAACTGGTTGCTACATT
GAAGGCTCTTTTGTACACTTGGTGGTAAGTT**CAACCCGGCTTTCATCACTG**ATATTGTTGCAG
CAATAAACTCTTGGAAAGCATGTCAGATCTTTGTACTCCAATCTTGCACAACCAAGTGCATGA
AATGGATTTAAAAAACTAACAAATGAAATAAATGCCTTAGCATAAGGGTGGTCTTCAATT

Sg3 target site
Sg1 target site
Sg2 target site
Sg6 target site
Sg5 target site
Sg4 target site
5' UTR
Edited exon 1

Figure 3-3. *X. laevis Rho.L* gene carrying the 12bp deletion at the start of exon 1. Highlighted in green are the PCR primers used to validate the edits via fragment analysis as well as Sanger sequencing. Highlighted in blue are the selected unique target sites for the designed guides.

3.2.3 Oligonucleotide ligation into the pDR274 and transformation

Upon resuspension and dilution of the ordered oligos from IDT to 100µM, the oligo annealing protocol was performed for the forward and reverse sequences ordered for each target site. For the annealing protocol, 1.5µl of Oligo A (100µM) and 1.5µl of Oligo B (100µM) were added to 5µl of NEBuffer3.1 and 42µl of dH₂O (Oligo A and B refer to the forward and reverse strands for each target site as designed by ZiFit). Each reaction was incubated in the thermocycler for 4 minutes at 95°C and then transferred to a 70°C water bath to prevent sudden cooling of the reaction. The

reaction was slowly cooled down to room temperature. Resulting annealed oligos were diluted in nuclease free water (1:10).

The pDR274 vector was prepared in the following manner: 3 μ g of cloned pDR274 plasmid was linearized using NEB *Bsa*I-HF restriction enzyme and then dephosphorylated with rSAP (30-minute incubation at 37°C). Linearized plasmid was then distinguished from uncut DNA on a 1% agarose gel, extracted and gel purified using the QIAEX II gel extraction kit (150). Ultimately, 20 μ l of purified linearized pDR274 was eluted. The concentration of DNA was measured and confirmed to be sufficient using Nanodrop (72 ng/ μ l).

Once the corresponding oligos were annealed together and the linearized pDR274 was prepared, ligation protocol was carried out to incorporate each oligo into the pDR274 plasmid. Each 10 μ l ligation reaction contained 1 μ l of annealed oligos, 1 μ l of linearized pDR274 template, 1 μ l of T4 DNA ligase buffer (10X) and 0.5 μ l of T4 DNA ligase. The reactions were then incubated at room temperature for 2 hours. Following the 2-hour ligation incubation period, transformation was performed into chemically competent *E. coli* cells and colonies were developed overnight. The following day, colonies were selected from each plate and grown in liquid culture overnight. Plasmid preparation was done by alkali lysis followed by Qiagen miniprep column.

3.2.4 Diagnostics to ensure proper insertion of the oligonucleotides

Once plasmid preparation was performed, diagnostics tests were carried out to ensure the proper insertion of each oligo into the plasmid vector. Primarily, restriction digest reactions were set up with *BsaI*. In the case that the insert was properly annealed, the *BsaI* digest should no longer be able to cut the plasmid containing the insert, while it would cut the control sample not containing the insert. The digested samples were then run on a 1% agarose gel for verification. One sample was selected for each designed oligo that was successfully inserted into the vector. Once confirmed, plasmid DNA was purified using the alkali lysis method followed by the Qiagen miniprep column's "purification of plasmid DNA prepared by other methods". DNA concentration was measured using Nanodrop following purification. All samples were sent for sequencing in order to verify the correctness of the inserted oligos.

3.2.5 PCR Primers

After selecting 6 target sites, 2 sets of PCR primers were also designed and ordered from IDT. PCR primers were selected in a way that they were unique to the *Rho.L* gene while encompassing all 6 selected sgRNA target sites. Since the region between the most upstream sgRNA and the most downstream one spans over 2000 base pairs, 2 sets of primers were designed and ordered to cover the entire region (Figure 3-3). The PCR primers were then tested on genomic DNA from a WT tadpole. Based on the annealing temperature of the ordered PCR oligos, PCR conditions were set and conducted. Since the initial attempt was not successful, a gradient PCR (54°C-67°C annealing temperatures) was performed after which ideal PCR conditions were identified (95°C for 2 minutes, 30 cycles of 95°C-15s, 62°C-15s, 68°C-60s and a final extension of 2 minutes at

68°C). The same PCR conditions were used for all experiments to validate the proper edits made to the genome.

3.2.6 *In-vitro* transcription of sgRNA

Once plasmids containing the inserts of interest were constructed, an *in-vitro* transcription reaction was performed to generate the sgRNAs corresponding to selected target sites. In order to perform the transcription reaction with the highest yield, the starting template must be linearized and highly purified. *Dra*I digest was used to linearize the pDR274 containing the insert of interest at a site at approximately 120 bp downstream of the T7 promoter. After a 1.5-hour digest, 1% agarose gel was used to confirm the efficient linearization of the plasmid. Once the linearization of the plasmid was ensured, DNA purification was carried out using the “Desalting and concentration DNA solutions” protocol from the QIAEX kit of Qiagen. At the final step of the purification protocol, 20µl of RNase free water was used to elute the purified linearized DNA, while using RNase free collection tubes, pipet tips and gloves in order to avoid RNase contamination into the sample for the next *in-vitro* transcription step. Lastly, Nanodrop was used to quantify the concentration of the resulting DNA. The concentration of all 6 samples were then brought to the same value by adding RNase free water in appropriate amounts. The HiScribe T7 High Yield RNA Synthesis Kit and the protocol provided for short RNA transcripts (<0.3kb) were then used to transcribe the sgRNAs *in-vitro*.

Once the sgRNAs were generated, they were treated with DNase I from NEB kit to remove the DNA template from all samples. Following the DNase treatment, the miRNeasy kit was used to purify sgRNAs from the HiScribe *in-vitro* assay. The final purified sgRNA concentration was quantified using Nanodrop and the correctness of size was confirmed via a 1% agarose gel.

3.2.7 CRISPR *in-vitro* digestion assay

The CRISPR *in-vitro* Assay is an approach to test the efficacy of designed guides *in-vitro* prior to *in-vivo* experiments. The protocol is adapted from NEB “*In vitro digestion of DNA with Cas9 Nuclease, S. pyogenes (M0386)*”. DNA templates were generated using the PCR primers that amplified the regions encompassing the target sites for six generated sgRNAs. Fragment analysis was performed using a 1% agarose gel to validate the editing efficacy of the designed sgRNAs *in-vitro*. Following these initial screening procedures, Sg5 and Sg6 unique target sites were selected within exon1 and Sg2 was chosen in the promoter regulatory region upstream from the start codon.

3.2.8 Designing a single-stranded oligonucleotide as an HDR template sequence

A 36-bases long insert was designed with 42 bases of homology arms on each end, resulting in a 120-bases long HDR template sequence. The insert begins immediately following the start codon, where the 12bp deletion occurs, and ends immediately preceding the Sg5 PAM sequence. The insert sequence is identical to the original WT sequence with two exceptions: 1. A silent mutation (CCC → CCA) was introduced to add an additional *ApoI* enzyme (NEB) restriction digest site (AAATTT) to be used as an assay for the efficiency of the HDR. 2. An M13F point mutation (ATG → TTT) was introduced to add a unique epitope distinguishable from the endogenous *X. laevis* rhodopsin. We also made sure that the Sg5 target sequence (AATTTT-ATATCCCCATGTCC) was different from the HDR template (AATTTTATATCCCCTTTTCC) to prevent Sg5 from editing the template sequence (Appendix B). The designed single-stranded oligonucleotide was then ordered from IDT with Polyacrylamide gel electrophoresis (PAGE) purification, recommended for maximum purity of full-length oligonucleotides longer than 60 bases¹¹⁶.

3.2.9 RNA microinjection

Microinjections were performed according to methods described by Feehan et al⁴⁹. Prior to conducting the experiment on our adRP animal model, the guides designed to edit the WT sequence were injected in WT embryos to test the efficacy of the designed guides. Once confirmed, a 12bp deletion adult female *X. laevis* was injected with HCG to induce ovulation prior to the experiment. In order to carry out the *in-vitro* fertilization of the female oocytes, an HCG-primed WT male *X. laevis* was sacrificed and the testes were removed. For each round of *in-vitro* fertilization, a single testis was split in half and macerated in 250 µl 0.1X MMR to release the sperm. Newly expelled oocytes from the female *X. laevis* were then covered with the extracted sperm and 0.1X MMR for a 20-minute incubation. The fertilized oocytes were dejellied in 2% cysteine pH 8 and approximately 100 embryos were arranged in a monolayer fashion inside injection plates covered with 0.4X MMR and 6% Ficoll. Previously prepared and diluted solutions of sgRNAs and GFP were then incubated with the Cas9 protein for 10 minutes at room temperature to form the Cas9/sgRNA RNPs. The solutions were then loaded into pulled glass micropipettes with a 20-25 µl bore and were attached to a Hamilton syringe pump and a micromanipulator. In order to inject 10nL of RNA per embryo, each embryo was injected for 1 second with the Hamilton pump set to deliver 36 µl/hr. Injected embryos were then transferred to an 18°C incubator for 2.5 hours, at which point they are expected to reach the 4-cell stage. Healthy embryos displaying proper cell division were selected and transferred into 0.1MMR, 6% Ficoll and 10 µg/mL gentamicin. At 36 hours post-fertilization, eGFP fluorescence screening was carried out using an epifluorescence-equipped Leica MZ16F dissecting microscope and GFP positive embryos (indicating sufficient injection) were transferred into 0.1X MMR to raise.

3.2.10 Genomic DNA extraction, fragment analysis and Sanger sequencing

Four unique PCR primer sites were also designed to specifically amplify the regions of interest and allow examination of the edits on the *Rho.L* sequence without amplifying the other rhodopsin encoding genes of *X. laevis* (highlighted in green in Figure 3-3). Genomic DNA was extracted from the tail of each sacrificed tadpole. DNA samples were PCR amplified using designed primers unique to the *Rho.L* gene to examine regions of interest. PCR products were then validated by electrophoresis on 1% agarose gel and were Sanger sequenced. Sanger sequencing allowed for distinguishing WT and 12bp-deletion animals in each group. Potential edits in the 12bp-deletion animals were also identified and validated through band sizes on a 1% agarose gel as well as genomic sequencing.

3.2.11 Dot blot assay, immunohistochemical labeling and confocal microscopy

Animal rearing, dot blot assay, immunohistochemical labeling and confocal microscopy were performed as described in the previous chapter (sections 2.2.4 and 2.2.5).

The dot blot probing antibodies in this chapter include: 514-18 anti-rhodopsin monoclonal antibody representing the epitope introduced by the M13F mutation in the HDR template (1:10 dilution, from cell culture supernatant, gift from Dr. P. Hargrave, University of Florida, Gainesville, FL). B630N¹⁰⁶ anti-rhodopsin monoclonal antibody representing total amount of rhodopsin (at 1:10 dilution from tissue culture supernatant, gift from W. C. Smith).

Sectioned eyes were labelled with the following primary antibodies: mAb 2B2¹⁰⁷, a primary antibody which specifically recognizes the N-terminus mammalian rhodopsin, used to detect the epitope introduced by the M13F mutation in the HDR template (at 1:10 dilution, cell culture supernatant, gift from R. S. Molday, University of British Columbia, Vancouver, British

Columbia, Canada). 11D5 antibody labeling c-terminus rhodopsin (at 1:30,000 dilution purified from ascites, gift from D. Deretic, University of New Mexico, Albuquerque, NM). B630N¹⁰⁶ anti-rhodopsin monoclonal antibody representing total amount of rhodopsin (at 1:10 dilution from tissue culture supernatant, gift from W. C. Smith).

3.2.12 Western Blotting

Western blots were carried out using solubilized eyes from 14-day old tadpoles as described previously. The protein samples (15µl/well) were electrophoresed through a 10% SDS-polyacrylamide gel and transferred to a PVDF membrane overnight. After blocking with 1% skim milk powder in PBS for 30 minutes at room temperature, the blot was cut into two pieces with identical samples. One piece of the membrane was probed with B630N antibody (at 1:15 dilution of tissue culture supernatant, labeling N-terminus rhodopsin) and the other half was probed with 11D5 (at 1:10,000 dilution purified from ascites, gift from D. Deretic, University of New Mexico, Albuquerque, NM, labeling C-terminus rhodopsin) in an overnight room-temperature incubation. After washing blots with PBS, IR-dye800-conjugated goat anti-mouse was used as secondary antibody at 1:10,000 of 1 mg/ml solution (LI-COR Biosciences). Following antibody probing, blots were imaged using LI-COR Odyssey imaging system.

3.2.13 ERG recordings

ERGs were recorded from untreated and Sg5-treated animals at 9-months of age. Prior to conducting the scotopic ERG recordings, animals were dark-adapted overnight. To maintain dark adaptation, all the following procedures were carried out in a dark room under red light illumination. Immediately prior to recordings, each animal was anesthetized in 0.1% tricaine solution in 0.1X MMR for approximately 10 minutes. Once completely unresponsive to physical

stimuli, the animal was placed on a stage mounted on a gold ECG electrode. A micromanipulator was then used to position a silver wire electrode immersed in a glass microcapillary filled with 1X MMR on the surface of the cornea. Electrodes were connected to the head stage of a Model 1800 AC amplifier (AM Systems) and the output of the amplifier was connected to the input of an Epsilon ERG unit (Diagnosys). The apparatus was then placed underneath a Ganzfeld dome. Photoreceptor responses were recorded by the Epsilon unit in response to varying intensities of blue light flashes (2.5, 25, 250, 750, 1250, 2500 cd·s/m²). The animal was exposed to each light intensity five consecutive times and the recorded responses were averaged. Following the recordings, blood samples were collected from each subject to identify their genotype (WT vs. 12bp deletion) via Sanger sequencing.

3.2.14 OCT and fundus photography

OCT and fundus imaging were conducted on 9-months old untreated animals. Each animal was anesthetized in 0.1% tricaine solution in 0.1X MMR for approximately 10 minutes. Once completely anesthetized, infrared OCT and fundus photography were performed using the mouse nosepiece with a Phoenix Micron IV system (Phoenix Research Labs, Pleasanton, CA, USA). After the imaging, blood samples were collected from each subject to identify their genotype (WT vs. 12bp deletion) via Sanger sequencing.

3.2.15 Statistical analyses

Statistical analyses were performed as described in the previous chapter (section 2.2.6) using GraphPad Prism software (version 9.0.0, San Diego, California, USA). The Mann-Whitney U test was used to compare levels of rhodopsin quantified from dot blot assays. Two-way ANOVA with

Sidak's post hoc test was used to analyze group effects, light intensity effects and interaction effects in ERG recordings.

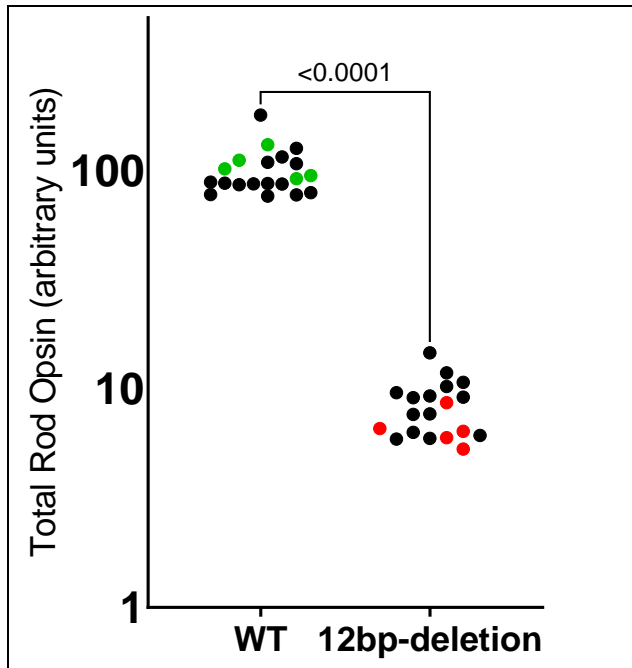
3.3 Results

3.3.1 Characterizing the animals with the 12bp deletion mutation

The 14-day old tadpoles generated from a mating between a WT and a heterozygous adult *X. laevis* carrying the 12bp deletion were characterized. Genotypically, the offspring were expected to be half WT and half heterozygous with the 12bp deletion. As anticipated, the dot blot assay illustrated a significantly lower levels of rhodopsin in 20 out of 40 of the eyes from the sacrificed tadpoles (n=20 per group; $p < 0.0001$ by Mann-Whitney U test; Figure 3-4, A). In accordance with the dot blot results, 5 subjects with high rhodopsin levels and 5 from the low rhodopsin levels were randomly selected and were sent for Sanger sequencing. The sequencing results demonstrated that all 5 animals with high rhodopsin levels were WT (highlighted in green, Figure 3-4, A) while all 5 animals with low rhodopsin levels carried the 12bp deletion (highlighted in red, Figure 3-4, A).

Immunohistochemical labelling of the contralateral eyes from the same subjects that were genetically typed further elucidated that the RD phenotype also corresponded with genotype of each sample. In WT animals, healthy retinas were observed with extended rhodopsin-expressing rods. In contrast, the 12bp deletion animals had significant RD apparent from confocal imaging with extensively disturbed and shortened rods of the retina (Figure 3-4, B).

A.



B.

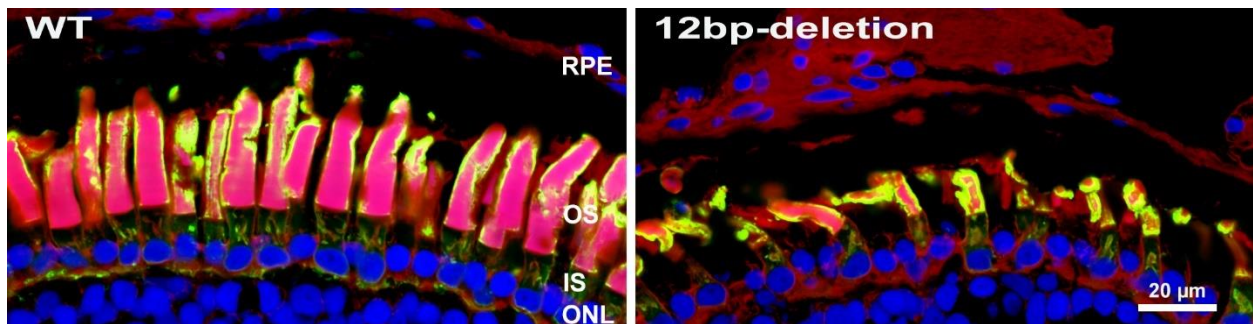


Figure 3-4. Retinal histology and rhodopsin levels in 12bp deletion animals compared to WT. (A) Total rod opsin levels assayed by dot blotting and rhodopsin labeling with B630N antibody. Rhodopsin levels are compared between the two groups on a log-scale (n=20 per group; $p<0.0001$; Mann-Whitney U test). Green=WT, red=12bp deletion, black=not sequenced (B) Significant RD was observed in 12bp deletion animals in histology sections. Green=B630N (rod opsin); red=WGA; blue=Hoechst dye.

3.3.2 *In-vitro* and *in-vivo* testing of the designed guides

***In-vitro* testing assay:** The six uniquely designed and generated sgRNAs were tested *in-vitro*. DNA templates were generated using the PCR primers that amplified the regions encompassing the target sites for six generated sgRNAs. The CRISPR *in-vitro* digestion assay is analogous to restriction digests, in that successful introduction of DSBs in DNA sequences are expected to result in different band sizes in fragment analyses. Through this assay, we were able to validate and compare the efficacy of our designed sgRNAs prior to *in-vivo* injections. As shown in Figure 3-5, we found that all six guides were able to introduce edits in the template DNA and correct band sizes were confirmed based on the location of designed guides (Refer to Figure 3-3 for the exact location of target sites and PCR primers).

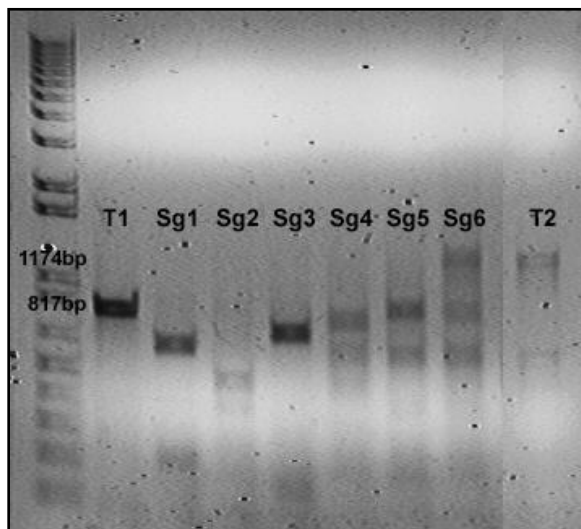


Figure 3-5. CRISPR *in-vitro* digestion assay. T1 (Template 1) refers to the 817bp-long PCR fragment amplified by primers encompassing the region containing Sg1-Sg3 target sites. T2 (Template 2) refers to the 1174bp-long PCR fragment amplified by primers encompassing the region containing Sg4-Sg6 target sites. Treatment with all 6 sgRNAs resulted in additional bands with expected sizes, validating the correctness and efficiency of the designed guide RNAs (1kb ladder, 1% agarose gel).

***In-vivo* testing assay:** The efficacy of the 4 guides that were not designed to specifically target the mutant allele were tested in WT embryos. Sg1, Sg2, Sg3 and Sg4 were designed to edit unique regions in the upstream regulatory region of the *Rho.L* gene, which are indistinguishable between the WT and 12bp deletion mutant alleles. Therefore, we were able to test these guides in WT embryos. The guides were injected in the following combinations in order to test their efficacy in introducing large deletions between the two guides: Sg1+Sg4, Sg2+Sg4, Sg3+Sg4. Performing similar fragment analysis as the *in-vitro* assay on genomic DNA extracted from these animals and comparing editing efficiencies, Sg2+Sg4 was found to be the most efficient in introducing large deletions (evidence for large deletions were observed in 7 out of 8 assayed embryos, Figure 3-6). Therefore, combining the findings of both the *in-vitro* and *in-vivo* assays, the Sg2 guide appeared to be the most effective guide to be used for the following experiments. From mutant specific sgRNAs, Sg5 and Sg6, only the *in-vitro* digestion assay was used to test their efficacy prior to injecting adRP mutant embryos.

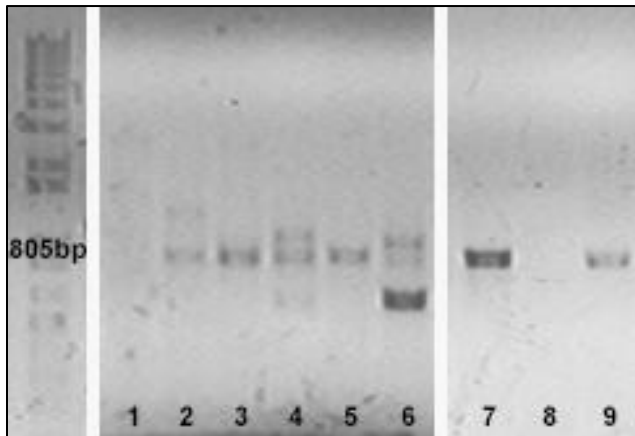


Figure 3-6. CRISPR *in-vivo* testing assay. Well 1 contained un-edited control DNA samples amplified by PCR primers that are 1971bp apart, therefore no bands were expected. Wells 2-9 contained DNA samples from embryos injected with Sg2+Sg4, where bands were expected to appear only if a 1166bp long sequence had been removed, resulting in 805bp long sequences. Evidence for large deletions was observed in 7 out of 8 assayed embryos (1kb ladder, 1% agarose gel).

3.3.3 Comparing the single-guide and double-guide CRISPR-based treatment approaches

The embryos generated from IVFs carried out between a WT male and a 12bp deletion female were separated into 5 groups:

1. The control group which remained untreated
2. Embryos injected with Sg5 alone (the first guide designed to edit the 12bp deletion sequence)
3. Embryos injected simultaneously with both Sg5 and Sg2 (the guide designed to edit the upstream promoter regulatory region of the *Rho.L* gene)
4. Embryos injected with Sg6 alone (the second guide designed to edit the 12bp deletion sequence)
5. Embryos injected simultaneously with both Sg6 and Sg2

3.3.4 Significantly higher rod opsin levels in the treated groups compared to untreated ones

The dot blot assay was utilized to compare rod opsin levels between different groups. As shown in Figure 3-7, untreated animals with the 12bp deletion (verified by Sanger sequencing) were found to have significantly lower levels of rhodopsin compared to WT animals. Single-guide treatment of the 12bp-deletion animals resulted in significantly higher levels of rod opsin compared to untreated animals. This effect was observed with both the Sg5 and Sg6 guides, targeting exon 1 of the *Rho.L* gene (untreated (n=9), Sg5-treated (n=19), $p < 0.0001$; untreated (n=11), Sg6-treated (n=11), $p = 0.0006$ by Mann-Whitney U test). However, rod opsin levels were still lower than WT animals. Combining the Sg5 and Sg6 guides with the Sg2 guide (targeting the upstream promoter)

also resulted in higher levels of rhodopsin compared to untreated 12bp-deletion group, although it was not found to be superior to the single-guide approach (untreated (n=9), Sg2+5-treated (n=10), p=0.0002; untreated (n=11), Sg2+6-treated (n=7), p=0.0028 by Mann-Whitney U test).

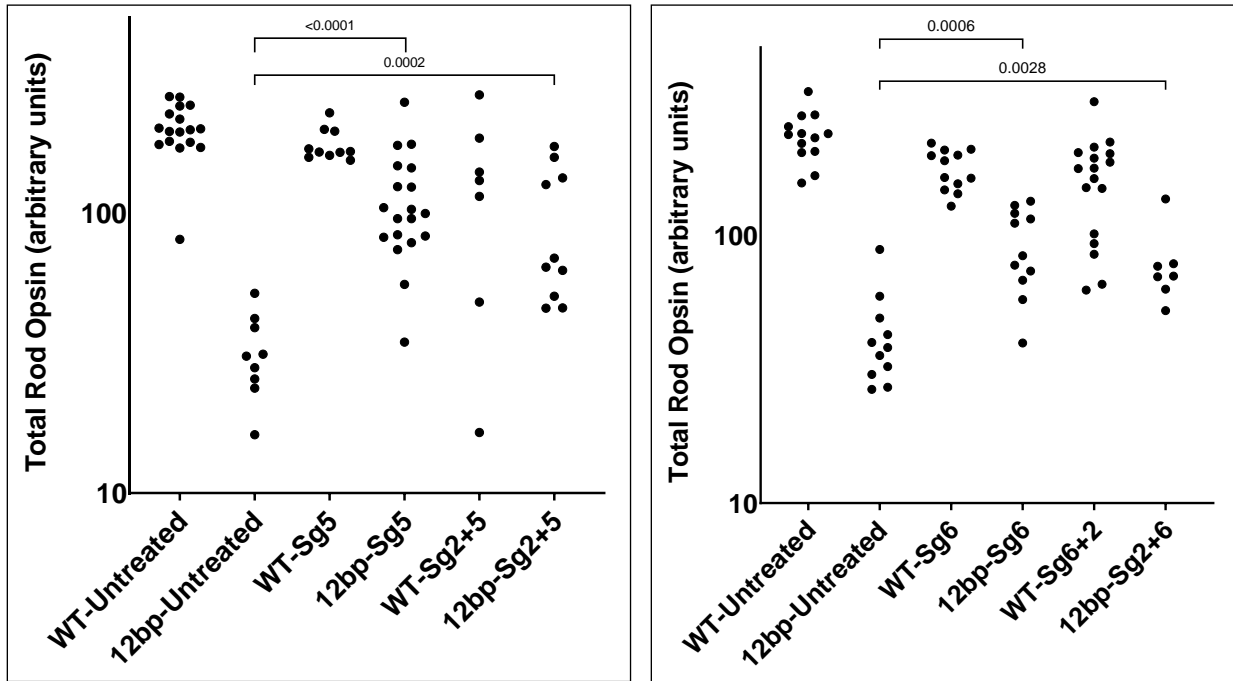


Figure 3-7. Total rod opsin levels assayed by dot blotting and rhodopsin labeling with B630N antibody. Rhodopsin levels are compared between groups on a log-scale. Left panel: WT-untreated (n=17), 12bp-untreated (n=9), WT-Sg5 (n=10), 12bp-Sg5 (n=19), WT-Sg2+5 (n=7), 12bp-Sg2+5 (n=10). Right panel: WT-untreated (n=13), 12bp-untreated (n=11), WT-Sg6 (n=12), 12bp-Sg6 (n=11), WT-Sg2+6 (n=17), 12bp-Sg2+6 (n=7). P-values were determined by Mann-Whitney U test to compare groups.

3.3.5 Retinal degeneration was prevented in 12bp-deletion animals treated with a single-guide edit in exon 1

As shown in Figure 3-8, the 12bp deletion in exon 1 of the *Rho.L* gene results in significant retinal degeneration and loss of rods. Retinal degeneration was prevented in animals treated with either the Sg5 or Sg6 guides. The single guide treatment of WT embryos with Sg5 and Sg6 also did not show to have any detrimental effects.

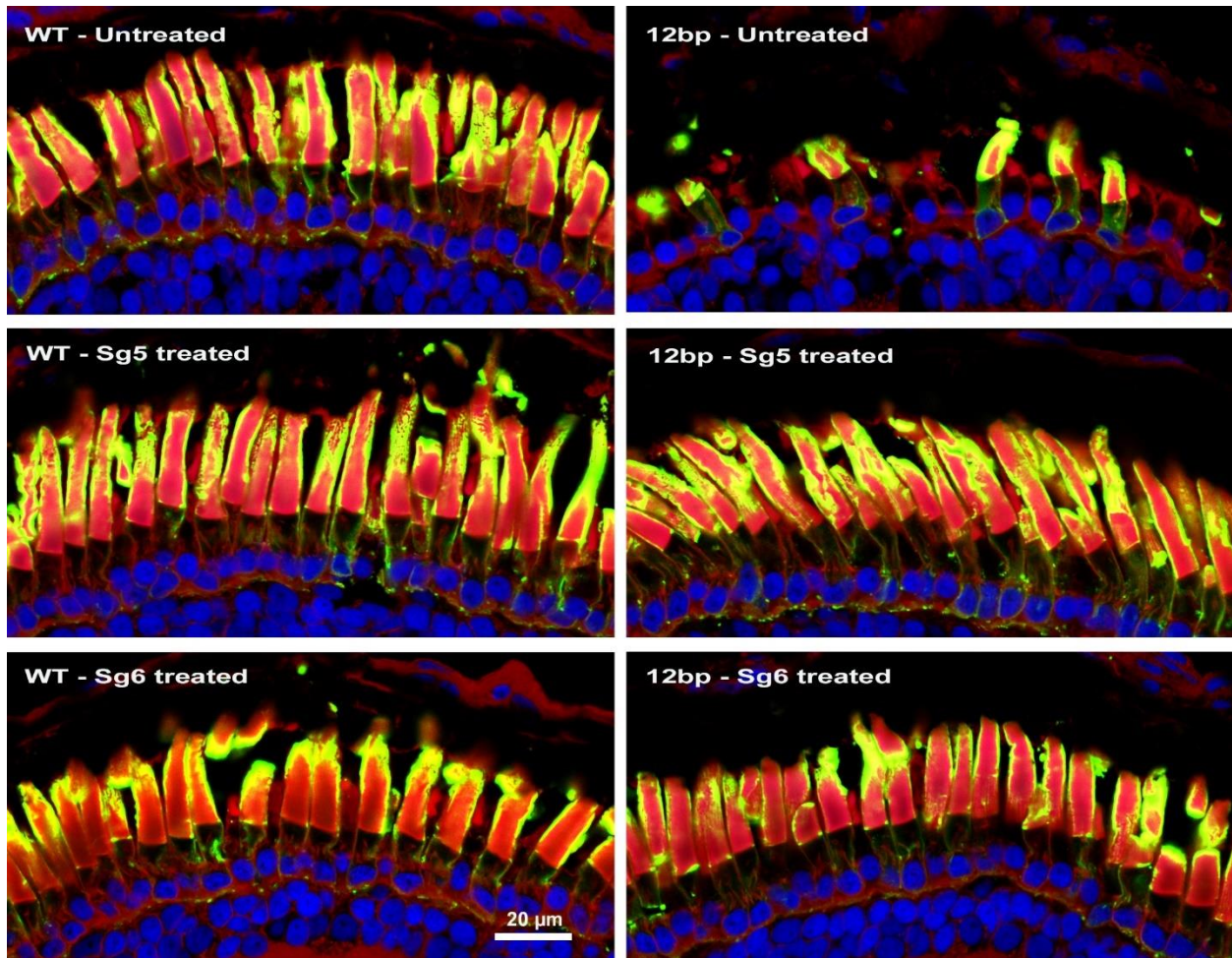


Figure 3-8. Significant RD observed in 12bp deletion animals was prevented in treated groups with a single guide. Histology sections from representative retinas in each group. Green=B630N (rod opsin); red=WGA; blue=Hoechst dye.

3.3.6 Simultaneous treatment with two guides also prevented RD

Significant RD was also prevented in animals simultaneously treated with two guides, in both Sg2+Sg5 and Sg2+Sg6 groups. However, Sanger sequencing illustrated that removal of the start codon did not occur in all subjects. Therefore, prevented RD in a subset of animals was likely attributed to the single edit of the 12bp deletion sequence. Overall, although the rod opsin levels were increased (Figure 3-7) and RD was prevented in the group treated with two guides (Figure 3-9), this treatment approach was not found to be superior to the single-guide approach.

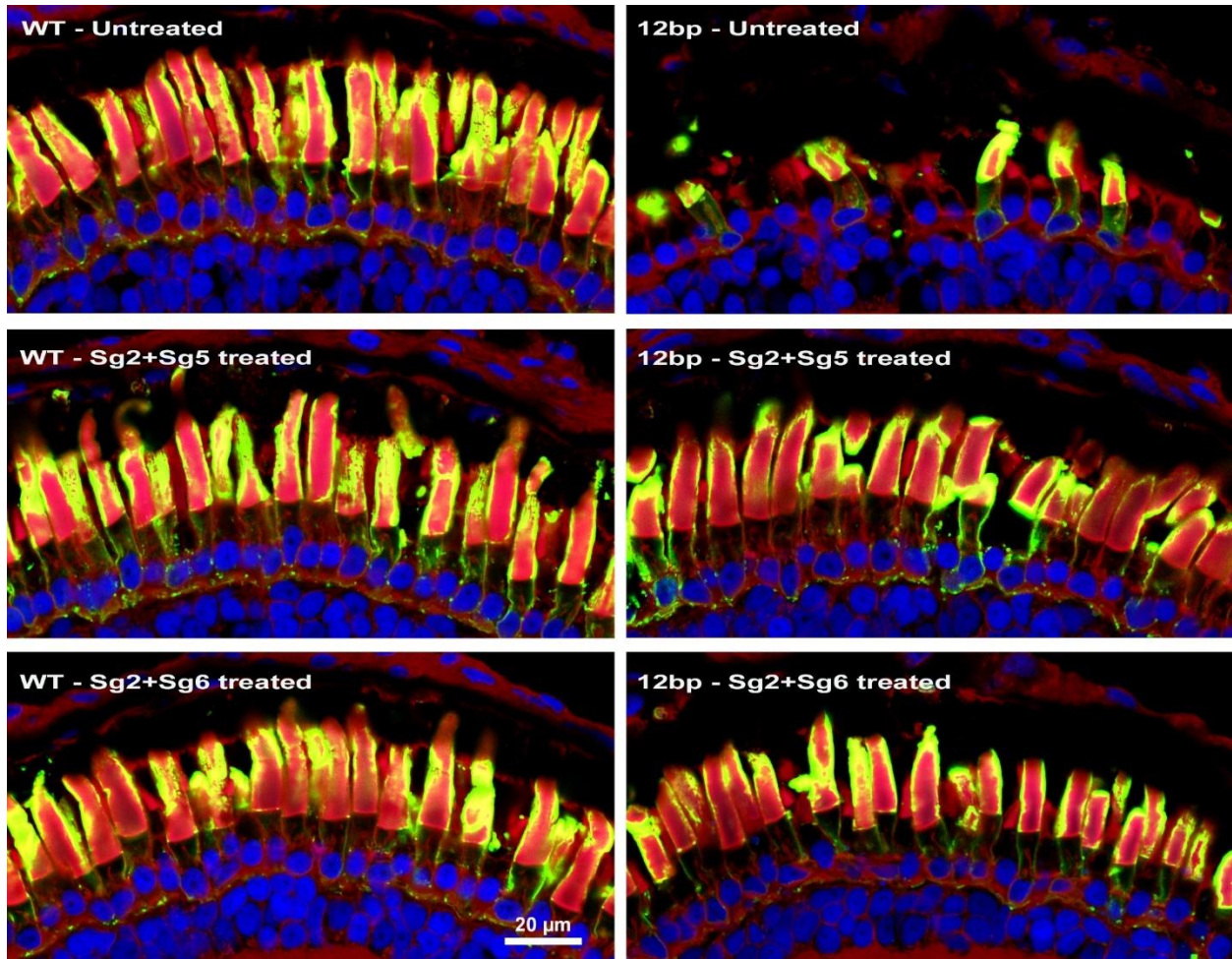


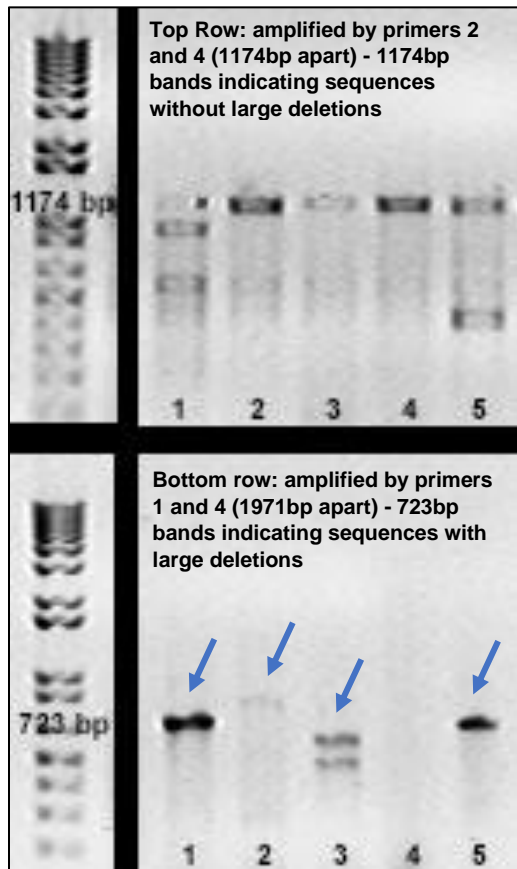
Figure 3-9. Significant RD observed in 12b deletion animals was prevented in treated groups with two guides. Histology sections from representative retinas in each group. Green=B630N (rod opsin); red=WGA; blue=Hoechst dye.

3.3.7 Simultaneous treatment with Sg2 and Sg5 resulted in large inactivating deletions in 7 out of 11 cases

The novel approach of attempting to knockout a mutant gene by inducing DSBs on both sides of the *Rho.L* gene start codon was successfully carried out in over half of the 12bp-deletion animals injected with Sg2 and Sg5, simultaneously. In those animals, a 1248bp long piece of DNA between the Sg2 and Sg5 guides containing the start codon for the *Rho.L* gene was removed. This large edit was validated via both band sizes of PCR products on 1% agarose gels as well as Sanger

sequencing (Figure 3-10, A). The large deletions also prevented significant retinal degeneration (Figure 3-10, B) and resulted in higher levels of rhodopsin detected by the dot blot assay (untreated (n=9), Sg2+5-treated (n=10), $p=0.0002$; untreated (n=11), Sg2+6-treated (n=7), $p=0.0028$ by Mann-Whitney U test; Figure 3-7). That being said, the histological outcomes and protein levels were not significantly improved by this approach relative to the single guide edit.

A.



B.

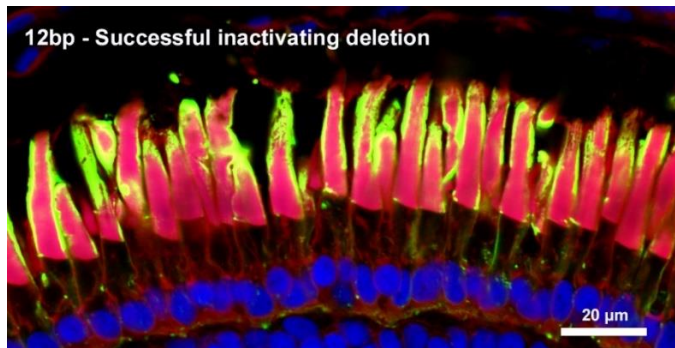
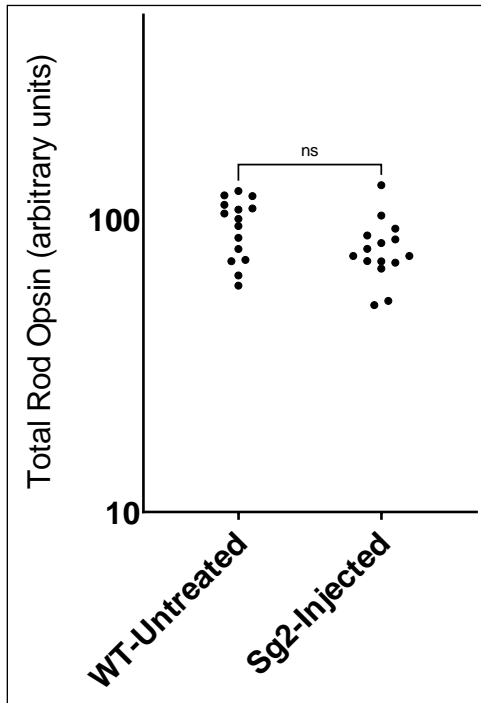


Figure 3-10. Removal of the start codon induced by large deletions in the 12bp-deletion animals prevented retinal degeneration in animals treated with simultaneous treatment of Sg2 and Sg5. (A) The evident 1248bp-long deletion was validated through PCR fragment analysis using different PCR primers as well as Sanger sequencing. Top row contains PCR products amplified with primers 2 and 4 that are 1174 bases apart, representing sequences without the large deletion. Bottom row contains PCR products of the corresponding samples amplified with primers 1 and 4, which are 1971 bases apart. Therefore, the appearance of bands around 720 bases represents the sequences with the large deletion. Blue arrows indicate samples where inactivating large deletions are evident and are confirmed with Sanger sequencing. Darker bands in the bottom row for samples 1 and 5 as well as the respectively lighter bands in the top row indicate that the large deletion must have occurred to a larger extent compared to samples 2 and 3. Sample 4 is an example of a 12bp deletion animal that was treated with Sg2 and Sg5, but the large deletion was not introduced successfully. 1kb ladder, 1% agarose gel (B) Representative histology sections from animals treated simultaneously with Sg2 and Sg5, where a successful large inactivating deletion took place. Green=B630N (rod opsin); red=WGA; blue=Hoechst dye.

3.3.8 The single guide (Sg2) editing the promoter regulatory region upstream from the start codon does not cause retinal degeneration

The dot blot assay demonstrated similar levels of rhodopsin in retinas from un-injected and Sg2-injected WT tadpoles, suggesting that minor disruptions of the promoter region caused by the Sg2 edit do not affect rhodopsin levels (n=15 per group; Mann Whitney U test, Figure 3-11, A). Additionally, the Sg2-injected WT animals were indistinguishable from untreated ones in histology and retinal degeneration was not observed in either group (Figure 3-11, B).

A.



B.

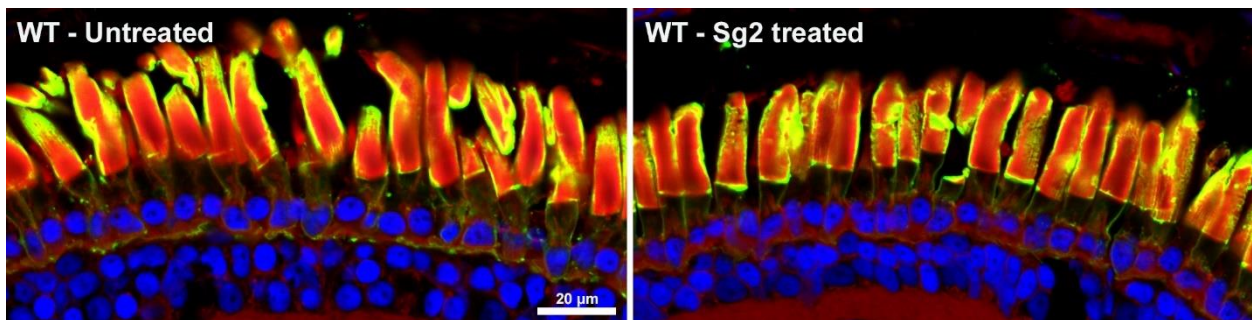


Figure 3-11. Comparing the Sg2-treated WT animals to untreated WT animals. (A) Total rod opsin levels assayed by dot blotting and rhodopsin labeling with B630N antibody. Rhodopsin levels are compared between the two groups on a log-scale (n=15 per group; Mann-Whitney U test). **(B)** WT Sg2-treated retinal sections appear indistinguishable from untreated WT retinas. Green=B630N (rod opsin); red=WGA; blue=Hoechst dye.

3.3.9 Distinguishing the mutant rhodopsin from WT endogenous rhodopsin protein via immunolabeling and western blotting

Immunolabeling: The primary monoclonal antibody B630N¹⁰⁶ binds to the N-terminus of the rhodopsin protein and represents the total amount of rhodopsin. Since the 12bp deletion site is also at the N-terminus, it is possible that the deletion interferes with the N-terminal 32 amino acids epitope of B630N. In order to test this effect, a subset of histology sections were labelled with 11D5 antibody, which binds to an epitope in the extreme C-terminus of rhodopsin¹¹⁷. Hence, we expected 11D5 labeling to detect the mutant rhodopsin in the 12bp-deletion animals that may no longer be recognizable by B630N. However, we did not observe a significant difference in labeling patterns between the two antibodies (Figure 3-12). This most likely indicates that the remaining amount of mutant protein are too small to be detected by either antibody in the context of a heterozygous animal, and that most of the mutant protein is effectively removed by the ER-associated protein degradation quality control pathways. It is possible that the B630N antibody may still be detecting the mutant rhodopsin despite the 12bp deletion mutation at the N-terminus. Another possibility is that the signal from the mutated rhodopsin generated by the single allele out of the three rhodopsin genes in the *X. laevis* may not be easily distinguishable. That being said, the mutated rhodopsin from that single allele is destructive enough to cause significant retinal degeneration in heterozygous animals.

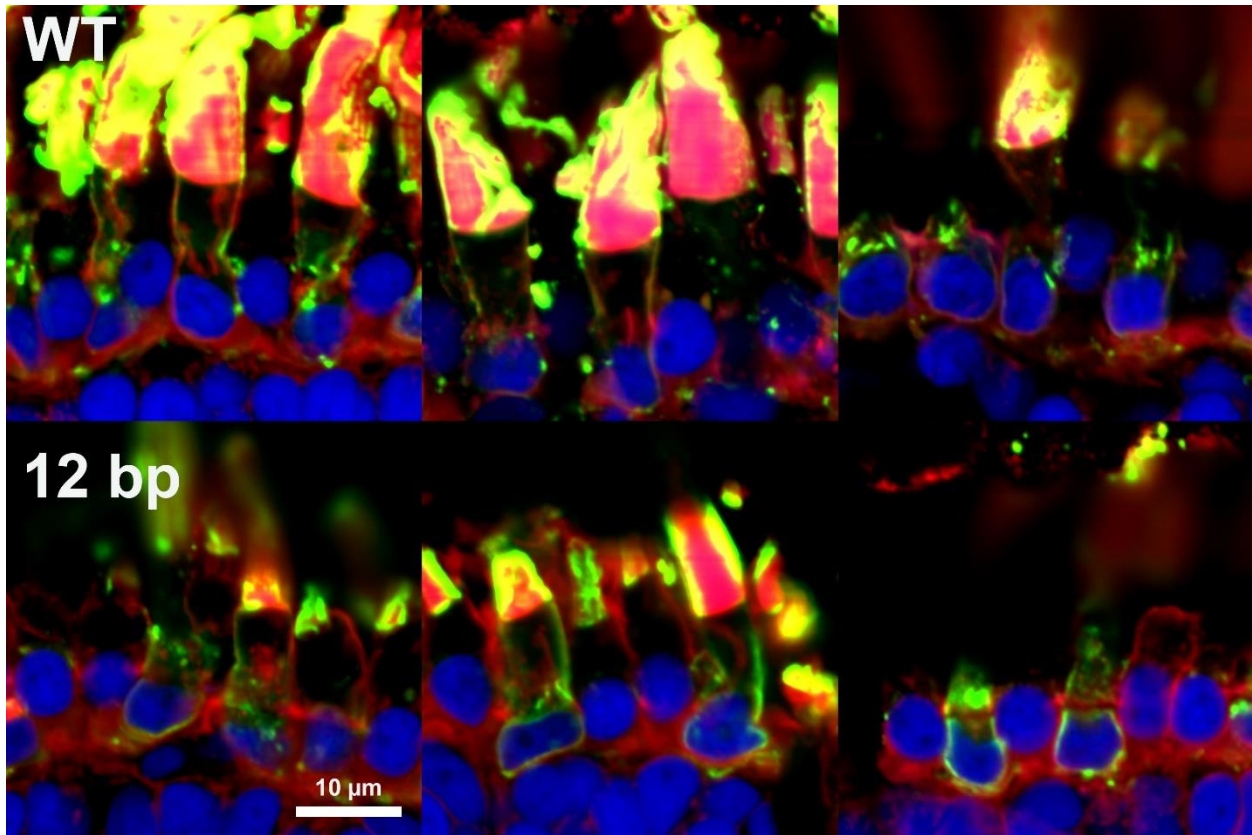


Figure 3-12. Rhodopsin localization in WT and 12bp deletion animals labelled by 11D5 antibody. Top row illustrates individual cells from three different WT animals. Bottom row includes three different 12bp deletion animals. Green=11D5 (rod opsin); red=WGA; blue=Hoechst dye.

Western Blotting: We also compared the B630N and 11D5 labeling in protein sample extracted from solubilized eyes of 12bp-deletion and WT animals using a western blot assay. We expected lower amounts of rhodopsin to be detected by both antibodies in 12bp deletion animals compared to controls. Additionally, we expected to observe potential extra bands in the 12bp deletion animals that would only be detected by the 11D5 antibody. Significantly higher levels of rhodopsin labeling were observed in WT compared to the 12bp deletion animals, detected similarly by both antibodies. However, we did not observe a significant difference between the 12bp deletion labeling of B630N and 11D5. No extra bands were observed with the 11D5 labeling (Figure 3-13).

One potential explanation is that the mutated rhodopsin protein has been destroyed and is no longer detectable.

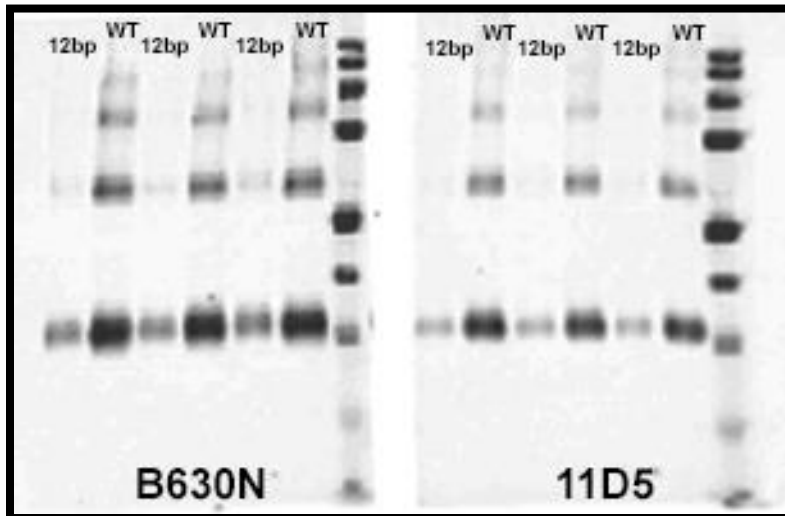


Figure 3-13. Western blotting to compare 11D5 and B630N rhodopsin labeling in three WT solubilized eyes and three 12bp deletion eyes. Duplicate membranes contain identical samples. The membrane on the left is probed with B630N antibody and the membrane on the right is probed with 11D5 antibody. Thicker bands indicating higher levels of rhodopsin are observed in columns containing WT samples compared to 12bp deletion samples. No difference in band patterns were observed between the two labeling antibodies.

3.3.10 ERG recordings from 9-months old animals

Rod photoreceptor function was compared between the 12bp deletion and WT animals using scotopic ERG measurements. The a-wave and b-wave amplitudes were measured in response to different blue light intensities (2.5, 25, 250, 750, 1250 and 2500 $\text{cd}\cdot\text{s}/\text{m}^2$). Mean a-wave amplitude was found to be significantly reduced ($p=0.0059$; two-way ANOVA) in 12bp deletion animals ($n=10$) compared to the WT ($n=6$). The average b-wave amplitude was not found to be statistically different between the two groups (Figure 3-14).

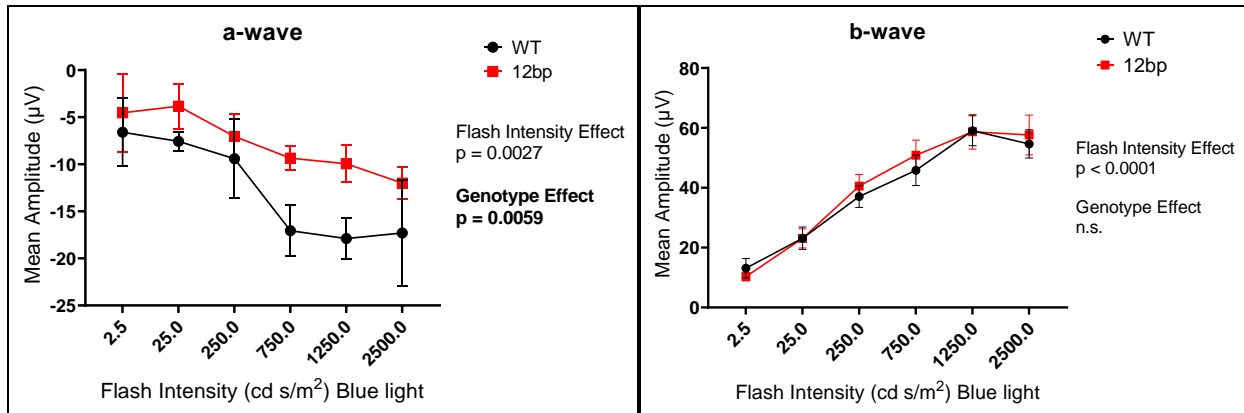


Figure 3-14. Scotopic ERG assay in 12bp deletion and WT animals. Mean a-wave and b-wave amplitudes in response to different light intensities from untreated WT (n=6) and 12bp deletion (n=10) animals. Genotype effect reflects the overall difference in mean amplitudes between WT and 12bp deletion animals. Flash intensity effect reflects the difference in response to varying blue light intensities. Data presented as mean \pm SEM. P-values were determined by two-way ANOVA with Sidak's post hoc test.

Subsequently, we assessed the effect of the Sg5-guide treatment on the 12bp deletion animals. As we had observed when comparing WT and 12bp deletion animals, no difference was found in mean b-wave amplitudes between the treated and untreated groups. However, mean a-wave amplitude was found to be significantly increased ($p=0.0001$; two-way ANOVA) in Sg5-treated animals (n=5) compared to the untreated adRP animals (n=8) (Figure 3-15). Hence, we were able to detect an improvement in scotopic ERG measurements in the treated group, comparable to WT animals as shown above.

Generally, the a-wave is associated with the overall physiological health of photoreceptors, while the b-wave is a reflection of bipolar and Müller cells' health within the inner retina¹¹⁸. Hence, we speculate that the reduction in a-wave amplitudes in our adRP model is likely due to the inability of sufficient functional photoreceptors in absorbing photons. However, the unaffected b-wave amplitudes reflect that a subset of photoreceptors remain functional at 9-months of age to relay

signals to the inner retina. Overall, our results are consistent with mild impairment of photoreceptors in our adRP model, that is prevented with the treatment.

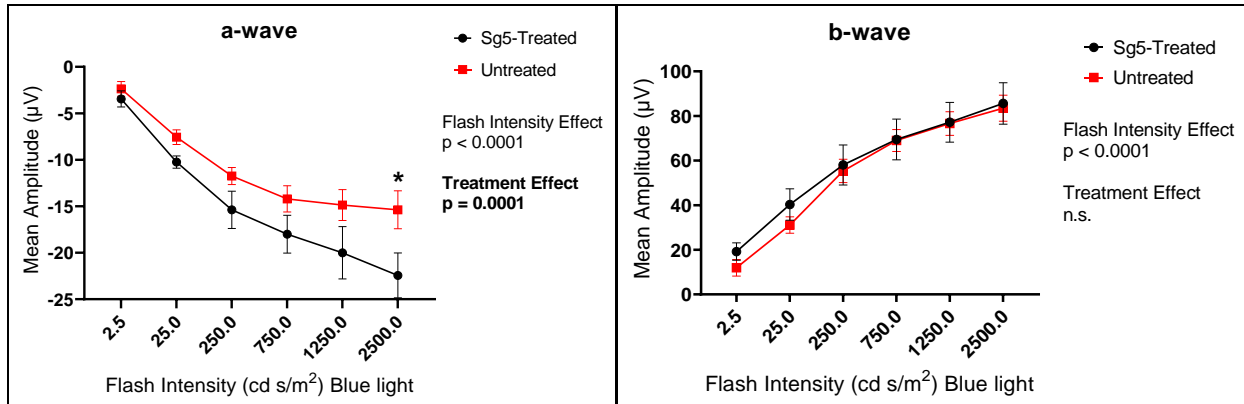


Figure 3-15. Scotopic ERG assay in treated and untreated animals. Mean a-wave and b-wave amplitudes in response to different light intensities from untreated 12bp deletion (n=8) and Sg5-treated 12bp deletion (n=5) animals. Treatment effect reflects the overall difference in mean amplitudes between treated and untreated animals. Flash intensity effect reflects the difference in response to varying blue light intensities. Data presented as mean \pm SEM. P-values were determined by two-way ANOVA with Sidak’s post hoc test.

3.3.11 OCT and fundus photography in 9-months old animals

Nakazawa *et al.*¹¹⁹ has reviewed reported differences in RP animal models using OCT. Particularly, degenerated photoreceptors in the retinal IS and OS layers of *RHO* P23H transgenic rats has been described as a ‘diffused hyperreflective zone’¹²⁰. Measurements from OCT have also been able to detect degenerating rod OS in *RHO* P23H *X. laevis* tadpole retinas, mainly characterized as decrease in retinal thickness¹²¹. To explore potential phenotypes with our adRP model, we acquired OCT and fundus images from WT and 12bp deletion untreated froglets at 9 months of age. Interestingly, we also observed the previously reported OCT diffused

hyperreflective zones in the OS of 12bp deletion animals, potentially associated with morphological abnormalities or disarrangement of OS discs due to disruption in rhodopsin trafficking to the outer segment. Given that we were able to distinguish WT and adRP retinas based on OCTs, prior to validating genotypes with Sanger sequencing, we believe that detectable discrepancies are evident between the two groups (Figure 3-16). Hence, OCT shows to be a viable tool for screening RD phenotype in our adRP model. Additionally, fundus images were acquired from the same animals. However, due to the small size of animals at the time of imaging, the resulting fundus images are of relatively low quality and we were unable to obtain meaningful information from fundus images.

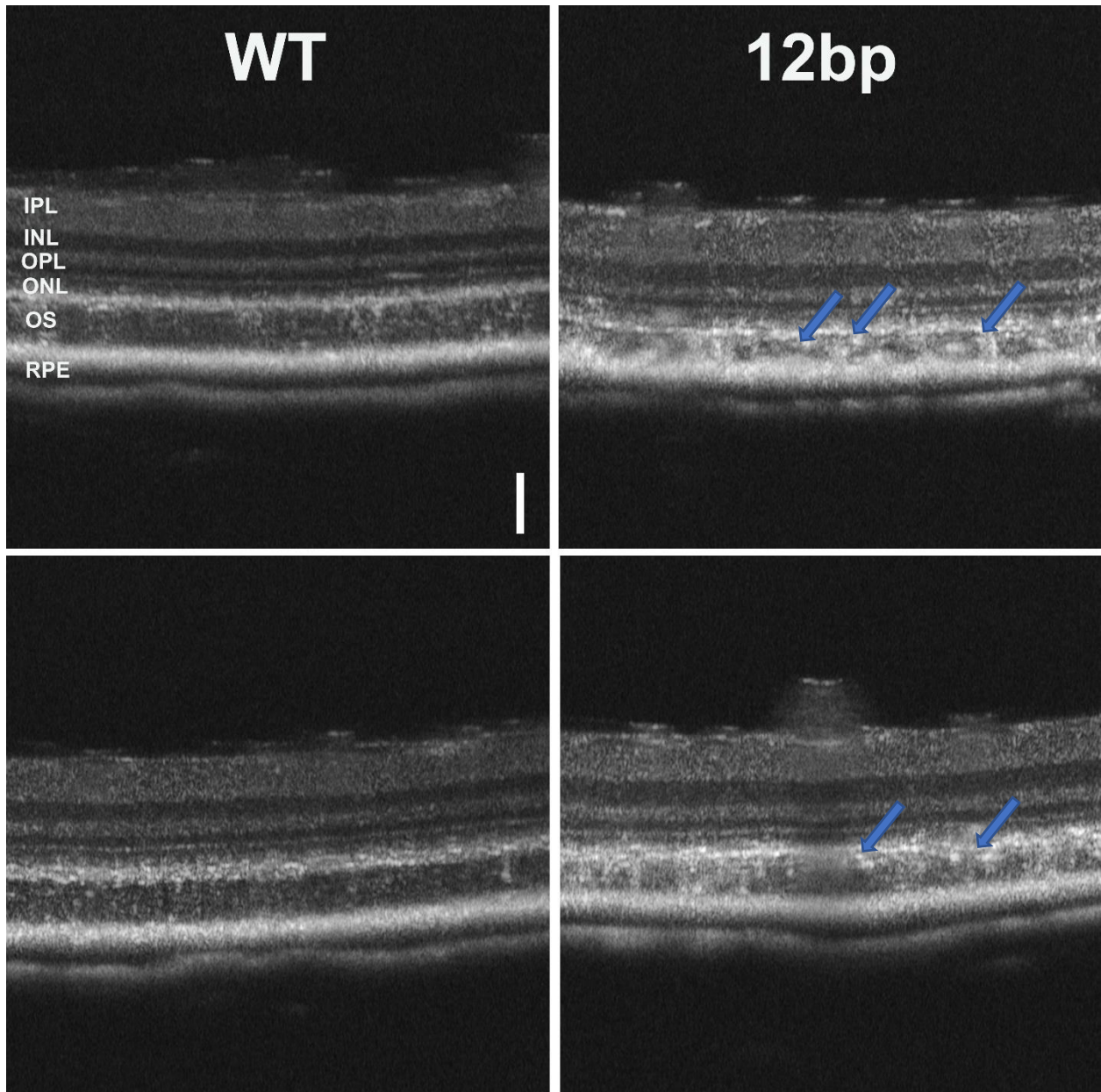


Figure 3-16. OCT comparing WT and 12bp deletion 9 months old *X. laevis*. The panels on the left demonstrate OCT images from two WT animals. The panels on the right demonstrate OCT images from two 12bp deletion animals. Blue arrows indicate diffused hyperreflective zones in the OS of 12bp deletion animals which are absent in the WT. Scale bar, 40 μm .

3.3.12 Histology sections from 9-months old animals

Animals at 9-months of age from untreated and Sg5-treated groups were sacrificed and genotyped using Sanger sequencing. Eyes were dissected, embedded, sectioned, labelled and imaged in the same manner as previously described to assess the long-term effects of both the 12bp deletion mutation and the persistence of the treatments. As shown in Figure 3-17, significant RD and loss of rods is observed in older froglets heterozygous for the 12bp deletion mutation. Remarkably, RD was prevented in the Sg5-treated animals, inferring that the beneficial effects of the treatment are long lasting.

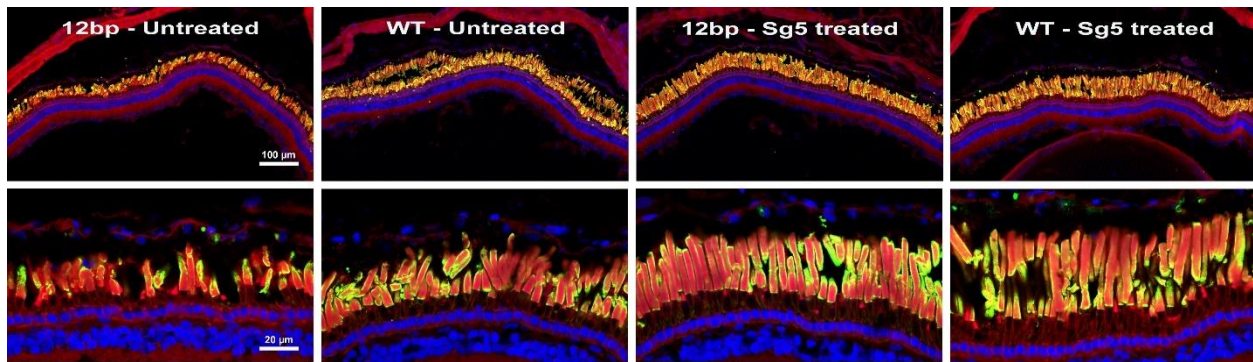


Figure 3-17. Histology sections from 9-months old animals. Significant RD is observed in untreated 9-months old 12bp deletion animal. RD is not apparent in Sg5-treated 12bp deletion animals. Treated animals appear to be indistinguishable from WT animals. Green=B630N (rod opsin); red=WGA; blue=Hoechst dye

3.3.13 CRISPR-mediated HDR as a treatment approach for adRP

Knocking out the allele carrying the 12bp deletion by relying on NMD as a result of indels introduced by the NHEJ repair mechanism was an effective approach in prevention of RD in our animal model. Due to the variability in the induced indels of NHEJ however, we only expected the KO strategy to be successful in two thirds of the photoreceptor cells due to an out-of-frame mutation. In the remaining one third of cases, an in-frame mutation may be neutral or aggravating.

Hence, we aimed to utilize the CRISPR-mediated HDR repair mechanism to improve treatment outcomes in our animal model. The HDR pathway is believed to produce error-free repairs compared to the NHEJ, as it uses a template sequence to repair a DSB. However, it is also found to have a lower efficiency¹²². Given that our treatment approach with a single guide (Sg5) and relying on the NHEJ repair mechanism was remarkably effective in preventing RD, we designed an experiment to compare its efficacy with the HDR repair mechanism.

In this experiment, the embryos generated from IVFs carried out between a WT male and a 12bp deletion female were separated into 3 groups:

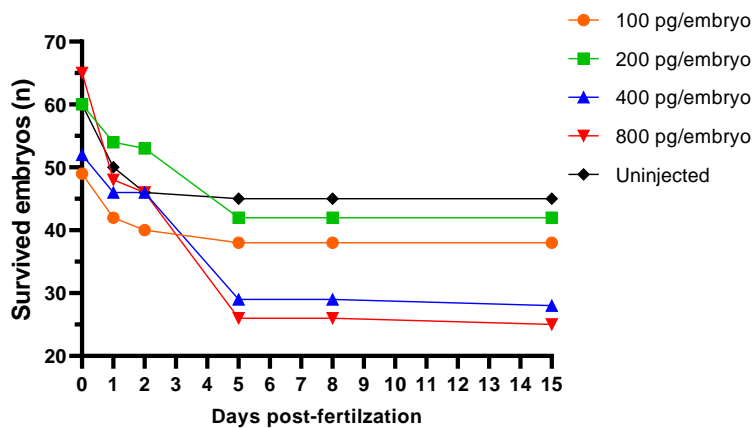
1. The control group which remained untreated
2. Embryos injected with Sg5 alone (designed to edit the 12bp deletion sequence) to induce the NHEJ repair mechanism
3. Embryos injected with a combination of Sg5 and the designed ssDNA template to induce the HDR repair mechanism

3.3.14 Toxicity test to optimize the amount of single-stranded oligonucleotide injected into each embryo

To maximize the efficiency of the HDR, we aimed to inject the highest amount of ssDNA into the oocytes without reaching toxic levels. In a previous study by Aslan *et al.* 200pg of a 200-base single-stranded oligonucleotide was successfully injected in *X. laevis* oocytes¹²³. Using this study as a reference point, we injected WT fertilized oocytes with varying amounts of 100, 200, 400 and 800pg of our 120-base long ssDNA per embryo. The resulting embryos were then raised to 15 days-old tadpoles in identical conditions as an un-injected control group. The survival rate of

animals in each group was monitored throughout. As shown in Figure 3-18, injecting 100pg of oligonucleotides seems to not influence the survival rate of embryos and is identical to un-injected animals. As the injected amount of oligonucleotide increased, fewer embryos survived the 15-day span of the experiment. Particularly, injection of 400 or 800pg appeared to be quite toxic and drastically reduced the survival rate. Therefore, 200pg/embryo was selected as the optimized amount to make the repair template abundantly available without inducing significant toxicity.

A.



B.

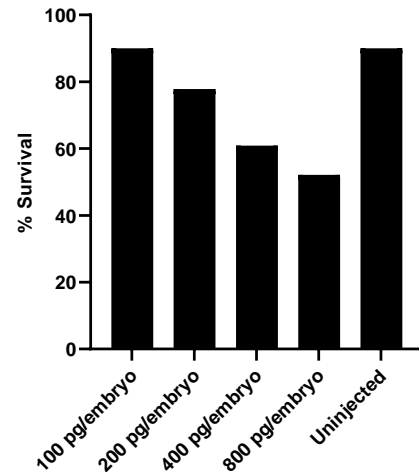


Figure 3-18. The effect of the concentration of ssDNA injected on the survival of *X. laevis* embryos. (A) Number of survived embryos at different timepoints over a 15-day long period for each of the injected concentrations. Starting number of animals in each group: Un-injected (n=60), 100pg (n=49), 200pg (n=60), 400pg (n=52), 800pg (n=65). (B) Percent survival of embryos with varying concentrations of ssDNA injected 15 days post-fertilization.

3.3.15 Significant improvement in phenotype was observed in treated groups

Similar to our findings in the previous experiment, significant RD was detected in untreated 12bp deletion animals. Severe RD was prevented in animals treated with Sg5 relying on the NHEJ repair mechanism (Figure 3-19, A). The improvement in phenotype was also validated with the dot blot assay showing a significant increase in rhodopsin levels of the treated groups compared to the untreated (Figure 3-19, B; n=32 per group; p=0.0266 by Mann-Whitney U test). Hence, the results of the previous experiment were reliably replicated. Significant RD was also prevented in the group of animals treated with Sg5 in combination with the designed ssDNA template (Figure 3-19, A). Rhodopsin levels were found to be significantly increased in this group compared to untreated animals (Figure 3-19, B; n=32 per group; p=0.0071 by Mann-Whitney U test). That being said, more investigations needed to be done to identify whether the improvements in phenotype were predominantly caused by the NHEJ or the HDR repair pathway.

The genotype of a subset of animals were identified through Sanger sequencing. As anticipated, rhodopsin levels were found to be at higher levels in WT animals compared to mutants in both treated and untreated groups. In the treated mutants, even animals with lower levels of rhodopsin were found to have significantly less RD with their rod OS fully intact. Therefore, although the treatment does not appear to increase rhodopsin quantities to WT levels in all animals, it is certainly highly effective in inhibiting RD.

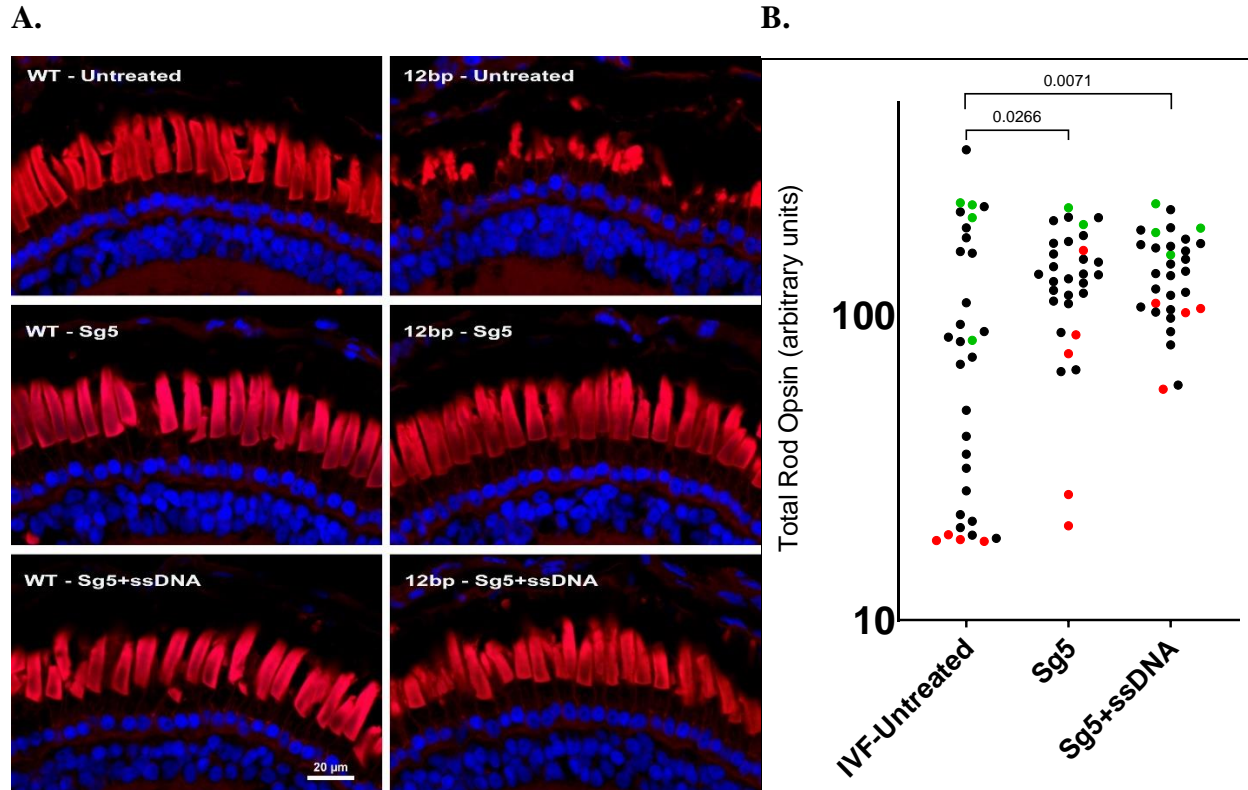


Figure 3-19. Comparing phenotypes between untreated, Sg5-treated and Sg5+ssDNA treated animals. (A) Demonstrated by labelled histology sections, significant RD observed in 12bp deletion animals was prevented in both treated groups. Red=WGA; blue=Hoechst dye. (B) Total rod opsin levels assayed by dot blotting and rhodopsin labeling with B630N antibody. Rhodopsin levels are compared between the groups on a log-scale. The genotype of a subset of animals were identified using Sanger sequencing. P-values were determined by Mann-Whitney U test to compare groups (n=32 per group). Green=WT, red=12bp deletion, black=not sequenced.

3.3.16 The HDR repair pathway was inefficient for the recombination of the designed ssDNA template into the mutant rhodopsin gene

Three main assays were carried out to assess the efficiency of the HDR repair mechanism in all 36 animals treated with Sg5-ssDNA:

1. *ApoI* restriction digests were carried out on *Rho.L* exon-I amplified PCR products of genomic DNA extracted from each animal. Given that an *ApoI* restriction site was introduced within the insert of our designed ssDNA, successful recombination of the repair template into genomic

DNA could be detected through fragment analysis. However, we were unable to detect any evidence supporting the introduction of an additional *ApoI* restriction site in our Sg5-ssDNA treated animals.

2. The dot blot assay was repeated and probed with different antibodies to detect potential evidence for the HDR pathway at a protein level. As mentioned previously, an M13F point mutation (ATG → TTT) was introduced within the insert of the ssDNA template to add a unique epitope distinguishable from the endogenous *X. laevis* rhodopsin. Through probing duplicate dot blots with 514-18 and B630N antibodies, we used the 514-18 to B630N labeling ratio to detect the potential recombination of the template and expression of the introduced epitope. No difference was observed in the ratios calculated between the experimental and control groups (Figure 3-20).

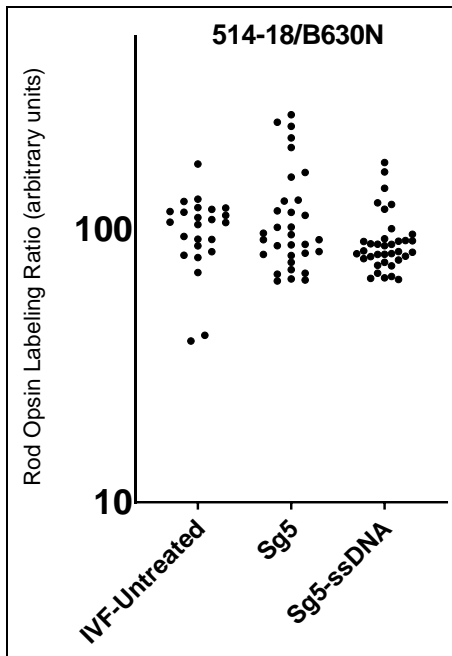


Figure 3-20. Dot blot assay comparing the 514-18 to B630N antibody labeling ratios between experimental and control groups. No statistical difference was detected between groups with Kruskal-Wallis test (n=32 per group). Since the 514-18 labeling is expected to detect potential

signals for HDR occurrence in the Sg5-ssDNA group, we were unable to find evidence of our designed insert recombination.

3. Retinal sections from all 36 animals were labelled with 2B2 antibody (distinctly recognizing the epitope resulting from the M13F mutation introduced in the ssDNA template) and imaged using confocal microscopy. Only a single cell in one of the sections was found to be 2B2-positive (Figure 3-21). Since 2B2 labeling was not detected in any other animal, we concluded that the HDR efficiency was relatively minimal. Considering the gathered evidence from multiple modes of testing for the efficacy of the HDR repair mechanism, it was concluded that the improved phenotype in the Sg5-ssDNA treated group was likely due to the NHEJ mechanism induced by the Sg5 edit, and not the HDR pathway.

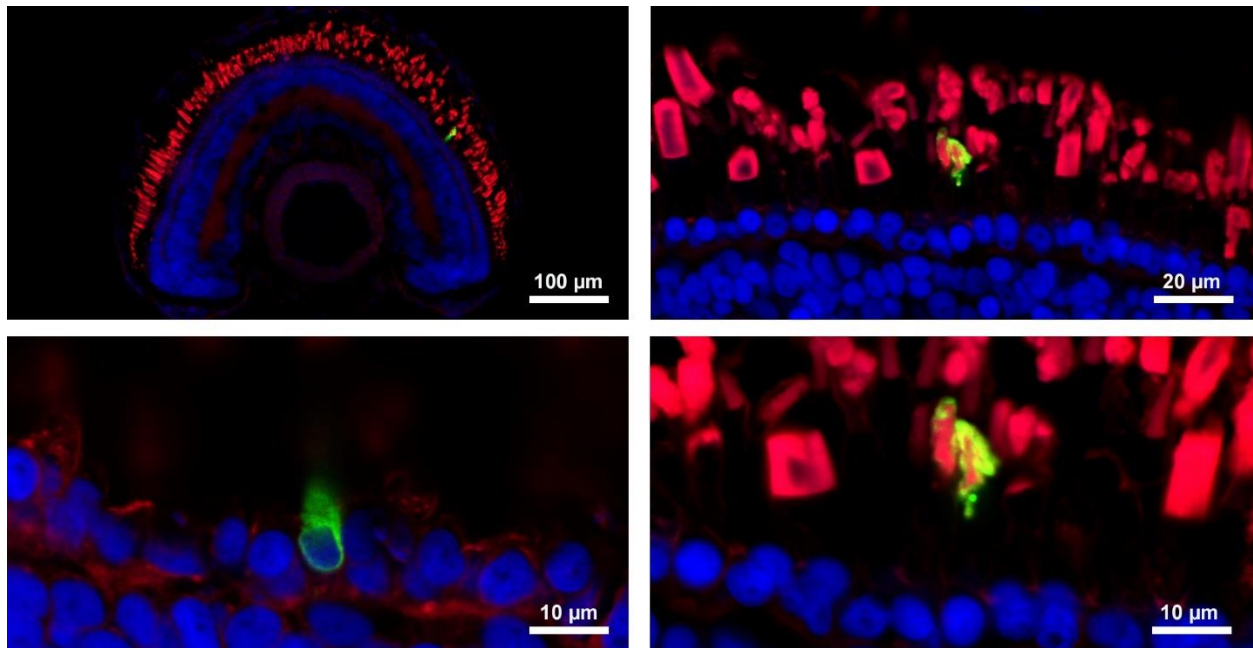


Figure 3-21. Histological evidence for a 2B2-positive cell, indicating the recombination of the designed template via HDR. The single cell was imaged with different magnifications for better visualization. The bottom two panels are imaged with the same magnification: bottom left panel was focused on the inner segment and bottom right panel was focused on the outer segment. Green=2B2; Red=WGA; blue=Hoechst dye.

4. CONCLUSION

As discussed in the second chapter of this dissertation, we designed a unique hybrid model for the RP-inducing T4K mutation in transgenic *X. laevis* carrying the mouse rhodopsin gene, with its first exon replaced with the human gene. We were further able to demonstrate that the light-exacerbated RD phenotype associated with the *RHO* T4K mutation remained present in our model. In fact, light-exacerbated RD appeared to be independent of the underlying *RHO* cDNA when compared to transgenic *X. laevis* with the human or mouse cDNAs alone. For tadpoles reared in cyclic light, T4K rhodopsin caused significant RD regardless of whether the transgene was human, mouse, or a human/mouse hybrid *RHO*. When raised in the dark, no significant RD was detected in tadpoles expressing T4K *RHO*, and rhodopsin levels were not significantly different from WT animals. This raises our confidence that the previously discussed humanized mouse model based on a hybrid *RHO* strategy will retain a mechanistically similar RD. Moreover, our results indicate that introduction of the T4K mutation into the mouse genome, without additional human sequence, would also be an effective means of modeling this type of RD.

Developing this unique model was critical for several reasons. Primarily, this model allowed us to characterize and confirm the observed phenotypes associated with the T4K mutation in a highly representative model that expresses the human exon-I in the mouse rhodopsin gene. Secondly, we aim to use this model as a stepping-stone in developing a knock-in humanized mouse model to study the mechanism of the human T4K rhodopsin mutation in a mammalian model. Lastly, this model can be used to further explore gene-editing therapeutic strategies directly on the human gene within our experimental animal model. By doing so, transferring gene therapeutics from lab benches into clinical trials can be done far more efficiently.

In the third chapter of this dissertation, multiple CRISPR-based gene editing strategies were explored as treatment approaches in an *X. laevis* model for adRP. This model was previously developed in our laboratory using the CRISPR/Cas9 gene editing system⁴⁹. The 12bp in-frame deletion in the first exon of the *X. laevis Rho.L* gene in this model resulted in a dominant phenotype of retinal degeneration. This is potentially caused by defects in biosynthesis and trafficking of the misfolded protein that result in cell death, similar to a number mutations identified in rhodopsin's N-terminus (i.e. T4K, T17M, P23H)^{16,39}. Therefore, analogous to human adRP, significant RD was observed in heterozygous animals carrying the mutation in only one of the alleles. Additionally, developing treatments in our adRP model was similar to developing treatments in human autosomal dominant diseases, in that the mutant allele would either need to be eliminated or restored¹¹⁰. In order to do so, allele-specific therapeutics were required to only target the mutant, leaving the WT unaffected. For these reasons, this model provided us with a viable context to test a variety of gene-editing treatment strategies for adRP. We believe that this model can be effectively utilized to further investigate therapeutics under idealized circumstances in which practical issues such as viral delivery of the therapy are eliminated, and allele specificity is highly optimized.

Comparing the efficacy of different treatment strategies explored in this dissertation, treating animals with a single sgRNA uniquely targeting the allele with the 12bp-deletion was overwhelmingly successful. We expected the NHEJ repair mechanism following the DSB to facilitate indel generation, resulting in out-of-frame mutations and nonsense mediated decay in approximately two-thirds of the photoreceptor cells. Hence, loss-of function mutation in the malfunctioning alleles was projected to prevent the majority, but not all, of the retinal degeneration. Remarkably, the treatment significantly prevented RD in almost all animals,

illustrating that selective editing even in a subset of cells can be used as a highly effective treatment approach. Additionally, we were able to demonstrate that a single-base discrepancy is sufficient for CRISPR to distinguish between the WT and mutant alleles. This is particularly important for potential clinical use of this editing strategy, as several human mutations are caused by a single point mutation. Most recently, Diakatou *et al.* have published their work in using the same editing strategy to treat G56R and NR2E3 adRP mutations in iPSCs⁵⁸. They designed unique sgRNAs to specifically target mutant alleles with a single-base difference and successfully utilized CRISPR/Cas9 to introduce NHEJ-mediated indels that KO the mutant allele⁵⁸. Latella *et al.* have also used a similar gene-editing approach in mouse retinas carrying the human P23H rhodopsin gene, through subretinal electroporation of plasmid-based CRISPR/Cas9¹²⁴. There are also limitations associated with NHEJ-based treatment for adRP. Primarily, although we have shown that CRISPR is able to discriminate between the mutant and WT alleles with high specificity, designing guides at the exact location of the mutation is not always possible. Secondly, in-frame mutations following an sgRNA edit can exacerbate the phenotype in a subset of cells or may leave them unaffected. Nonetheless, our findings emphasize that even an imperfect treatment strategy can be highly effective, elucidating that complex approaches may not be necessary for developing effective treatments for dominant retinal diseases.

Despite the remarkable success of the single guide treatment approach in preventing RD in our adRP model, we also tested more complex editing strategies, designed to eliminate the remaining 1/3 of cells where in-frame edits were expected. In attempting to restore the mutated allele into WT in our adRP model through the HDR repair mechanism, we found that HDR appears to be quite inefficient in *X. laevis* using the described protocol. Although reasons remain unclear, similar results were also obtained by Feehan *et al.* in our laboratory, despite modifications in our

methodology⁴⁹. Here, we attempted to improve HDR efficiency by means of a 120nt single stranded oligonucleotide as the repair template, as opposed to the 1200bp long double-stranded DNA template used by Feehan *et al.*⁴⁹. Yet, HDR efficiency remained relatively low compared to the NHEJ repair pathway. It should be noted that incidence and efficiency of HDR-mediated repair is also reported to be extremely low in mammalian cells⁶⁴. Maruyama *et al.* have reported HDR repair efficiencies ranging from 0.5% to 20%, compared to 20-60% NHEJ-mediated repair in mouse models¹²⁵. To improve HDR efficiency, Lin *et al.* have proposed a novel strategy to synchronize cells into late S and G2 phases of the cell cycle, where HDR predominantly takes place¹²⁶. Alternatively, other research groups have attempted to suppress NHEJ by targeting its unique components such as DNA ligase IV, allowing for HDR to become a more dominant repair pathway following DNA damage^{127,128}.

Generating large deletions in genomic DNA through combining two different sgRNAs with the Cas9 protein was another key finding of this dissertation. We attempted a unique KO strategy in which the start codon of the mutated gene was removed after introducing two separate DSBs upstream and downstream from the *Rho.L* gene's start codon. Remarkably, removing the start codon of the mutated allele resulted in viable retinas without RD. Tsai *et al.* has previously successfully carried out a similar treatment approach in human rhodopsin knock-in adRP mouse models using AAV injections¹²⁹. Utilizing double gRNAs in combination with Cas9 protein, they introduced two DSBs upstream and downstream from the rhodopsin gene's start codon (363bp apart), resulting in large inactivating deletions in both alleles. Simultaneous with the elimination of the targeted gene, they enabled the expression of WT rhodopsin through an exogenous cDNA¹²⁹. Our treatment approach, however, was unique in that one of the sgRNAs designed to introduce the large inactivating deletion was selected specifically to only target the mutant allele. The second

non-specific sgRNA was also designed to introduce an edit upstream from the promoter regulatory region, in a non-conserved region so that it does not disrupt the WT allele. Therefore, our strategy did not require an addition of exogenous cDNA, and the endogenous WT allele was sufficient in expressing WT phenotype.

Although the introduction of large deletions was not 100% efficient in our experiment and was only detected in a subset of our animals (7 out of 11), this is a notable finding that can be optimized and replicated in gene therapeutics as well as in creating KO genetic models. One contributing factor to the efficiency of simultaneous breaks may be the physical distance between the two target sites. In our experiment, the designed sites were 1248bp apart. Shorter or longer distance between the target sites may affect the proficiency of the edit. Nonetheless, this KO approach provides more flexibility in the selection of guide RNA target sites compared to the single guide approach. A key limitation in designing guides is finding target sites that are unique to the mutated allele and do not edit the WT allele. A double guide approach is less restricted because unique target sites can be identified within a larger number of bases upstream and downstream from the desired gene's start codon.

Although CRISPR/Cas9 is a highly robust and flexible gene editing tool, its translation as a therapeutic tool in human patients is not free of challenges. The delivery of CRISPR/Cas9 based gene therapies is complicated by the large size of the Cas9 protein, concerns about off target effects and the requirement for a PAM site adjacent to the site to be edited⁶⁴. Currently, CRISPR/Cas9 components can be delivered via physical delivery methods (mainly microinjection and electroporation), viral vectors (i.e., AAVs) and non-viral vectors (i.e., lipid nanoparticles)¹³⁰. However, available delivery methods are still associated with major limitations when it comes to

clinical applications. Physical deliveries, although remarkably efficient in laboratory settings, are generally not suitable for patient treatment¹³⁰. In case of microinjections, individual cells need to be targeted which is typically not feasible, and electroporation can be damaging to mammalian cells¹³¹. Viral vectors that are extensively used in gene therapy are limited in the size of cargo they can deliver, especially in cases where multiple sgRNAs or HDR templates are also required⁶⁴. Non-viral vectors have not yet been highly optimized and in many cases are unable to escape being degraded by internal protective cellular mechanisms, leading to reduced efficiencies¹³². To address these challenges, more work needs to be done for more efficient and potent delivery methods to emerge. Recent developments in lipid nanoparticles for CRISPR delivery labelled as selective organ targeting (SORT)¹³³ or the use of biphotonic laser-assisted surgery tool (BLAST)¹³⁴ for delivery of CRISPR cargo may hold the future for delivery of this powerful gene editing tool. Furthermore, The PAM motif requirement for designing sgRNAs is limiting in selecting the desired location of target site, while its repetition throughout the genome also reduces the specificity of guides. For instance, the *S. pyogenes*'s Cas9 PAM sequence (NGG) has been reported to, on average, occur once every 8bps¹³⁵. Fortunately, however, more Cas proteins from other species are becoming characterized with diverse PAM sequences, allowing for more flexibility and specificity in designing sgRNAs⁶⁴. Moreover, in cases like in our animal model, the mutation itself offers a unique sequence that is absent in the WT or anywhere else in the genome, allowing us to design guides that uniquely edit the mutant.

Overall, our results indicate that, more complex strategies such as those we have explored here may be theoretically superior, but ultimately not as efficacious if their efficiency is lower. In addition, NHEJ is active in both proliferating and non-dividing cells, whereas activating HDR in post-mitotic cells such as photoreceptors can be challenging¹³⁶. Therefore, should the challenges

of efficient CRISPR delivery be overcome, it would be possible to develop a highly efficacious therapy for adRP based simply on the NHEJ repair mechanism.

BIBLIOGRAPHY

1. Sung CH, Chuang JZ. Review series: The cell biology of vision. *J Cell Biol.* 2010;190(6):953-963.
2. Purves D, Augustine GJ, Fitzpatrick D, et al. *The Retina.* 2001. <https://www.ncbi.nlm.nih.gov/books/NBK10885/>. Accessed March 24, 2021.
3. Simple Anatomy of the Retina by Helga Kolb – Webvision. <https://webvision.med.utah.edu/book/part-i-foundations/simple-anatomy-of-the-retina/>. Accessed March 24, 2021.
4. Diakotou M, Manes G, Bocquet B, Meunier I, Kalatzis V. Genome editing as a treatment for the most prevalent causative genes of autosomal dominant retinitis pigmentosa. *Int J Mol Sci.* 2019;20(10). doi:10.3390/ijms20102542
5. Baccus SA. Timing and computation in inner retinal circuitry. *Annu Rev Physiol.* 2007;69:271-290. doi:10.1146/annurev.physiol.69.120205.124451
6. Fain GL, Hardie R, Laughlin SB. Phototransduction and the Evolution of Photoreceptors. *Curr Biol.* 2010;20(3):R114-24. doi:10.1016/j.cub.2009.12.006
7. Athanasiou D, Aguila M, Bellingham J, et al. The molecular and cellular basis of rhodopsin retinitis pigmentosa reveals potential strategies for therapy. *Prog Retin Eye Res.* 2018;62:1-23. doi:10.1016/j.preteyeres.2017.10.002
8. Hoon M, Okawa H, Della Santina L, Wong ROL. Functional architecture of the retina: Development and disease. *Prog Retin Eye Res.* 2014;42:44-84. doi:10.1016/j.preteyeres.2014.06.003
9. Perkins BD, Fadool JM. *Photoreceptor Structure and Development. Analyses Using GFP Transgenes.* Vol 100. NIH Public Access; 2010. doi:10.1016/B978-0-12-384892-5.00007-4
10. Arikawa K, Molday LL, Molday RS, Williams DS. Localization of peripherin/rds in the disk membranes of cone and rod photoreceptors: Relationship to disk membrane morphogenesis and retinal degeneration. *J Cell Biol.* 1992;116(3):659-667. doi:10.1083/jcb.116.3.659
11. Mustafi D, Engel AH, Palczewski K. Structure of cone photoreceptors. *Prog Retin Eye Res.* 2009;28(4):289-302. doi:10.1016/j.preteyeres.2009.05.003
12. Park PSH. Constitutively Active Rhodopsin and Retinal Disease. In: *Advances in Pharmacology.* Vol 70. Academic Press Inc.; 2014:1-36. doi:10.1016/B978-0-12-417197-8.00001-8
13. Leskov IB, Klenchin VA, Handy JW, et al. The gain of rod phototransduction: Reconciliation of biochemical and electrophysiological measurements. *Neuron.* 2000;27(3):525-537. doi:10.1016/S0896-6273(00)00063-5

14. Klapper SD, Swiersy A, Bamberg E, Busskamp V. Biophysical properties of optogenetic tools and their application for vision restoration approaches. *Front Syst Neurosci.* 2016;10(SEP):74. doi:10.3389/fnsys.2016.00074
15. Obin MS, Jahngen-Hodge J, Nowell T, Taylor A. *Ubiquitinylation and Ubiquitin-Dependent Proteolysis in Vertebrate Photoreceptors (Rod Outer Segments)*. <http://www.jbc.org/>. Accessed April 10, 2020.
16. Tam BM, Moritz OL. The role of rhodopsin glycosylation in protein folding, trafficking, and light-sensitive retinal degeneration. *J Neurosci.* 2009;29(48):15145-15154. doi:10.1523/JNEUROSCI.4259-09.2009
17. Tatour Y, Ben-Yosef T. Syndromic inherited retinal diseases: genetic, clinical and diagnostic aspects. *Diagnostics.* 2020;10(10). doi:10.3390/diagnostics10100779
18. Berger W, Kloeckener-Gruissem B, Neidhardt J. The molecular basis of human retinal and vitreoretinal diseases. *Prog Retin Eye Res.* 2010;29(5):335-375. doi:10.1016/j.preteyeres.2010.03.004
19. Hamel CP. Cone rod dystrophies. *Orphanet J Rare Dis.* 2007;2(1):7. doi:10.1186/1750-1172-2-7
20. Narayan DS, Wood JPM, Chidlow G, Casson RJ. A review of the mechanisms of cone degeneration in retinitis pigmentosa. *Acta Ophthalmol.* 2016;94(8):748-754. doi:10.1111/aos.13141
21. Kolomeyer AM, Zarbin MA. Trophic factors in the pathogenesis and therapy for retinal degenerative diseases. *Surv Ophthalmol.* 2014;59(2):134-165. doi:10.1016/j.survophthal.2013.09.004
22. Punzo C, Kornacker K, Cepko CL. Stimulation of the insulin/mTOR pathway delays cone death in a mouse model of retinitis pigmentosa. *Nat Neurosci.* 2009;12(1):44-52. doi:10.1038/nn.2234
23. Shen J, Yang X, Dong A, et al. Oxidative damage is a potential cause of cone cell death in retinitis pigmentosa. *J Cell Physiol.* 2005;203(3):457-464. doi:10.1002/jcp.20346
24. Gupta N, Brown KE, Milam AH. Activated microglia in human retinitis pigmentosa, late-onset retinal degeneration, and age-related macular degeneration. *Exp Eye Res.* 2003;76(4):463-471. doi:10.1016/S0014-4835(02)00332-9
25. Van Rossum D, Hilbert S, Straßenburg S, Hanisch UK, Brück W. Myelin-phagocytosing macrophages in isolated sciatic and optic nerves reveal a unique reactive phenotype. *Glia.* 2008;56(3):271-283. doi:10.1002/glia.20611
26. Van Antwerp DJ, Martin SJ, Kafri T, Green DR, Verma IM. Suppression of TNF- α -induced apoptosis by NF- κ B. *Science (80-).* 1996;274(5288):787-789. doi:10.1126/science.274.5288.787
27. Boje KM, Arora PK. Microglial-produced nitric oxide and reactive nitrogen oxides mediate neuronal cell death. *Brain Res.* 1992;587(2):250-256. doi:10.1016/0006-

8993(92)91004-X

28. Ripps H. Cell death in retinitis pigmentosa: Gap junctions and the “bystander” effect. *Exp Eye Res.* 2002;74(3):327-336. doi:10.1006/exer.2002.1155
29. Viringipurampeer IA, Metcalfe AL, Bashar AE, et al. NLRP3 inflammasome activation drives bystander cone photoreceptor cell death in a P23H rhodopsin model of retinal degeneration. *Hum Mol Genet.* 2016;25(8):1501-1516. doi:10.1093/hmg/ddw029
30. Samardzija M, Masarini K, Ueffing M, Trifunović D. HDAC Inhibition Prevents Primary Cone Degeneration Even After the Onset of Degeneration. In: *Advances in Experimental Medicine and Biology.* Vol 1185. Springer; 2019:383-387. doi:10.1007/978-3-030-27378-1_63
31. Samardzija M, Corna A, Gomez-Sintes R, et al. HDAC inhibition ameliorates cone survival in retinitis pigmentosa mice. *Cell Death Differ.* 2021;28(4):1317-1332. doi:10.1038/s41418-020-00653-3
32. Hamel C. Retinitis pigmentosa. *Orphanet J Rare Dis.* 2006;1(1):40. doi:10.1186/1750-1172-1-40
33. Retinitis Pigmentosa - Fighting Blindness Canada (FBC). <https://www.fightingblindness.ca/eye-diseases-pathways/retinitis-pigmentosa/>. Accessed April 10, 2020.
34. Verbakel SK, van Huet RAC, Boon CJF, et al. Non-syndromic retinitis pigmentosa. *Prog Retin Eye Res.* 2018;66:157-186. doi:10.1016/j.preteyeres.2018.03.005
35. Parmeggiani F, Sorrentino F, Ponzin D, Barbaro V, Ferrari S, Di Iorio E. Retinitis Pigmentosa: Genes and Disease Mechanisms. *Curr Genomics.* 2011;12(4):238-249. doi:10.2174/138920211795860107
36. Hartong DT, Berson EL, Dryja TP. Retinitis pigmentosa. *Lancet.* 2006;368(9549):1795-1809. doi:10.1016/S0140-6736(06)69740-7
37. Hellsten U, Harland RM, Gilchrist MJ, et al. The genome of the western clawed frog *Xenopus tropicalis*. *Science (80-).* 2010;328(5978):633-636. doi:10.1126/science.1183670
38. Wheeler GN, Brändli AW. Simple vertebrate models for chemical genetics and drug discovery screens: Lessons from zebrafish and *Xenopus*. *Dev Dyn.* 2009;238(6):1287-1308. doi:10.1002/dvdy.21967
39. Tam BM, Moritz OL. Dark rearing rescues P23H rhodopsin-induced retinal degeneration in a transgenic *Xenopus laevis* model of retinitis pigmentosa: A chromophore-dependent mechanism characterized by production of N-terminally truncated mutant rhodopsin. *J Neurosci.* 2007;27(34):9043-9053. doi:10.1523/JNEUROSCI.2245-07.2007
40. Horb M, Wlizla M, Abu-Dayā A, et al. *Xenopus* resources: Transgenic, inbred and mutant animals, training opportunities, and web-based support. *Front Physiol.* 2019;10(APR):387. doi:10.3389/fphys.2019.00387

41. Rivas MA, Vecino E. Animal models and different therapies for treatment of retinitis pigmentosa. *Histol Histopathol.* 2009;24(10):1295-1322. doi:10.14670/HH-24.1295
42. Zelinka CP, Sotolongo-Lopez M, Fadool JM. Targeted disruption of the endogenous zebrafish rhodopsin locus as models of rapid rod photoreceptor degeneration. *Mol Vis.* 2018;24:587-602. <http://www.molvis.org/molvis/v24/587>. Accessed May 5, 2021.
43. Wilhelm M, Gábriel R. Functional anatomy of the photoreceptor and second-order cell mosaics in the retina of *Xenopus laevis*. *Cell Tissue Res.* 1999;297(1):35-46. doi:10.1007/s004410051331
44. Witkovsky P. Photoreceptor classes and transmission at the photoreceptor synapse in the retina of the clawed frog, *Xenopus laevis*. *Microsc Res Tech.* 2000;50(5):338-346. doi:10.1002/1097-0029(20000901)50:5<338::AID-JEMT3>3.0.CO;2-I
45. Elurbe DM, Paranjpe SS, Georgiou G, et al. Regulatory remodeling in the allo-tetraploid frog *Xenopus laevis*. *Genome Biol.* 2017;18(1):198. doi:10.1186/s13059-017-1335-7
46. Session AM, Uno Y, Kwon T, et al. Genome evolution in the allotetraploid frog *Xenopus laevis*. *Nature.* 2016;538(7625):336-343. doi:10.1038/nature19840
47. Bowes JB, Snyder KA, Segerdell E, et al. Xenbase: gene expression and improved integration. *Nucleic Acids Res.* 2009;38(suppl_1):D607-D612. doi:10.1093/nar/gkp953
48. Colella P, Cotugno G, Auricchio A. Ocular gene therapy: current progress and future prospects. *Trends Mol Med.* 2009;15(1):23-31. doi:10.1016/j.molmed.2008.11.003
49. Feehan JM, Chiu CN, Stanar P, Tam BM, Ahmed SN, Moritz OL. Modeling Dominant and Recessive Forms of Retinitis Pigmentosa by Editing Three Rhodopsin-Encoding Genes in *Xenopus Laevis* Using Crispr/Cas9. *Sci Rep.* 2017;7(1):1-14. doi:10.1038/s41598-017-07153-4
50. Wilson JH, Wensel TG. The Nature of Dominant Mutations of Rhodopsin and Implications for Gene Therapy. In: *Molecular Neurobiology.* Vol 28. Humana Press; 2003:149-158. doi:10.1385/MN:28:2:149
51. Hafler BP, Comander J, Difranco CW, Place EM, Pierce EA. Course of ocular function in PRPF31 retinitis pigmentosa. *Semin Ophthalmol.* 2016;31(1-2):49-52. doi:10.3109/08820538.2015.1114856
52. Auricchio A, Smith AJ, Ali RR. The Future Looks Brighter After 25 Years of Retinal Gene Therapy. *Hum Gene Ther.* 2017;28(11):982-987. doi:10.1089/hum.2017.164
53. Herskowitz I. Functional inactivation of genes by dominant negative mutations. *Nature.* 1987;329(6136):219-222. doi:10.1038/329219a0
54. Illing ME, Rajan RS, Bence NF, Kopito RR. A rhodopsin mutant linked to autosomal dominant retinitis pigmentosa is prone to aggregate and interacts with the ubiquitin proteasome system. *J Biol Chem.* 2002;277(37):34150-34160. doi:10.1074/jbc.M204955200

55. Athanasiou D, Aguila M, Bellingham J, et al. The molecular and cellular basis of rhodopsin retinitis pigmentosa reveals potential strategies for therapy. *Prog Retin Eye Res.* 2018;62:1-23. doi:10.1016/j.preteyeres.2017.10.002
56. Mendes HF, Van Der Spuy J, Chapple JP, Cheetham ME. Mechanisms of cell death in rhodopsin retinitis pigmentosa: Implications for therapy. *Trends Mol Med.* 2005;11(4):177-185. doi:10.1016/j.molmed.2005.02.007
57. Cideciyan A V., Sudharsan R, Dufour VL, et al. Mutation-independent rhodopsin gene therapy by knockdown and replacement with a single AAV vector. *Proc Natl Acad Sci U S A.* 2018;115(36):E8547-E8556. doi:10.1073/pnas.1805055115
58. Diakatou M, Dubois G, Erkilic N, Sanjurjo-Soriano C, Meunier I, Kalatzis V. Allele-specific knockout by crispr/cas to treat autosomal dominant retinitis pigmentosa caused by the g56r mutation in nr2e3. *Int J Mol Sci.* 2021;22(5):1-21. doi:10.3390/ijms22052607
59. Tsai YT, Wu WH, Lee TT, et al. Clustered Regularly Interspaced Short Palindromic Repeats-Based Genome Surgery for the Treatment of Autosomal Dominant Retinitis Pigmentosa. *Ophthalmology.* 2018;125(9):1421-1430. doi:10.1016/j.ophtha.2018.04.001
60. Foltz LP, Howden SE, Thomson JA, Clegg DO. Functional assessment of patient-derived retinal pigment epithelial cells edited by CRISPR/Cas9. *Int J Mol Sci.* 2018;19(12). doi:10.3390/ijms19124127
61. Hsu PD, Lander ES, Zhang F. Development and applications of CRISPR-Cas9 for genome engineering. *Cell.* 2014;157(6):1262-1278. doi:10.1016/j.cell.2014.05.010
62. Jinek M, Chylinski K, Fonfara I, Hauer M, Doudna JA, Charpentier E. A programmable dual-RNA-guided DNA endonuclease in adaptive bacterial immunity. *Science (80-).* 2012;337(6096):816-821. doi:10.1126/science.1225829
63. Rath D, Amlinger L, Rath A, Lundgren M. The CRISPR-Cas immune system: Biology, mechanisms and applications. *Biochimie.* 2015;117:119-128. doi:10.1016/j.biochi.2015.03.025
64. Lino CA, Harper JC, Carney JP, Timlin JA. Delivering CRISPR: a review of the challenges and approaches. doi:10.1080/10717544.2018.1474964
65. Wang D, Zhang C, Wang B, et al. Optimized CRISPR guide RNA design for two high-fidelity Cas9 variants by deep learning. *Nat Commun.* 2019;10(1):1-14. doi:10.1038/s41467-019-12281-8
66. Liu C, Zhang L, Liu H, Cheng K. Delivery strategies of the CRISPR-Cas9 gene-editing system for therapeutic applications. *J Control Release.* 2017;266:17-26. doi:10.1016/j.jconrel.2017.09.012
67. Ran FA, Hsu PD, Wright J, Agarwala V, Scott DA, Zhang F. Genome engineering using the CRISPR-Cas9 system. *Nat Protoc.* 2013;8(11):2281-2308. doi:10.1038/nprot.2013.143
68. Fu Y, Foden JA, Khayter C, et al. High-frequency off-target mutagenesis induced by

- CRISPR-Cas nucleases in human cells. *Nat Biotechnol.* 2013;31(9):822-826.
doi:10.1038/nbt.2623
69. Shen B, Zhang W, Zhang J, et al. Efficient genome modification by CRISPR-Cas9 nickase with minimal off-target effects. *Nat Methods.* 2014;11(4):399-402.
doi:10.1038/nmeth.2857
 70. Li L, Hu S, Chen X. Non-viral delivery systems for CRISPR/Cas9-based genome editing: Challenges and opportunities. *Biomaterials.* 2018;171:207-218.
doi:10.1016/j.biomaterials.2018.04.031
 71. Kim S, Kim D, Cho SW, Kim J, Kim JS. Highly efficient RNA-guided genome editing in human cells via delivery of purified Cas9 ribonucleoproteins. *Genome Res.* 2014;24(6):1012-1019. doi:10.1101/gr.171322.113
 72. Zaboikin M, Zaboikina T, Freter C, Srinivasakumar N. Non-homologous end joining and homology directed DNA repair frequency of double-stranded breaks introduced by genome editing reagents. *PLoS One.* 2017;12(1). doi:10.1371/journal.pone.0169931
 73. Chapman JR, Taylor MRG, Boulton SJ. Playing the End Game: DNA Double-Strand Break Repair Pathway Choice. *Mol Cell.* 2012;47(4):497-510.
doi:10.1016/j.molcel.2012.07.029
 74. Baker KE, Parker R. Nonsense-mediated mRNA decay: Terminating erroneous gene expression. *Curr Opin Cell Biol.* 2004;16(3):293-299. doi:10.1016/j.ceb.2004.03.003
 75. Ferreira MG, Cooper JP. Two modes of DNA double-strand break repair are reciprocally regulated through the fission yeast cell cycle. *Genes Dev.* 2004;18(18):2249-2254.
doi:10.1101/gad.315804
 76. Branzei D, Foiani M. Regulation of DNA repair throughout the cell cycle. *Nat Rev Mol Cell Biol.* 2008;9(4):297-308. doi:10.1038/nrm2351
 77. Tang XD, Gao F, Liu MJ, Fan QL, Chen DK, Ma WT. Methods for enhancing clustered regularly interspaced short palindromic repeats/Cas9-mediated homology-directed repair efficiency. *Front Genet.* 2019;10(JUN):551. doi:10.3389/fgene.2019.00551
 78. Arnoult N, Correia A, Ma J, et al. Regulation of DNA repair pathway choice in S and G2 phases by the NHEJ inhibitor CYREN. *Nature.* 2017;549(7673):548-552.
doi:10.1038/nature24023
 79. Salsman J, Dellaire G. Precision genome editing in the CRISPR era. *Biochem Cell Biol.* 2017;95(2):187-201. doi:10.1139/bcb-2016-0137
 80. Miura H, Gurumurthy CB, Sato T, Sato M, Ohtsuka M. CRISPR/Cas9-based generation of knockdown mice by intronic insertion of artificial microRNA using longer single-stranded DNA. *Sci Rep.* 2015;5. doi:10.1038/srep12799
 81. Yoshimi K, Kunihiro Y, Kaneko T, Nagahora H, Voigt B, Mashimo T. SsODN-mediated knock-in with CRISPR-Cas for large genomic regions in zygotes. *Nat Commun.* 2016;7.
doi:10.1038/ncomms10431

82. Okamoto S, Amaishi Y, Maki I, Enoki T, Mineno J. Highly efficient genome editing for single-base substitutions using optimized ssODNs with Cas9-RNPs. *Sci Rep.* 2019;9(1):1-11. doi:10.1038/s41598-019-41121-4
83. Paix A, Folkmann A, Goldman DH, et al. Precision genome editing using synthesis-dependent repair of Cas9-induced DNA breaks. *Author Contrib AP GS Des Res.* doi:10.1073/pnas.1711979114
84. Richardson CD, Ray GJ, DeWitt MA, Curie GL, Corn JE. Enhancing homology-directed genome editing by catalytically active and inactive CRISPR-Cas9 using asymmetric donor DNA. *Nat Biotechnol.* 2016;34(3):339-344. doi:10.1038/nbt.3481
85. Jacobi AM, Rettig GR, Turk R, et al. Simplified CRISPR tools for efficient genome editing and streamlined protocols for their delivery into mammalian cells and mouse zygotes. *Methods.* 2017;121-122:16-28. doi:10.1016/j.ymeth.2017.03.021
86. Ding Y, Li H, Chen LL, Xie K. Recent advances in genome editing using CRISPR/Cas9. *Front Plant Sci.* 2016;7(MAY2016):703. doi:10.3389/fpls.2016.00703
87. Perlman I. *The Electroretinogram: ERG. 2001 May 1 [Updated 2007 Jun 27].* (Kolb H, Fernandez E, Nelson R, eds.). University of Utah Health Sciences Center; 2007. <http://www.ncbi.nlm.nih.gov/pubmed/21413407>. Accessed April 7, 2021.
88. Brandli A, Stone J. Using the electroretinogram to assess function in the rodent retina and the protective effects of remote limb ischemic preconditioning. *J Vis Exp.* 2015;2015(100):52658. doi:10.3791/52658
89. Creel DJ. *Clinical Electrophysiology.* University of Utah Health Sciences Center; 1995. <http://www.ncbi.nlm.nih.gov/pubmed/21413406>. Accessed April 7, 2021.
90. Li Y, Cohen ED, Qian H. Rod and Cone Coupling Modulates Photopic ERG Responses in the Mouse Retina. *Front Cell Neurosci.* 2020;14:305. doi:10.3389/fncel.2020.566712
91. Benchorin G, Calton M, Beaulieu M, Vollrath D. Assessment of Murine Retinal Function by Electroretinography. *BIO-PROTOCOL.* 2017;7(7). doi:10.21769/bioprotoc.2218
92. Abramoff MD, Garvin MK, Sonka M. Retinal imaging and image analysis. *IEEE Rev Biomed Eng.* 2010;3:169-208. doi:10.1109/RBME.2010.2084567
93. Brancati N, Frucci M, Gragnaniello D, Riccio D, Di Iorio V, Di Perna L. Automatic segmentation of pigment deposits in retinal fundus images of Retinitis Pigmentosa. *Comput Med Imaging Graph.* 2018;66:73-81. doi:10.1016/j.compmedimag.2018.03.002
94. Fujimoto JG, Pitris C, Boppart SA, Brezinski ME. Optical coherence tomography: An emerging technology for biomedical imaging and optical biopsy. *Neoplasia.* 2000;2(1-2):9-25. doi:10.1038/sj.neo.7900071
95. Garcia-Martin E, Pinilla I, Sancho E, et al. Optical coherence tomography in retinitis pigmentosa: Reproducibility and capacity to detect macular and retinal nerve fiber layer thickness alterations. *Retina.* 2012;32(8):1581-1591. doi:10.1097/IAE.0b013e318242b838

96. Tam BM, Lai CC-L, Zong Z, Moritz OL. Generation of Transgenic *X. laevis* Models of Retinal Degeneration. In: Humana Press, Totowa, NJ; 2012:113-125. doi:10.1007/978-1-62703-080-9_8
97. Paskowitz DM, LaVail MM, Duncan JL. Light and inherited retinal degeneration. *Br J Ophthalmol*. 2006;90(8):1060-1066. doi:10.1136/bjo.2006.097436
98. Tam BM, Noorwez SM, Kaushal S, Kono M, Moritz OL. Photoactivation-induced instability of rhodopsin mutants T4K and T17M in rod outer segments underlies retinal degeneration in *X. laevis* transgenic models of retinitis pigmentosa. *J Neurosci*. 2014;34(40):13336-13348. doi:10.1523/JNEUROSCI.1655-14.2014
99. White DA, Hauswirth WW, Kaushal S, Lewin AS. Increased sensitivity to light-induced damage in a mouse model of autosomal dominant retinal disease. *Investig Ophthalmol Vis Sci*. 2007;48(5):1942-1951. doi:10.1167/iovs.06-1131
100. Iwabe S, Ying GS, Aguirre GD, Beltran WA. Assessment of visual function and retinal structure following acute light exposure in the light sensitive T4R rhodopsin mutant dog. *Exp Eye Res*. 2016;146:341-353. doi:10.1016/j.exer.2016.04.006
101. Daiger SP, Sullivan LS, Bowne SJ. Genes and mutations causing retinitis pigmentosa. *Clin Genet*. 2013;84(2):132-141. doi:10.1111/cge.12203
102. Tam BM, Qazalbash A, Lee HC, Moritz OL. The dependence of retinal degeneration caused by the rhodopsin P23H mutation on light exposure and vitamin a deprivation. *Investig Ophthalmol Vis Sci*. 2010;51(3):1327-1334. doi:10.1167/iovs.09-4123
103. Miura H, Quadros RM, Gurusurthy CB, Ohtsuka M. Easi-CRISPR for creating knock-in and conditional knockout mouse models using long ssDNA donors. *Nat Protoc*. 2018;13(1):195-215. doi:10.1038/nprot.2017.153
104. Gibson DG, Young L, Chuang RY, Venter JC, Hutchison CA, Smith HO. Enzymatic assembly of DNA molecules up to several hundred kilobases. *Nat Methods*. 2009;6(5):343-345. doi:10.1038/nmeth.1318
105. Tam BM, Xie G, Oprian DD, Moritz OL. Mislocalized rhodopsin does not require activation to cause retinal degeneration and neurite outgrowth in *Xenopus laevis*. *J Neurosci*. 2006;26(1):203-209. doi:10.1523/JNEUROSCI.3849-05.2006
106. Adamus G, Zam ZS, Arendt A, Palczewski K, McDowell JH, Hargrave PA. Anti-rhodopsin monoclonal antibodies of defined specificity: Characterization and application. *Vision Res*. 1991;31(1):17-31. doi:10.1016/0042-6989(91)90069-H
107. Mackenzie D, Molday RS, Arendt A, Hargrave P, McDowell JH. Localization of Binding Sites for Carboxyl Terminal Specific Anti-Rhodopsin Monoclonal Antibodies Using Synthetic Peptides. *Biochemistry*. 1984;23(26):6544-6549. doi:10.1021/bi00321a041
108. Mann--Whitney Test. In: *The Concise Encyclopedia of Statistics*. New York, NY: Springer New York; 2008:327-329. doi:10.1007/978-0-387-32833-1_243
109. Kruskal-Wallis Test. In: *The Concise Encyclopedia of Statistics*. New York, NY: Springer

- New York; 2008:288-290. doi:10.1007/978-0-387-32833-1_216
110. Meng D, Ragi SD, Tsang SH. Therapy in Rhodopsin-Mediated Autosomal Dominant Retinitis Pigmentosa. *Mol Ther*. 2020;28(10):2139-2149. doi:10.1016/j.ymthe.2020.08.012
 111. Lem* † ‡ J, Krasnoperova N V, Calvert PD, et al. *Morphological, Physiological, and Biochemical Changes in Rhodopsin Knockout Mice*. Vol 96.; 1999. www.pnas.org. Accessed May 31, 2021.
 112. Rosenfeld PJ, Cowley GS, McGee TL, Sandberg MA, Berson EL, Dryja TP. A Null mutation in the rhodopsin gene causes rod photoreceptor dysfunction and autosomal recessive retinitis pigmentosa. *Nat Genet*. 1992;1(3):209-213. doi:10.1038/ng0692-209
 113. Kartasasmita A, Fujiki K, Iskandar E, Sovani I, Fujimaki T, Murakami A. A novel nonsense mutation in rhodopsin gene in two Indonesian families with autosomal recessive retinitis pigmentosa. *Ophthalmic Genet*. 2011;32(1):57-63. doi:10.3109/13816810.2010.535892
 114. Wen RH, Stanar P, Tam B, Moritz OL. Autophagy in *Xenopus laevis* rod photoreceptors is independently regulated by phototransduction and misfolded RHOP23H. *Autophagy*. 2019;15(11):1970-1989. doi:10.1080/15548627.2019.1596487
 115. Feehan JM, Stanar P, Tam BM, Chiu C, Moritz OL. Generation and Analysis of *Xenopus laevis* Models of Retinal Degeneration Using CRISPR/Cas9. In: *Methods in Molecular Biology*. Vol 1834. Humana Press Inc.; 2019:193-207. doi:10.1007/978-1-4939-8669-9_14
 116. Which type of oligo purification should I choose? <https://www.idtdna.com/pages/education/decoded/article/which-type-of-purification-should-i-choose->. Accessed March 15, 2021.
 117. Deretic D, Papermaster DS. Polarized sorting of rhodopsin on post-Golgi membranes in frog retinal photoreceptor cells. *J Cell Biol*. 1991;113(6):1281-1293. doi:10.1083/jcb.113.6.1281
 118. Miller RF, Dowling JE. Intracellular responses of the Müller (glial) cells of mudpuppy retina: their relation to b-wave of the electroretinogram. *J Neurophysiol*. 1970;33(3):323-341. doi:10.1152/jn.1970.33.3.323
 119. Nakazawa M, Hara A, Ishiguro SI. Optical Coherence Tomography of Animal Models of Retinitis Pigmentosa: From Animal Studies to Clinical Applications. *Biomed Res Int*. 2019;2019. doi:10.1155/2019/8276140
 120. Monai N, Yamauchi K, Tanabu R, Gonome T, Ishiguro S ichi, Nakazawa M. Characterization of photoreceptor degeneration in the rhodopsin P23H transgenic rat line 2 using optical coherence tomography. *PLoS One*. 2018;13(3). doi:10.1371/journal.pone.0193778
 121. Lee DC, Xu J, Sarunic M V., Moritz OL. Fourier domain optical coherence tomography as a noninvasive means for in vivo detection of retinal degeneration in *Xenopus laevis*

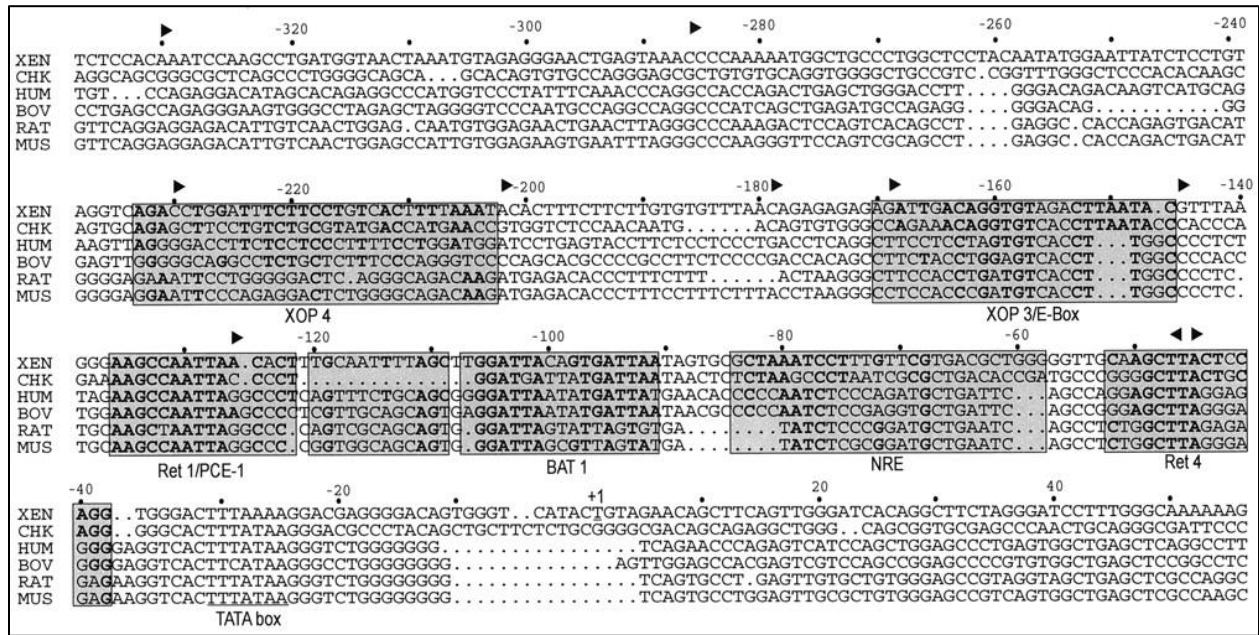
- tadpoles. *Investig Ophthalmol Vis Sci.* 2010;51(2):1066-1070. doi:10.1167/iovs.09-4260
122. Liu M, Rehman S, Tang X, et al. Methodologies for improving HDR efficiency. *Front Genet.* 2019;10(JAN):691. doi:10.3389/fgene.2018.00691
 123. Aslan Y, Tadjuidje E, Zorn AM, Cha SW. High-efficiency non-mosaic CRISPR-mediated knock-in and indel mutation in F0 *Xenopus*. *Dev.* 2017;144(15):2852-2858. doi:10.1242/dev.152967
 124. Latella MC, Di Salvo MT, Cocchiarella F, et al. In vivo Editing of the Human Mutant Rhodopsin Gene by Electroporation of Plasmid-based CRISPR/Cas9 in the Mouse Retina. *Mol Ther - Nucleic Acids.* 2016;5(11):e389. doi:10.1038/mtna.2016.92
 125. Maruyama T, Dougan SK, Truttmann MC, Bilate AM, Ingram JR, Ploegh HL. Increasing the efficiency of precise genome editing with CRISPR-Cas9 by inhibition of nonhomologous end joining. *Nat Biotechnol.* 2015;33(5):538-542. doi:10.1038/nbt.3190
 126. Lin S, Staahl BT, Alla RK, Doudna JA. Enhanced homology-directed human genome engineering by controlled timing of CRISPR/Cas9 delivery. *Elife.* 2014;3:e04766. doi:10.7554/eLife.04766
 127. Vartak S V., Raghavan SC. Inhibition of nonhomologous end joining to increase the specificity of CRISPR/Cas9 genome editing. *FEBS J.* 2015;282(22):4289-4294. doi:10.1111/febs.13416
 128. Srivastava M, Nambiar M, Sharma S, et al. An inhibitor of nonhomologous end-joining abrogates double-strand break repair and impedes cancer progression. *Cell.* 2012;151(7):1474-1487. doi:10.1016/j.cell.2012.11.054
 129. Tsai YT, Wu WH, Lee TT, et al. Clustered Regularly Interspaced Short Palindromic Repeats-Based Genome Surgery for the Treatment of Autosomal Dominant Retinitis Pigmentosa. *Ophthalmology.* 2018;125(9):1421-1430. doi:10.1016/j.ophtha.2018.04.001
 130. Yip BH. Recent advances in CRISPR/Cas9 delivery strategies. *Biomolecules.* 2020;10(6). doi:10.3390/biom10060839
 131. Young JL, Dean DA. Electroporation-Mediated Gene Delivery. *Adv Genet.* 2015;89:49-88. doi:10.1016/bs.adgen.2014.10.003
 132. Ramamoorth M, Narvekar A. Non viral vectors in gene therapy - An overview. *J Clin Diagnostic Res.* 2015;9(1):GE01-GE06. doi:10.7860/JCDR/2015/10443.5394
 133. Cheng Q, Wei T, Farbiak L, Johnson LT, Dilliard SA, Siegwart DJ. Selective organ targeting (SORT) nanoparticles for tissue-specific mRNA delivery and CRISPR-Cas gene editing. *Nat Nanotechnol.* 2020;15(4):313-320. doi:10.1038/s41565-020-0669-6
 134. Wu YC, Wu TH, Clemens DL, et al. Massively parallel delivery of large cargo into mammalian cells with light pulses. *Nat Methods.* 2015;12(5):439-444. doi:10.1038/nmeth.3357
 135. Ramakrishna S, Kwaku Dad AB, Beloor J, Gopalappa R, Lee SK, Kim H. Gene disruption

- by cell-penetrating peptide-mediated delivery of Cas9 protein and guide RNA. *Genome Res.* 2014;24(6):1020-1027. doi:10.1101/gr.171264.113
136. Suzuki K, Tsunekawa Y, Hernandez-Benitez R, et al. In vivo genome editing via CRISPR/Cas9 mediated homology-independent targeted integration. *Nature.* 2016;540(7631):144-149. doi:10.1038/nature20565
 137. Mani SS, Batni S, Whitaker L, Chen S, Engbretson G, Knox BE. Xenopus rhodopsin promoter. Identification of immediate upstream sequences necessary for high level, rod-specific transcription. *J Biol Chem.* 2001;276(39):36557-36565. doi:10.1074/jbc.M101685200
 138. Dalkara D, Goureau O, Marazova K, Sahel JA. Let There Be Light: Gene and Cell Therapy for Blindness. *Hum Gene Ther.* 2016;27(2):134-147. doi:10.1089/hum.2015.147

APPENDICES

Appendix A. Rhodopsin promoter sequence

The highly conserved region in the rhodopsin promoter sequence of *X. laevis* aligned with other animal models (Figure acquired from Mani *et al.*¹³⁷)



Appendix B. HDR template design

Original WT Sequence – *Rho.L*:

GTAGAACAGCTTCAGTTGGGATCACAGGCTTCTAAGGATCCTTTGGGCAAAAAAGAAACAGAGAAGGCATTCTTT
CTATACAAGAAAGGACTTGATAGAGCTGCTACCATGAACGGAACAGAGGGTCCCAATTTTTATATCCCCATGTCCA
ACAAAACGGGGTGGTACGAAGCCCATTTCGATTACCCTCAGTATTACTTAGCAGAGCCATGGCAATATTCAGCACT
GGCTGCTTACAT

12bp (11+1) deletion:

GTAGAACAGCTTCAGTTGGGATCACAGGCTTCTAAGGATCCTTTGGGCAAAAAAGAAACAGAGAAGGCATTCTTT
CTATACAAGAAAGGACTTGATAGAGCTGCTACCATGAACGGAACAGAGGGTCCCAATTTTTATATCCCCATGTCCA
ACAAAACGGGGTGGTACGAAGCCCATTTCGATTACCCTCAGTATTACTTAGCAGAGCCATGGCAATATTCAGCACT
GGCTGCTTACAT

12bp deleted Sequence:

GTAGAACAGCTTCAGTTGGGATCACAGGCTTCTAAGGATCCTTTGGGCAAAAAAGAAACAGAGAAGGCATTCTTT
CTATACAAGAAAGGACTTGATAGAGCTGCTACCATGGGGTCCCAATTTTTATATCCCCATGTCCAACAAAACGGGG
TGGTACGAAGCCCATTTCGATTACCCTCAGTATTACTTAGCAGAGCCATGGCAATATTCAGCACTGGCTGCTTACAT

Final HDR Template (120nt):

TTCTTTCTATACAAGAAAGGACTTGATAGAGCTGCTACCATG[AACGGAACAGAGGGTCCAAATTTTTATATCCCC
TT]TCCAACAAAACGGGGTGGTACGAAGCCCATTTCGATTACCCT

Start codon

11+1 deletion

Sg5 target sequence

[Insert = 36nt]

M13F mutation: ATG → TTT

ApoI digestion site silent mutation: CAATTT → AAATTT

42nt homology arms on each side

42+42+36 = 120nt

Sg5 target sequence: AATTTT-ATATCCCCATGTCC

Corresponding HDR template: AATTTTTATATCCCCTTTCC